

NON-STOICHIOMETRY IN TITANIUM DIOXIDE (RUTILE)

Thesis submitted in supplication

for the Degree of

DOCTOR OF PHILOSOPHY

(under special regulations)

by

PETER WILLIAM GRAVES, B.Sc. (Hons.)

Department of Physical Metallurgy

University of Birmingham

May 1963

UNIVERSITY OF
BIRMINGHAM

University of Birmingham Research Archive

e-theses repository

This unpublished thesis/dissertation is copyright of the author and/or third parties. The intellectual property rights of the author or third parties in respect of this work are as defined by The Copyright Designs and Patents Act 1988 or as modified by any successor legislation.

Any use made of information contained in this thesis/dissertation must be in accordance with that legislation and must be properly acknowledged. Further distribution or reproduction in any format is prohibited without the permission of the copyright holder.

SYNOPSIS

The present investigation, which forms part of a general programme of research into the effects of departures from the stoichiometric composition on the physical and mechanical properties of ceramic compounds, is concerned with the defect structure of non-stoichiometric rutile. The physical properties of rutile, with particular reference to the effects of departure from the stoichiometric composition, have been briefly reviewed.

The development and design of an apparatus, incorporating a sensitive microbalance, capable of measuring departures from the stoichiometric composition in rutile at low pressures of oxygen and at temperatures up to a maximum of 1300°C is described in detail.

The defect structure of non-stoichiometric rutile has been shown to alter as departure from the ideal composition increases. It is concluded that at small departures from the stoichiometric composition free anion vacancies are present, whereas at large departures the vacancies cluster on planes of the {100}, {101} and {110} types, which subsequently collapse by displacement of $\frac{1}{2}\langle 101 \rangle$ forming interstitial cations.

The departures from stoichiometric composition which have been observed in high-purity rutile are very small - much smaller than those previously reported in the literature. Larger departures found to occur in impure rutile can be attributed directly to electronic effects associated with impurity atoms. Much further work of a systematic and long-term nature will have to be carried out before the role of impurity atoms on the defect structure of non-stoichiometric rutile is understood.

CONTENTS

	<u>Page</u>
I INTRODUCTION	1
II TITANIUM DIOXIDE - RUTILE	3
1. Structural Data	3
1.1. Crystal Structure	3
1.2. Crystal Bonding	4
1.3. Homogeneity Range of Rutile	5
2. Possible Non-Stoichiometric Structural Defects in Rutile	8
3. Physical Property Data	12
3.1. Electrical Conductivity	12
3.2. Hall Coefficient	17
3.3. Magnetic Susceptibility	18
3.4. Dielectric Constant	20
3.5. Optical Absorption	21
3.6. Density	23
3.7. Coefficient of Thermal Expansion	24
4. Band Structure of Rutile	25
5. Imperfections in Non-Stoichiometric Rutile - Conclusions	26
6. The Present Investigation	28

	<u>Page</u>
III APPARATUS AND EXPERIMENTAL PROCEDURES	31
1. General Considerations	31
1.1. Chemical Methods	31
1.2. Physical Methods	33
1.3. Method Chosen for the Present Investigation	34
2. Quartz Microbalance	35
2.1. Design and Construction	36
2.2. Electromagnetic Balancing Arrangement	36
2.3. Movement-Detection System	37
2.4. Calibration	38
3. Reasons for Abandoning the Quartz Microbalance	39
4. Sartorius Vacuum Electrono Microbalance	41
4.1. Electrical Circuit	41
4.2. Microbalance Beam	43
4.3. Microbalance Housing	44
4.4. Specimen Suspension	44
5. Specimen Tube and Temperature Measurement	45
6. Vacuum System and Pressure Measurement	47
7. General Assembly	51
8. Corrections to Meter Readings	52
8.1. Scale Reading	52

	<u>Page</u>
8.2. Temperature Effects	53
8.3. Buoyancy Effects	54
9. Operation of the Apparatus	58
10. Specimen Source and Pre-Treatment	61
11. Estimation of Errors	62
IV EXPERIMENTAL METHODS USED FOR THE DILATOMETRIC AND DENSITY STUDIES OF NON-STOICHIOMETRIC RUTILE	63
1. Dilatometric Studies	63
1.1. Introduction	63
1.2. Apparatus	64
1.3. Preparation of Specimens	66
1.4. Experimental Procedure	67
2. Density Measurements	67
V EXPERIMENTAL RESULTS	69
1. Variation of Non-Stoichiometry with Oxygen Pressure	69
1.1. Pressure Range	69
1.2. Vacuum Reduction	69
1.3. Treatment of Results	71
1.4. Temperatures below 1000°C	71
1.5. Temperatures above 1000°C	74

	<u>Page</u>
1.6. Electronic Effects of Non-Stoichiometry in Rutile	101
1.7. Origins of the Driving Force, and Possible Nuclei for Clustering	107
2. Maximum Extent of Non-Stoichiometry in Rutile	113
2.1. Non-Stoichiometry of Rutile at Low Temperatures	114
2.2. Maximum Extent of Non-Stoichiometry at Various Temperatures	115
3. Future Work	119
VII REFERENCES	121
VIII ACKNOWLEDGEMENTS	127
APPENDICES	

Table I

ELEMENT COMPOUND	Ti	Zr	Hf	V	Nb	Ta	Cr	Mo	W	U
(METAL)	1460	1860	2230	1915	2410	2850	1850	2620	3410	1130
MONOCARBIDE	3250	3175	3890	2830	3500	3880		2695	2630 ^x	2475
MONONITRIDE	2930	2980	3310	2050	2050	3090	1500			2650
DIBORIDE	2980	3040	3250	2100 ^x	>2900 ^x	3000 ^x	1850	2100		

DIOXIDE	1840	2677	2777	1550						3280
SESQUOXIDE	1900			1977	1772		2265			

Melting points (in °C) of the early transition metals and their "refractory" compounds. Table compiled from data given in Schwarzkopf and Kieffer⁽¹⁾, and Campbell⁽²⁾. The superscript^x indicates that the compound decomposes.

I INTRODUCTION

The work described here forms part of a more general study of the behaviour of inorganic compounds characterised by a high melting point. Compounds of this type are almost entirely restricted to the oxides, carbides, nitrides and borides of the transition metals^(1,2), and one of the interests in these compounds is the effect of departures from the stoichiometric composition on their physical and mechanical properties. The reasons for the studies being undertaken in a Department of Physical Metallurgy are threefold, namely (i) the compounds may possibly be used at some future date as high-temperature constructional materials, in place of the usual metallic materials, (ii) as a more direct approach to the understanding of such metallurgical phenomena as oxidation, carburising and nitriding, and (iii) the interest in solid-state electronic devices based on unusual electrical and magnetic characteristics.

The number of inorganic compounds of the transition metals with a high melting point is large, as can be seen from Table I. Of these compounds the one chosen for the initiation of the studies was titanium dioxide, interest being restricted to its modification known as rutile. The reasons for this choice were that rutile is the most stable crystal modification of titanium

dioxide, and that it is available commercially in highly purified forms - facilities are not yet available in this Department for the preparation of any of the compounds. Also previous work had shown that rutile, when heated in vacuo, exhibits large departures from the stoichiometric composition, occurring by loss of oxygen from the lattice, although reports in the literature differed as to the maximum extent of the non-stoichiometry, and to the nature of the structural defects formed. Furthermore none of the earlier studies had been carried out using rutile of such a high purity as that available in this laboratory.

In the following sections much of the existing physical property data of rutile has been collected together, in order to give some idea of the present state of our knowledge of this material. Particular emphasis is placed on the effects produced by departures from the stoichiometric composition.

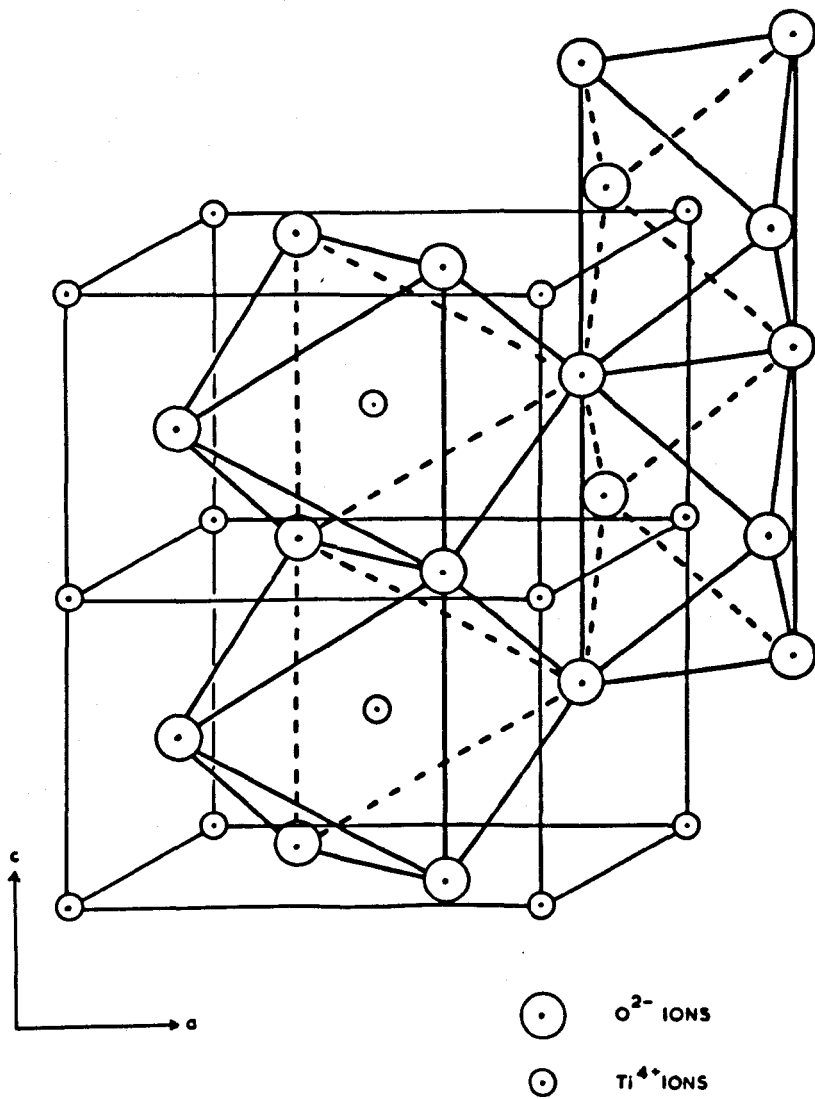


Fig. 2. Octahedral structure of rutile (after Breckenridge and Hosler⁽²⁷⁾).

Table II

Bond	Type	No./unit cell	Length (Å)
Ti - O	1	4	1.94 ± 0.004
Ti - O	2	2	1.98 ± 0.006
O - O	3	8	2.730 ± 0.002
O - O	4	2	2.520 ± 0.012
O - O	5	2	2.959 ± 0.002
Angle			Value
O - Ti - O	1 - 1 (lesser)	2	80.8°
O - Ti - O	1 - 1 (greater)	2	99.2°
O - Ti - O	1 - 2	8	90.0°
Ti - O - Ti	C - B - A		130.4°

Bond lengths and interbound angles in rutile (after Grant⁽⁴⁾).

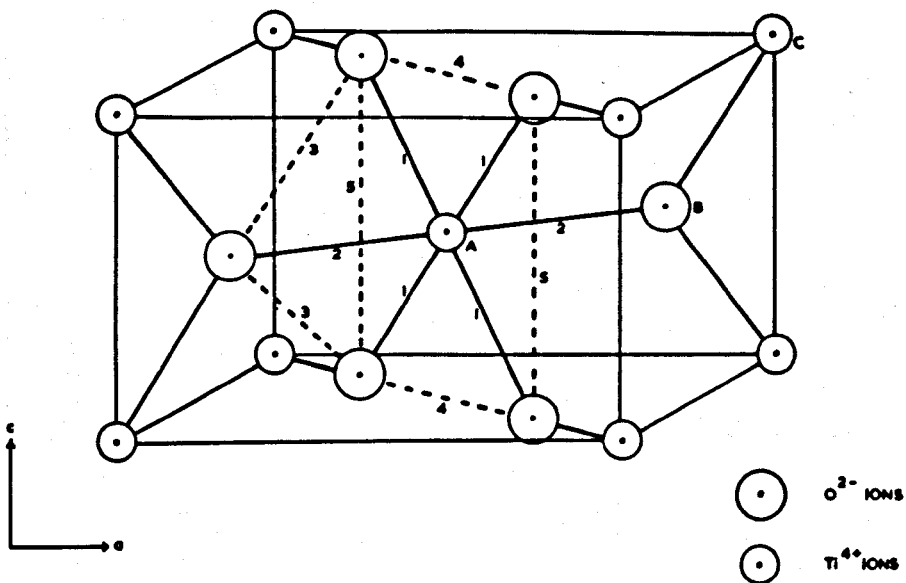


Fig. 1. Arrangement of the ions in the unit cell of rutile. The numbers refer to the bond lengths given in Table II (After Grant⁽⁴⁾).

II TITANIUM DIOXIDE - RUTILE

1. Structural Data

1.1 Crystal Structure

On a simple ionic model titanium dioxide can be thought of as being formed from titanium and oxygen in their +4 and -2 valence states respectively. The rutile modification of titanium dioxide possesses a tetragonal unit cell, the parameters of which are⁽³⁾:

$$a = 4.594 \pm 0.003 \text{ \AA}, \quad c = 2.959 \pm 0.002 \text{ \AA}, \quad \frac{c}{a} = 0.6441.$$

If the Ti^{4+} cations are considered to be situated at $(0,0,0)$ and $(\frac{1}{2}, \frac{1}{2}, \frac{1}{2})$, then the O^{2-} anions are in the positions $\pm(x, x, 0)$ and $\pm(\frac{1}{2} + x, \frac{1}{2} - x, \frac{1}{2})$, where $x = 0.306 \pm 0.001$ ⁽³⁾. The ionic arrangement of rutile is illustrated in Fig. 1, the numbers on the diagram referring to the bond lengths and angles given in Table II.

From Fig. 1 it is evident that each cation is situated at the centre of an octahedron described by six surrounding anions. Rutile can therefore be visualised as being built of a series of chains of octahedra parallel to the c axis, each octahedron sharing an edge in the (001) plane with adjacent members of the chain, and corners with neighbouring chains (see Fig. 2). The octahedra are, however, distorted, owing to two of the anions

being at a greater distance from the cation than the other four (see Table II and Fig. 1).

1.2 Crystal Bonding

The difference in the Ti-O bond lengths is attributed^(4,5) to a covalent contribution to the crystal bonding. Some support for the view that the bonding is partly covalent comes from the low solubility of rutile in polar solvents. Also if rutile is assumed to be purely ionic in nature, the calculated values of the axial ratio⁽⁶⁾, corresponding to a maximum of the Madelung constant, and of the parameter x ⁽⁷⁾ do not agree with the values obtained by experiment. The discrepancies indicate that the bonding in rutile is not completely ionic.

The most conclusive evidence for a covalent contribution to the crystal bonding has been given by Baur⁽³⁾, who carried out a Fourier projection of the elementary unit cell of rutile, perpendicular to the [001] axis. If the structure were completely ionic the electron density would be expected to fall to zero between the ions, as in sodium chloride⁽⁸⁾. The electron density did fall to zero between anions and cations in the (001) plane, i.e. ions B and A of Fig. 1, but a finite electron density was found to exist between anions in the (001) plane and the body-centred cation. From these observations the length of bond BC,

of a covalent nature, would be expected to be less than the length of the ionic bond AB, due to the sharing of electrons in the former case. This, in fact, agrees with the observed bond lengths (see Table II). No attempt was made to deduce the degree of the covalency in the crystal bonding, but Hannay and Smyth⁽⁹⁾ using the calculated electro-negativities of O^{2-} and Ti^{4+} , have estimated it to be 57%.

1.3 Homogeneity Range of Rutile

X-ray studies have shown^(10,11,12,13) that titanium dioxide maintains the rutile structure over a range of composition, corresponding to oxygen:titanium atomic ratios of less than 2:1, see Fig. 3⁽¹⁴⁾. Single phases of variable composition are found in many ionic compounds, including the halides, oxides and sulphides, and in the majority of the cases of binary compounds, a phase only extends on one side of the stoichiometric composition⁽¹⁵⁾.

Zirconia (ZrO_2), like rutile, is restricted to the oxygen deficient side of the stoichiometric composition⁽¹⁶⁾, the lower oxygen limit varying from 63 atomic % at 1900°C to 65.5 atomic % at 700°C⁽¹⁷⁾.

In urania (UO_2), on the other hand, the cubic dioxide phase is maintained for an excess of oxygen, up to a composition of $UO_{2.2}$ ⁽¹⁸⁾.

Loss of oxygen from rutile can be brought about by heating a specimen of rutile in a vacuum or oxygen at reduced

pressure to above 800°C ^(13,19). Larger losses can be obtained by the use of a reducing agent such as hydrogen⁽²⁰⁾, carbon monoxide⁽¹¹⁾, or titanium metal^(10,12).

The upper limit of oxygen composition of rutile is unequivocally considered^(10,11,12,13) to be stoichiometric TiO_2 , but there is considerable disagreement about the lower limit. In an X-ray study, Ehrlich⁽¹⁰⁾ found that extra diffraction lines, indicating the presence of a second phase, appeared at a composition of $\text{TiO}_{1.90}$. Andersson⁽¹²⁾, however, found that the X-ray diffraction pattern of the material corresponding to the composition $\text{TiO}_{1.90}$ indicated that it was composed of two oxide phases. Although the first trace of the rutile diffraction lines appeared at $\text{TiO}_{1.95}$, the resolving power of the X-ray camera used was not high enough to reveal the co-existence of two phases between $\text{TiO}_{1.9}$ and $\text{TiO}_{1.95}$. The value of $\text{TiO}_{1.95}$, for the lower limit of oxygen composition of rutile must therefore be accepted with caution, especially as the author considers that equilibrium conditions are not easily reached in this border region. Both workers prepared their specimens by heating or melting mixtures of rutile and titanium metal, the composition of the material being computed from the aliquot portions used. This procedure is not altogether satisfactory since additional changes in composition may occur as a result of loss of oxygen from the sample at high temperature. X-ray studies⁽¹¹⁾ of rutile reduced by carbon monoxide, which is perhaps a more reliable method,

showed that $\text{TiO}_{1.90}$ is the lower compositional limit, but unfortunately no details were given of the experimental procedures used.

Straumanis et al.⁽¹³⁾, using highly refined X-ray techniques, have found that extra diffraction lines attributed to a second phase, appeared in the rutile diffraction pattern at a composition of $\text{TiO}_{1.983}$. The failure of other workers to detect extra lines at this composition was attributed to the use of thick samples which cause extensive background fogging of the X-ray film. In this work great care was taken in preparing the samples (heating at 1400°C under controlled oxygen pressures) and in determining their composition. For the latter a combination of the density of the sample and the volume of the unit cell computed from the X-ray measurements was used.

These workers also found that the lattice constants of the unit cell of rutile varied only slightly with loss of oxygen, the a parameter decreased while c increased. The findings are in complete contradiction to those of Andersson et al.⁽¹²⁾ who maintain that the opposite effects occur i.e. a increases and c decreases with decreasing oxygen content. However, neither the values of a and c nor the precision of the measurements of the latter workers compare with those of Straumanis et al.⁽¹³⁾, whose values for the parameters a and c agree very favourably with the generally accepted values⁽³⁾.

The many different values reported for the range of oxygen concentrations over which rutile is homogeneous, suggest that any specimen of rutile having a composition lying between $\text{TiO}_{1.983}$ and $\text{TiO}_{1.90}$ may well have contained two phases, and was thus not strictly non-stoichiometric.

2. Possible Non-Stoichiometric Structural Defects in Rutile

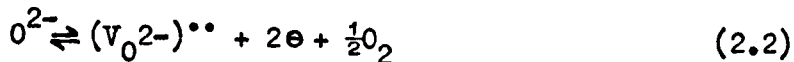
Departure from the stoichiometric composition occurs in rutile by a reversible process, and hence can be represented by a defect equation of the type:



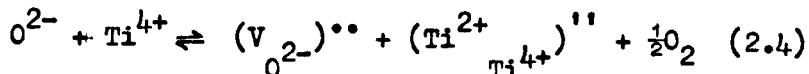
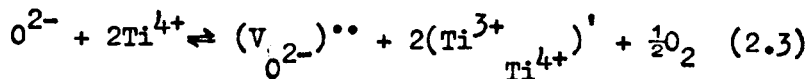
where \ominus represents an electron. The equation is incomplete, however, since the formation of vacant oxygen (anion) sites in the rutile lattice must also be included. It is to be expected that the electrons will associate themselves with either the anion vacancies or the cations, and the formation of all possible types of imperfection in rutile, of non-stoichiometric composition, can be described by means of defect reactions. Some of these reactions are given below, and in them the imperfections, etc., are described in terms of the ionic notation* used by Kroger and Vink⁽²¹⁾.

If the two electrons remain free in the conduction band of the crystal:

* For details of this and other notations, see Appendix I.



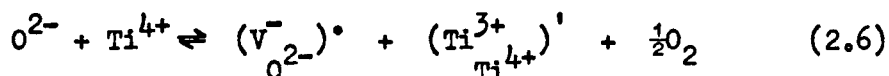
Some of the Ti^{4+} ions could be converted to either Ti^{3+} or Ti^{2+} ions, according to:



If the two electrons remain associated with an anion vacancy:



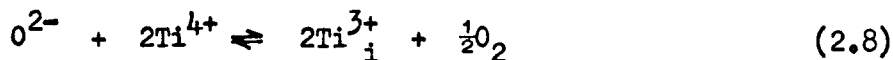
Alternatively Ti^{3+} ions and anion vacancies with a single associated electron could be formed:



In these reactions the Ti^{3+} and Ti^{2+} ions are represented as remaining at normal Ti^{4+} lattice sites, but there is a possibility that ions move to interstitial positions. The general reaction for the creation of this type of imperfection is, according to Hurlen⁽²²⁾:



If only interstitial trivalent ions are formed:



In defect reaction (2.7) n is an integer of value between

nought and four only.

By application of the law of mass action to these equilibria, the relationship between the equilibrium concentrations of the various imperfections can be obtained. As an illustration let us consider equation (2.3). If the concentrations of the various reactants are denoted by [], and the concentration of oxygen in the gaseous phase is expressed⁽²¹⁾ in terms of its equilibrium partial pressure, P_{O_2} , then

$$\frac{\left[\left(\frac{Ti^{3+}}{Ti^{4+}} \right)' \right]^2 \cdot \left[(v_{O^{2-}})^{\bullet\bullet} \right]}{\left[Ti^{4+} \right]^2 \cdot \left[O^{2-} \right]} \cdot P_{O_2}^{\frac{1}{2}} = \text{constant}$$

Now if the departure from stoichiometric composition is small, then the formation of a small number of Ti^{3+} ions and O_v will not affect, to a first approximation, the overall concentration of Ti^{4+} and O^{2-} ions in the crystal⁽²¹⁾. Thus:

$$\left[\left(\frac{Ti^{3+}}{Ti^{4+}} \right)' \right]^2 \cdot \left[(v_{O^{2-}})^{\bullet\bullet} \right] \cdot P_{O_2}^{\frac{1}{2}} = \text{constant} \quad (2.9)$$

As two Ti^{3+} ions are formed for every oxygen vacancy,

$$\left[\left(\frac{Ti^{3+}}{Ti^{4+}} \right)' \right] = 2 \left[(v_{O^{2-}})^{\bullet\bullet} \right] \quad (2.10)$$

On substitution of (2.10) in (2.9)

$$\left[(v_{O^{2-}})^{\bullet\bullet} \right]^3 \cdot P_{O_2}^{\frac{1}{2}} = \text{constant}$$

$$\text{i.e. } \left[(v_{O^{2-}})^{\bullet\bullet} \right] \propto P_{O_2}^{-1/6} \quad (2.11)$$

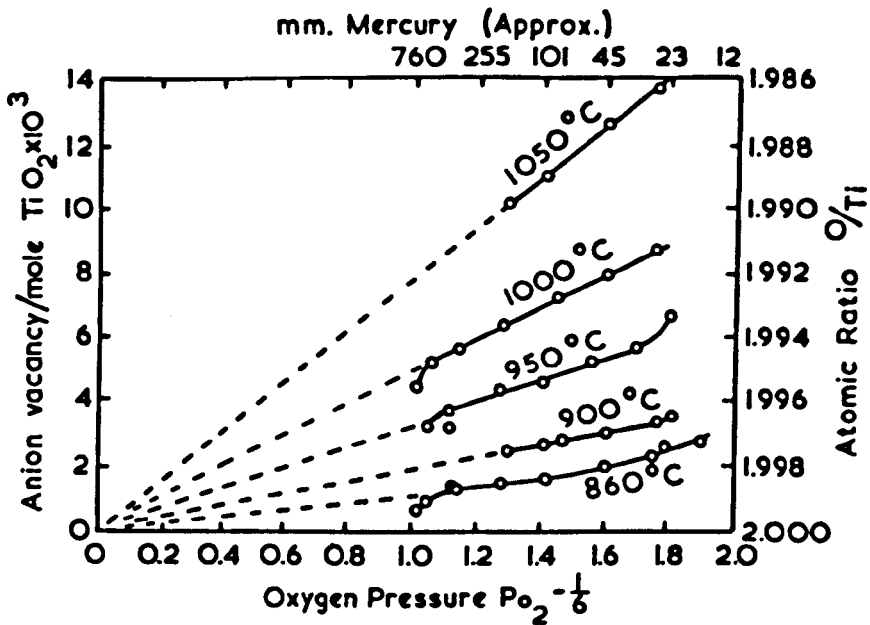


Fig. 4. Dependence of the concentration of oxygen (anion) vacancies in rutile on the pressure of oxygen (after Buessem and Butler⁽¹⁹⁾).

Thus on departure from the stoichiometric composition, the concentration of vacant oxygen lattice sites, in a sample of rutile, should be proportional to the inverse one-sixth power of the oxygen pressure in equilibrium with the sample.

By treating the other reactions in a similar way, it can be shown that for

$$\text{Equation (2.2), } [(V_{O_{2-}})^{\bullet\bullet}] \propto P_{O_2}^{-1/6} \quad (2.12)$$

$$\text{Equation (2.4), } [(V_{O_{2-}})^{\bullet\bullet}] \propto P_{O_2}^{-1/6} \quad (2.13)$$

$$\text{Equation (2.5), } [V_{O_{2-}}^{2-}] \propto P_{O_2}^{-1/2} \quad (2.14)$$

$$\text{Equation (2.6), } [(V_{O_{2-}})^{\bullet}] \propto P_{O_2}^{-1/4} \quad (2.15)$$

$$\text{Equation (2.7), } [(V_{O_{2-}})^{\bullet\bullet}] \propto P_{O_2}^{-1/n + 1} \propto \Theta \quad (2.16.1)$$

$$\text{Equation (2.8), } [Ti_i^{3+}] \propto [(V_{O_{2-}})^{\bullet\bullet}] \propto P_{O_2}^{-1/4} \quad (2.16.2)$$

In one sample of rutile, the number of oxygen (anion) vacancies per mole has been found⁽¹⁹⁾ to depend on $P_{O_2}^{-1/6}$ - see Fig. 4. However, as this indicated the formation of either Ti^{3+} ions or free electrons (equations 2.3 and 2.2) other data had to be consulted before a decision could be made as to the exact nature of the imperfections. Expressions for the equilibrium constants of reactions (2.2) and (2.3) were derived, and on substituting experimental enthalpy data, values for the two equilibrium constants were obtained⁽¹⁹⁾. Comparison of these

values with the value obtained by experiment indicated that imperfections of the type given by equation (2.3), i.e. Ti^{3+} ions, were formed.

Assayag et al.⁽¹¹⁾, on the other hand, have found that the concentration of oxygen vacancies in another sample of rutile was proportional to $P_{O_2}^{-1/5}$. Since this power of the oxygen pressure does not correspond to any of those calculated from equations (2.2) to (2.8), it suggests that possibly more than one type of imperfection is formed.

It is evident, therefore, that a study of the dependence of the concentration of oxygen vacancies on the equilibrium pressure of oxygen can only give an indication of the most probable types of imperfection existing in rutile of non-stoichiometric composition. Their exact nature is more likely to be found by consideration of the effects of departure from the stoichiometric composition on the physical properties of rutile.

3. Physical Property Data

3.1 Electrical Conductivity

If the bonding in rutile were entirely ionic, then it would be an insulator when of the stoichiometric composition, and would be an ionic conductor if defects such as vacant anion sites were present. The room temperature resistivity of stoichiometric

rutile is about 10^{13} ohm cm⁽²³⁾, but on applying an electric field electronic, not ionic, conduction takes place^(23,24) since a current can be passed for hours through a specimen of rutile without any chemical separation of cation and anion taking place. The intrinsic conductivity σ , in $(\text{ohm cm})^{-1}$, of rutile, resulting from the excitation of electrons from the filled valency band to a conduction band, has been found to depend on temperature (T , °K) and crystal direction in the following way⁽²³⁾:

Direction perpendicular to the c axis:

$$623 - 1123^{\circ}\text{K}: \quad \ln \sigma = 7.92 - 17,600/T \quad (2.17)$$

$$1123 - 1673^{\circ}\text{K}: \quad \ln \sigma = 11.10 - 21,200/T \quad (2.18)$$

Direction parallel to the c axis:

$$773 - 1223^{\circ}\text{K}: \quad \ln \sigma = 8.43 - 17,600/T \quad (2.19)$$

$$1223 - 1673^{\circ}\text{K}: \quad \ln \sigma = 11.30 - 21,200/T \quad (2.20)$$

In both cases the activation energies for conduction at low and high temperatures were 1.53 and 1.84 eV respectively. Few details were given of the experimental procedures used, and unless the measurements were made in an atmosphere of oxygen, the test samples may well have assumed a non-stoichiometric composition above 1123°K (850°C). However, using the low temperature value of the activation energy (1.53 eV), the energy gap between the filled valency and the conduction band was computed to be about 3.05 eV. This value lies between the limits of 1 and 7 eV which are typical values of the width of the energy gap of an intrinsic

semi-conductor on the one hand, and an insulator such as diamond on the other⁽²⁵⁾. Before, however, discussing the energy band structure of rutile in more detail we must first consider other physical properties of the material.

Since the electrical conductivity of an intrinsic semi-conductor, besides being strongly dependent on temperature, is also affected by physical structure and chemical composition⁽²⁶⁾, it is to be expected that the conductivity of rutile will change when it departs from the stoichiometric composition. This has already been shown to occur by loss of oxygen from the lattice, and leads to the production of two electrons per oxygen vacancy in the material, according to equation (2.1). The presence of these electrons will result in further electronic energy levels being introduced above the valency band, and hence can be expected to lead an increase in conductivity since electrons in these extra levels can be excited more easily into the conduction band. Breckenridge and Hosler⁽²⁷⁾ have shown that after a 15 minute reduction in hydrogen at 600°C, the resistivity of a single crystal of rutile falls to about 10 ohm cm, and the material behaves like an n-type semi-conductor. Its conductivity could be further enhanced by increasing the time or temperature of reduction, since both processes lead to a greater departure from stoichiometric composition and thus to an increase in the number of electrons in

bound states which give rise to energy levels lying between the valency and conduction bands. The energy separation between these levels and the conduction band has been calculated, by combining the above conductivity data with Hall coefficient data obtained from similar non-stoichiometric specimens.

The anisotropy of the conductivity of single crystals of rutile arises from the low crystallographic symmetry of the tetragonal unit cell of the rutile structure ($c/a \neq 1$). As a result of a detailed study of the change in the anisotropy in rutile, arising from departures from the stoichiometric composition, it has been found^(28,29) that as the concentration of oxygen vacancies increases, the wave functions of their associated electrons begin to overlap and form an energy band. Furthermore it was shown that this occurs first in the c direction and then later in the a direction. However, the concentrations of oxygen vacancies in the various specimens was unknown, so the precise compositions at which these overlaps occur are not known. Moreover, the possibility exists that the specimens may have consisted of two oxide phases.

It is to be expected that the conductivity of a sample of rutile will be dependent on the pressure of oxygen surrounding the sample, since equations (2.11) to (2.16) in Section 2 can equally well be expressed in terms of the number of electrons

present in non-stoichiometric rutile, rather than the number of oxygen vacancies. The only data available^(24,30) of this effect has been obtained from measurements made on rutile in the form of powder that has been compressed and subsequently sintered at a high temperature, the density of the sintered compact being about 90% of that of a single crystal of rutile. Earle⁽²⁴⁾ found that the conductivity (σ) depended on the pressure of oxygen (P_{O_2}) according to the following relationships:

$$\ln \sigma = A - B \ln P_{O_2} \quad (2.21)$$

The constant B was found to be both temperature and pressure dependent, having values between $\frac{1}{4}$ and $\frac{1}{2}$, and from these numerical values Earle concluded that Ti^+ ions were formed in non-stoichiometric rutile. This conclusion is rather strange since titanium rarely, if at all, forms ions in the +1 valence state. A relationship similar to (2.21) was found by Hauffe et al.⁽³⁰⁾, but B fell within the limits $\frac{1}{4.4}$ to $\frac{1}{5.3}$. These numerical values are considered to indicate the formation of Ti^{3+} ions either at normal lattice sites⁽¹⁹⁾, or in interstitial positions⁽²²⁾.

The wide range of values reported for the value of the constant B in equation (2.21), and hence for the type of defects present in non-stoichiometric rutile, probably arises from differences both in the purity of the rutile powder used for the specimens, and in the state of aggregation of the latter. Great

care must be exercised when interpreting physical property data obtained from sintered powder compacts⁽³¹⁾. The main objections⁽³¹⁾ to the use of this type of material are that the specimens are rarely free of voids, and that powder particles are generally covered by a surface layer whose electrical properties are significantly different to those of the interior. These surface effects can control the electrical properties of the sintered powder compact, and so mask or modify the true properties of the material.

In none of the studies mentioned above was the composition of the material under test known, so that, as yet, changes in the conductivity of rutile cannot be correlated with its composition.

3.2. Hall Coefficient

The change in Hall coefficient with temperature has been studied⁽²⁷⁾ in both sintered compacts and single crystals of rutile, made non-stoichiometric i.e. semi-conducting by reduction in hydrogen.

By combining the Hall coefficient data with the results of electrical conductivity measurements on similar samples, the number and mobility of the charge carriers (shown to be electrons) in the various samples were calculated. The mobility of the conduction electrons was extremely low, between 0.1 and 10 cm²/volt sec., which with the anomalously high effective electron mass

Table III

Source	Temperature	Susceptibility 10^{-6} e.m.u./gm
Leyer (32)	230°K	0.37
Wedekind (33)	room	0.066
Berkman (34)	room	-0.20
Hüttig (35)	room	-0.30
Raychaudhuri (36)	0.073
Ehrlich (10)	90 and 293°K	0.02
Zimms (37)	0.134
Hill (38)	-0.3
Reyerson (39)	301°K	0.061
Gray (40)	room	0.075
Senftle (41)	55 to 272°K	0.067

Values reported for the magnetic susceptibility of rutile (after Senftle et al. (41)).

(between 30 and 130 times the free electron mass) are probably indicative of a very narrow conduction band. The variation in the number of conduction electrons with temperature was interpreted⁽²⁷⁾ in terms of two types of donor centre, in one of which the electrons have a very small activation energy for excitation into the conduction band. This implies that some centres would be ionized even at low temperatures. The two donor centres were suggested⁽²⁷⁾ to be oxygen ion vacancies with either one or two associated electrons, which may be considered as being trapped as Ti^{3+} ions.

3.3 Magnetic Susceptibility

Many values for the magnetic susceptibility of rutile have been reported in the literature, see Table III. The lack of consistency in the values must be attributed to the range of impurity contents and departures from the stoichiometric composition of the materials used. The most reliable value of those presented in Table III is probably $+0.067 \times 10^{-6}$ e.m.u./gm obtained by Senftle et al.⁽⁴¹⁾, since the purest available form of rutile was used, and extreme care was taken to eliminate departure from the stoichiometric composition and presence of absorbed water vapour. The susceptibility was found to have an almost negligible temperature coefficient between 55 and 372°K⁽⁴¹⁾.

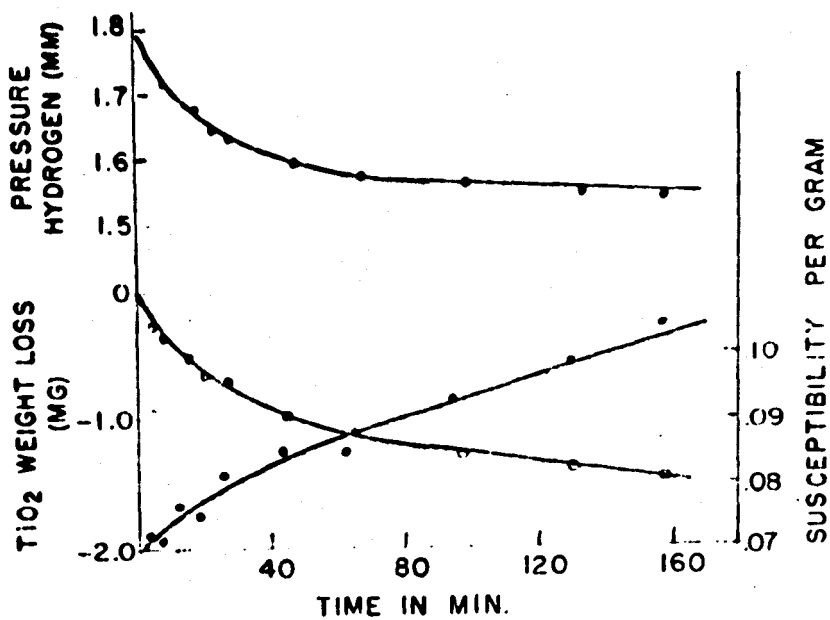


Fig. 5. Change of Hydrogen pressure, sample weight and paramagnetic susceptibility during the surface reduction of rutile (after Gray⁽⁴³⁾).

If the bonding in rutile were purely ionic it would not be expected to exhibit paramagnetism (positive susceptibility), since it would be composed of ions having completely filled outer electronic levels, which would lead to a temperature-independent, diamagnetic (negative) susceptibility^(42,25,26). As mentioned earlier (see Section 1.2), however, it has been shown that there is probably a considerable covalent contribution to the crystal bonding in rutile, and this is thought^(4,42) to be partly responsible for its observed paramagnetic susceptibility. The precise origins of the latter are considered⁽⁴²⁾ to be rather difficult to define.

The paramagnetic susceptibility of rutile increases on departure from the stoichiometric composition, owing to the formation of Ti^{3+} ions. These ions are paramagnetic^(10,40,41,42) since they contain a single electron in their outermost electronic level. Gray et al.⁽⁴³⁾ have directly correlated the increase in susceptibility of a sample of rutile with its change in weight on reduction in hydrogen, see Fig. 5. The data is not truly representative of the properties of non-stoichiometric rutile, however, since the surface of the samples was reduced to a greater extent than the interior. Furthermore, the material used in this investigation contained anatase (the other tetragonal modification of TiO_2 , $c/a > 1$), the presence of which can lead to erroneous values for the susceptibility (anatase has a susceptibility of $+0.02 \times 10^{-6}$ e.m.u./gm⁽⁴¹⁾).

The magnetic susceptibilities of samples of rutile in the composition range from $\text{TiO}_{1.97}$ to $\text{TiO}_{1.9}$ have been measured by Ehrlich⁽¹⁰⁾. The number of electrons per mole of sample contributing to the susceptibility - calculated on the assumption that the magnetic electrons were associated with Ti^{3+} - were always found to be less than the total number of such electrons that would be expected to have formed, as a result of the known oxygen deficiency. This agrees with the view of Breckenridge and Hosler⁽²⁷⁾ who consider that besides Ti^{3+} ions, oxygen vacancies with associated electrons are also present in rutile of non-stoichiometric composition. Such electrons would not be expected to make a large contribution to the paramagnetic susceptibility of the material⁽²⁵⁾.

3.4 Dielectric Constant

The dielectric constants of rutile of stoichiometric composition are 89 and 173 in the a and c directions respectively^(44,45). The dielectric constant of sintered compacts of rutile is approximately 100^(46,47), and decreases with increasing temperature⁽⁴⁸⁾. The values of the dielectric constant have been found to have only a slight dependence on the frequency of the applied electric field up to at least several hundred megacycles per sec^(46,47). In fact no large dependence on frequency would be expected⁽⁴⁹⁾ unless the frequency of the applied field could be increased to a value that

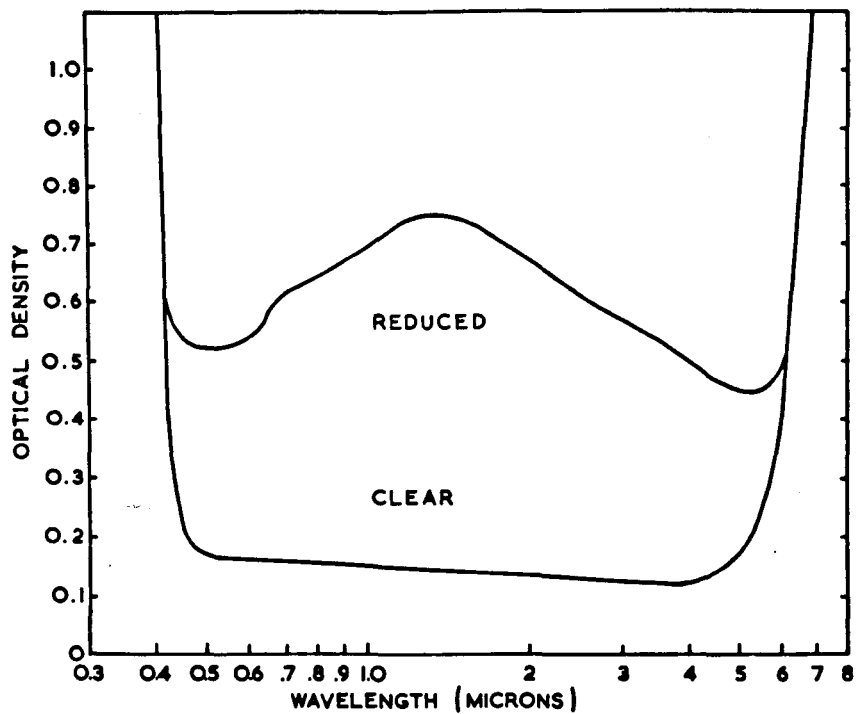


Fig. 6. Optical density of stoichiometric (clear) and non-stoichiometric (reduced) rutile. Graph compiled from data reported by Breckenridge and Hosler⁽²⁷⁾.

approached the natural frequency of vibration of the ions in the lattice, i.e. 10^6 to 10^7 megacycles per sec.

Departures from the stoichiometric composition have been found to cause the dielectric constant of rutile to become dependent on the frequency of the applied field^(44,50). Using a low frequency method of measurement, the dielectric constant of non-stoichiometric rutile was shown⁽⁵⁰⁾ to increase as the number of defects increases, but no details were given of the reduction treatment. It has been reported^(51,52) that the defects in rutile are anisotropic, since their effect on the dielectric constant could only be detected with the applied field in the c direction. In none of these studies, however, has the composition of the material been determined - only some arbitrary reduction treatment has been given.

3.5 Optical Absorption

Stoichiometric rutile does not exhibit any marked absorption of light in the visible region (see Fig. 6), but at $4,100 \text{ \AA}$ there is a sharp absorption edge^(23,53,27). Soffer⁽⁵⁴⁾ has carefully examined the absorption spectrum of single crystals of rutile in the near infrared region, and found that there is a narrow band at 0.4 eV, which was identified as arising from the presence of hydroxyl, OH^- , groups in the rutile lattice. Such a

conclusion is not surprising, since single crystals of rutile are prepared⁽⁵⁵⁾ by the Verneuil⁽⁵⁶⁾ flame-fusion process, the basis of which is to drop powder through an oxy-hydrogen flame. The hydrogen diffuses out of the rutile lattice when heated to temperatures above 800°C either in vacuo or an atmosphere free of both hydrogen and water vapour⁽⁵⁴⁾. In this respect Soffer considers that rutile is an excellent scavenger of hydrogen and water vapour, since only small concentrations of these gases are necessary to give rise to the characteristic absorption band of the hydroxyl group in rutile.

The presence of the hydroxyl group, not only in stoichiometric single crystals of rutile but also in material reduced in hydrogen - a reducing agent commonly used to promote non-stoichiometry in rutile^(23,27,40) - will have to be taken into consideration when interpreting physical property data of rutile^(57,58).

Departures from the stoichiometric composition lead to light absorption in the visible region, due to the formation^(27,59) of a broad absorption band centred in the infrared at about 17,000 Å (0.73 eV) - see Fig. 6 - giving rise to the characteristic blue-grey colour of reduced rutile. As the departure from the stoichiometric composition increases, the peak at 0.73 eV suddenly gives way⁽⁵⁹⁾ to a larger peak at 1.18 eV, at a composition corresponding to a sample resistivity of about 4 ohm cm. It has

been suggested⁽⁵⁹⁾ that these peaks correspond to the ionisation of the first and second electrons from the oxygen vacancies. Furthermore, that the thermal activation energy of ionisation of one of the electrons from the vacancy has fallen to zero when the composition reaches about $\text{TiO}_{1.997}$, so that below this composition oxygen vacancies having two associated electrons are not present as imperfections in non-stoichiometric rutile.

3.6 Density

The density of rutile of stoichiometric composition is 4.2496 gm per cu.cm at 25°C⁽¹³⁾. Straumanis et al.⁽¹³⁾ have reported that the density of rutile decreases when departure from the stoichiometric composition occurs, falling to 4.2356 gm/cc (at 25°C) at the limit of the single phase region i.e. $\text{TiO}_{1.983}$.

From the data given by these workers the rate of decrease of density with composition can be calculated, and is -0.83 gm/cc/anion vacancy/molecule TiO_2 . Prener⁽⁶⁰⁾, on the other hand, using high precision density measurements has shown that the density increases with increasing non-stoichiometry, at a rate of +0.34.

This confliction in the variation of the density of non-stoichiometric rutile may arise from differences in the forms of the specimens used for the density determinations. The former workers used powders, which can lead to erroneous values of density due to the presence of minute air bubbles adhering to the particles of powder.

Prener used single crystal specimens, which are more likely to give correct values, but unfortunately no details are available as to the accuracy with which the sample composition was known. There is obviously a need for a re-investigation of the effect of departure from the stoichiometric composition on the density of rutile.

3.7 Coefficient of Thermal Expansion

The coefficients of thermal expansion have been calculated from X-ray data to be 6.9 and 9.9 ($\times 10^{-6}/^{\circ}\text{C}$) in the a and c directions respectively⁽¹³⁾.

It has been reported⁽⁶¹⁾ that the coefficient in the c direction changes from 9.2 to 10.5 ($\times 10^{-6}/^{\circ}\text{C}$) when the composition of rutile is altered from TiO_2 to $\text{TiO}_{1.97}$. Straumanis et al.⁽¹³⁾, however, have found no systematic change in their values for the coefficient of thermal expansion, at least up to the limit of the single-phase region i.e. $\text{TiO}_{1.983}$. The value of $10.5 \times 10^{-6}/^{\circ}\text{C}$ reported above may represent the coefficient of thermal expansion of a two-phase sample.

Up to the present time no direct measurements of the coefficient of the thermal expansion have been made on a specimen of rutile.

4. Band Structure of Rutile

Below 1123°K the forbidden energy gap between the valency and conduction bands has been found⁽²³⁾ to be 3.05 eV. The conduction band in rutile is considered^(62,63) to be of the same type as that in the other oxides of titanium, and in the oxides of the closely related element vanadium. In these compounds a conduction band is formed as a result of the overlap of the 3d-electrons from adjacent cations. In rutile of stoichiometric composition, this 3d-conduction band is, of course, empty since the Ti^{4+} ion has no 3d-electrons.

Above 1123°K the width of the energy gap increases by over 0.6 eV, to 3.67 eV⁽²³⁾, and Morin⁽⁶²⁾ has suggested two reasons for this increase. Either the 4s-band in rutile is situated 0.6 eV above the 3d-band, so that at high temperatures transitions occur between the valency and 4s-bands, or the 3d-band consists of two sub-bands, spaced 0.6 eV part. Morin⁽⁶²⁾ considers, however, the second explanation to be the most likely, and Goodenough⁽⁶³⁾ supports this view, because it has been shown⁽⁶⁴⁾ that the fivefold degeneracy⁽⁶⁵⁾ of the 3d-electronic level of a free atom is removed when the atom forms a solid compound, by the 3d-level splitting into two, more stable, states.

It is interesting and perhaps significant, to note that the energy gap increases in the temperature range where rutile

begins to lose oxygen, when in vacuo or under low pressures of oxygen. In the absence of experimental details regarding the atmosphere in which the measurements⁽²³⁾ of electrical conductivity (used for the computation of the energy gap) were made, it cannot be assumed that the specimens remained stoichiometric.

When departures from the stoichiometric composition occur in rutile, Ti^{3+} ions are formed and, as they contain one 3d-electron, the conduction band contains a small number of electrons. The low mobility and high effective mass⁽²⁷⁾ of these electrons indicate that the 3d-conduction band is exceedingly narrow. This is to be expected since the large separation of the cations in the oxides of the transition metals will result in only a small overlap of the 3d-electrons^(62,63,66). In addition two energy levels are introduced in the energy gap between the valency and conduction bands, owing to the creation of oxygen vacancies with one or two associated electrons. As the concentration of oxygen vacancies increases, only oxygen vacancies with one associated electron exist⁽⁵⁹⁾, and the energy level corresponding to this defect gives rise to a further conduction band^(4,23,59,62,67) situated about 0.015 eV below the 3d-conduction band⁽⁶⁷⁾.

5. Imperfections in Non-Stoichiometric Rutile - Conclusion

It is evident from the data presented above that several types of imperfection may well be present in rutile of non-

stoichiometric composition, and not just Ti^{3+} ions and oxygen vacancies as suggested by Buessem and Butler⁽¹⁹⁾. However, as the latter workers used material of only 99% purity, it is possible that the nature of the defect structure of non-stoichiometric rutile can be modified by the presence of impurity atoms.

By combining the results of various workers it appears that the following imperfections are formed in rutile, when departures from the stoichiometric composition occur: Ti^{3+} ions, oxygen vacancies, and oxygen vacancies with one or two associated electrons. Below a composition of $\text{TiO}_{1.997}$, oxygen vacancies with two associated electrons are not considered⁽⁵⁹⁾ to exist. The concentrations of each type of imperfection present at a specific composition are expected to alter with temperature, as well as with composition. No data concerning these effects are yet available; that obtained by Ehrlich⁽¹⁰⁾ - see section 3.3 - was for rutile of composition $\text{TiO}_{1.97}$ - $\text{TiO}_{1.90}$, which may be in the two-phase region.

There is considerable disagreement regarding the position that the Ti^{3+} ions occupy in the lattice, the two main views being that the Ti^{3+} ions are either at normal cation lattice sites^(13,19,41), or in interstitial positions⁽²²⁾. The former view is perhaps the most obvious, and much of the evidence is in its favour. Furthermore, Chester⁽⁵⁸⁾ has shown from electron spin resonance

studies of rutile that interstitial Ti^{3+} ions can only be detected in samples of rutile which have been reduced in hydrogen. Defects of this type cannot be detected in samples that have been reduced in vacuo. Since the former type of reduction treatment is far more severe than the latter, it is conceivable that samples of rutile reduced in hydrogen may contain two phases. This view gains support from observations⁽¹²⁾ of the X-ray diffraction patterns of rutile with a composition less than $TiO_{1.96}$, which indicate that the crystal structure consists of planes of interstitial ions in a pseudo-rutile structure.

It is evident, therefore, that the exact nature of the defect structure of non-stoichiometric rutile is rather confused. Much of the confusion has undoubtedly arisen because some of the data has been obtained from material reduced to such an extent that it contains two phases. In this respect it is far better to control the reduction of rutile using oxygen at reduced pressure, since conditions then prevail which completely define⁽⁶⁸⁾ a non-stoichiometric compound.

6. The Present Investigation

It would appear to be impossible, from the existing data, to derive any consistent picture of the exact nature and number of imperfections produced in rutile when departures from the stoichiometric composition occur. Results so far obtained do, however, indicate that striking changes in the physical properties

of this material can take place as a result of its defect structure, whether this be caused by oxygen deficiency or impurity content. Before the details of these effects can be elucidated satisfactorily it will be necessary to carry out much systematic work on specimens of rutile which have been very carefully prepared from pure materials. The object of the present work is to initiate this type of protracted study.

In the present investigation it is intended that a study shall be commenced of departures from the stoichiometric composition on some of the physical properties of rutile, using material of very high purity (99.99%)*, so that the effects of impurities will be small. Initially the composition of this material, in the as-received powdered form, will be studied as a function of temperature and oxygen pressure, in order to determine the form of the dependence of the concentration of oxygen vacancies on the pressure of oxygen. It will then be possible to obtain some indication of the nature of the imperfections present, using the equations discussed in section 2. It will also be of interest to compare the type of oxygen-pressure dependence of the vacancies in this high-purity material with that obtained by other workers using less pure material.

Once the composition of the material is known as a function of temperature and oxygen pressure, it will then be possible to

*The author is indebted to the Research Manager, British Titan Products Ltd., Billingham, Co. Durham for supplying this material and also details of its purity.

interpret any physical property data obtained from the material in a more logical manner than has hitherto been achieved.

III APPARATUS AND EXPERIMENTAL PROCEDURES

1. General Considerations

A variety of methods have been used to determine the composition of samples of non-stoichiometric rutile, some of which are discussed briefly below. No fundamentally new method was envisaged for the present investigation, so a method was chosen that was most easily adaptable to a high sensitivity.

1.1. Chemical Methods

The oxygen:titanium ratio in a sample of rutile can be determined by chemical analysis, with an accuracy of "one milliatom of oxygen ($\pm 10\%$) per molecule of material".⁽⁶⁹⁾ The basis of the method is to dissolve, under vacuo, part (about 0.25 gm) of the sample of rutile in sulphuric acid containing an excess of ferric sulphate. Any Ti^{3+} ions present in the sample convert an equivalent number of ferric (Fe^{3+}) ions to ferrous (Fe^{2+}) ions, and the concentration of the latter in the solution is determined by titration with potassium permanganate.

The main disadvantages with the method are that it is destructive, that parasitic oxygen can cause spurious effects and that only the concentration of Ti^{3+} ions in the material is determined. It has already been shown that the concentration of these ions in a non-stoichiometric sample of rutile need not be equal to twice the

concentration of anion vacancies, since various types of defect may be formed. Thus the method does not give the exact oxygen:titanium ratio. A further disadvantage arises when the sample is in the form of a single crystal, since in order to dissolve the crystal it has to be first fused with sodium carbonate at 950°C for 3 hours. During this process it is assumed that the composition of the material does not vary.

In addition to the above disadvantages, a further one arises owing to the fact that the analyses have to be made on material quenched from the reaction conditions. Errors can be introduced by using material of this type, since there is no control over compositional changes that occur during the time of quenching⁽²¹⁾. In general, therefore, methods involving the use of quenched material are to be avoided.

The composition of non-stoichiometric rutile can be controlled at any desired value by heating a specimen of rutile in carbon monoxide⁽¹¹⁾, or a mixture of hydrogen and water vapour⁽²⁰⁾. The composition of the sample and the equilibrium pressure of oxygen corresponding to this composition can then be determined by (i) measuring the amounts of carbon dioxide and water vapour formed, and (ii) using the values found in conjunction with the known equilibrium constants of the $\text{CO} - \text{CO}_2$ and $\text{H}_2 - \text{H}_2\text{O}$ (vapour) reactions. Both methods, however, use rather noxious

gases which have to be circulated in a closed system. The $H_2 - H_2O$ (vapour) method has recently been used to study departures from the stoichiometric composition in zirconia⁽⁷⁰⁾, an accuracy of ± 0.0005 atoms of oxygen per molecule of ZrO_2 being obtained. However, for a fixed value of the partial pressure of oxygen surrounding the sample, the resulting composition was dependent on the rate of flow of gas over the sample.

On the whole, therefore, it appears that the above methods are not sufficiently accurate or reliable for the present investigation.

1.2 Physical Methods

The composition of a sample of rutile can be calculated from its density, assuming the volume of the unit cell of rutile remains constant as departures from the stoichiometric composition occur⁽¹³⁾. However, opinions differ as to whether the volume of the unit cell does remain constant, due to conflicting reports on the effect of non-stoichiometry on the density of rutile (see Sec. 3.6 above). Under these circumstances it appears inadvisable to consider this method. In addition, if the use of quenched materials is to be avoided, then the density measurements would have to be made immediately after subjecting a specimen of rutile to the specified conditions and at the same temperature. This would create practical difficulties, however, since the medium in the system would have to be changed to one suitable for the determination

of density^(71,72), without altering the composition of the sample.

The composition of a sample of non-stoichiometric rutile can be determined by calculating the number of molecules present in the unit cell⁽¹³⁾. X-ray measurements of the latter are normally made at room temperature, so that quenched samples are normally used for this type of work. In order to overcome this disadvantage, the X-ray measurements of the unit cell would have to be made simultaneously at a high temperature and in a controlled atmosphere, both of which involve considerable practical difficulties.

A change in the oxygen content of a sample of rutile results in a change in its weight, so that departures from the stoichiometric composition can be determined by a weighing method. By enclosing a suitable balance in a closed system the weight of a sample of rutile could be determined continuously while the sample was subjected to the reaction conditions. A method of this type has been used to a limited extent with rutile^(19,73), and appears to be very attractive for the present investigation as it avoids the use of quenched material.

1.3 The Method Chosen for the Present Investigation

Of the methods discussed above, the one most readily adaptable to the determination of the composition of a sample of rutile, under controlled conditions, is that based on the weight of the sample. The most convenient way of accurately and

continuously weighing a sample in a closed system is to use a microbalance, since these instruments can be made extremely sensitive and, being small, can be easily installed in the closed system. For these reasons it was decided to use a microbalance to follow the changes in composition of a sample of rutile on heating it in oxygen at various pressures.

When the studies described in this thesis were started, commercial microbalances were not available in this country and so one had to be constructed. At a later date, however, a commercial microbalance of W. German manufacture, suitable for use in a high vacuum system, became available to the author, and was subsequently used to obtain most of the data presented in Part IV of this thesis. In view of this fact only a brief description will be given of the microbalance that was constructed by the author, after which the reasons for changing to the commercial instrument will be given.

2. The Quartz Microbalance

It was decided to construct a microbalance of the type described by Gulbransen⁽⁷⁴⁾, since instruments of this type had been used extensively for the study of oxidation⁽⁷⁵⁾, surface activity and surface gas absorption⁽⁷⁶⁾ of metals, both at high temperatures and in controlled atmospheres, i.e. conditions similar to those envisaged for the present investigation.

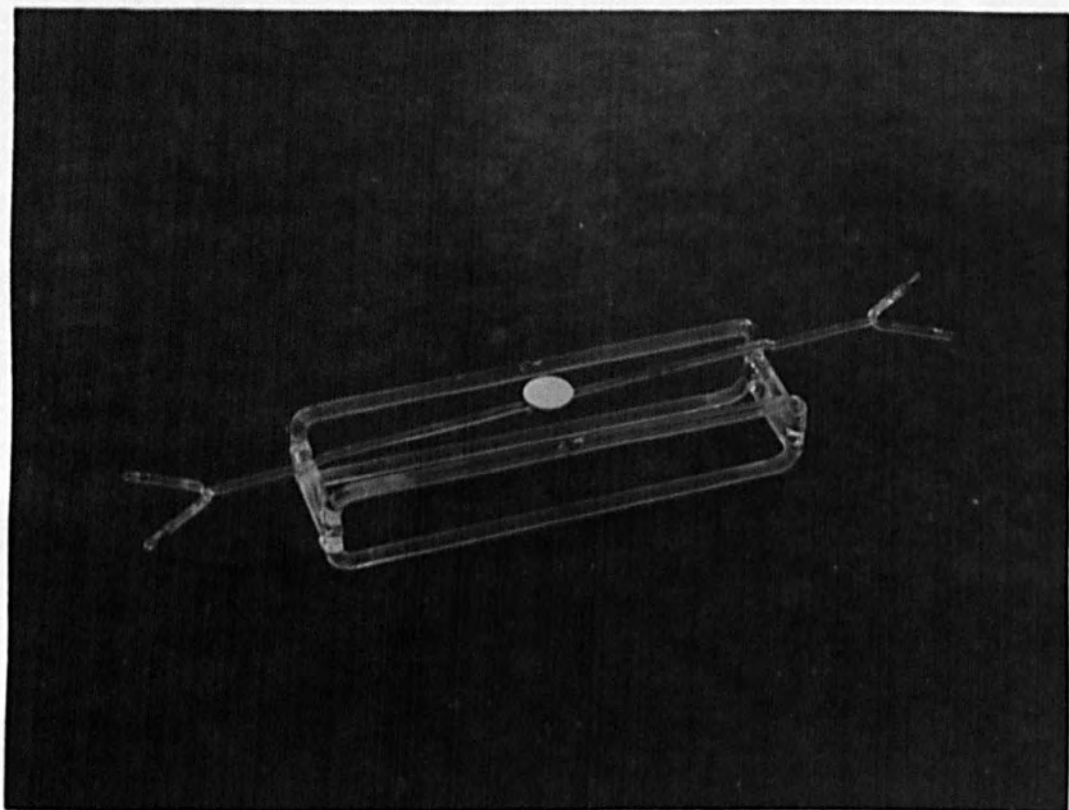


Fig. 8. A photograph of the quartz microbalance that was constructed (about three-quarters actual size).

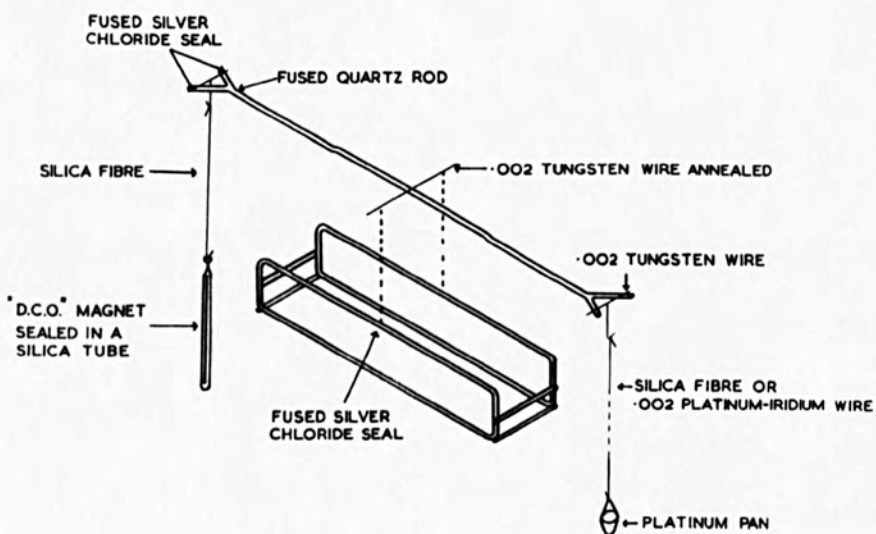


Fig. 7. Diagrammatic view of the Gulbransen-type microbalance.

2.1 Design and Construction

The design of the Gulbransen-type of microbalance is shown diagrammatically in Fig. 7, the shape and dimensions of the beam having been chosen⁽⁷⁴⁾ after detailed considerations of the expressions for the sensitivity, period etc., of a beam balance.

The beam and frame of the microbalance were constructed from fused quartz rod, chosen for its high strength/weight ratio and low coefficient of thermal expansion. The rod was manipulated to the required shape in an oxy-coal gas flame, with the aid of jigs machined from graphite. The beam was supported on an annealed tungsten wire (0.002" diameter) stretched across the frame (see Fig. 7) the wire being attached to the quartz using fused silver chloride seals. A tungsten wire was also fixed, using fused silver chloride seals, across the yokes at each end of the beam. At the mid point of each wire a small hook, fashioned from tungsten wire, was attached, again using a fused silver chloride seal. From these hooks the specimen and counter balance weight were suspended (see Fig. 7).

A photograph of a microbalance that has been constructed in this manner is given in Fig. 8.

2.2. Electromagnetic Balancing Arrangement

The beam was maintained in the balanced position by

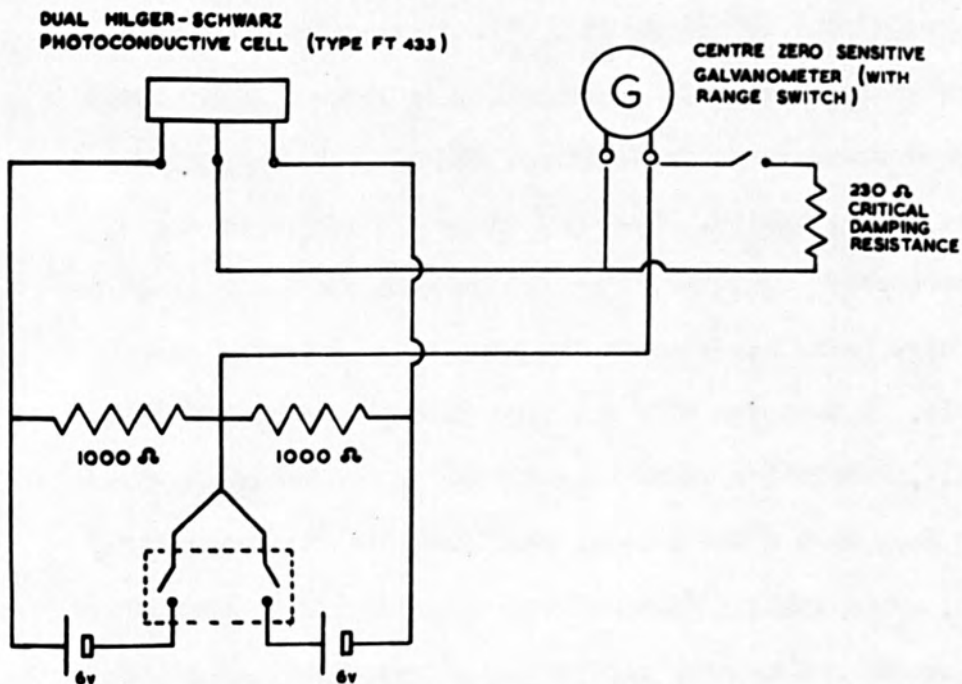


Fig. 10. The balance indicating circuit of the deflection-detection system.

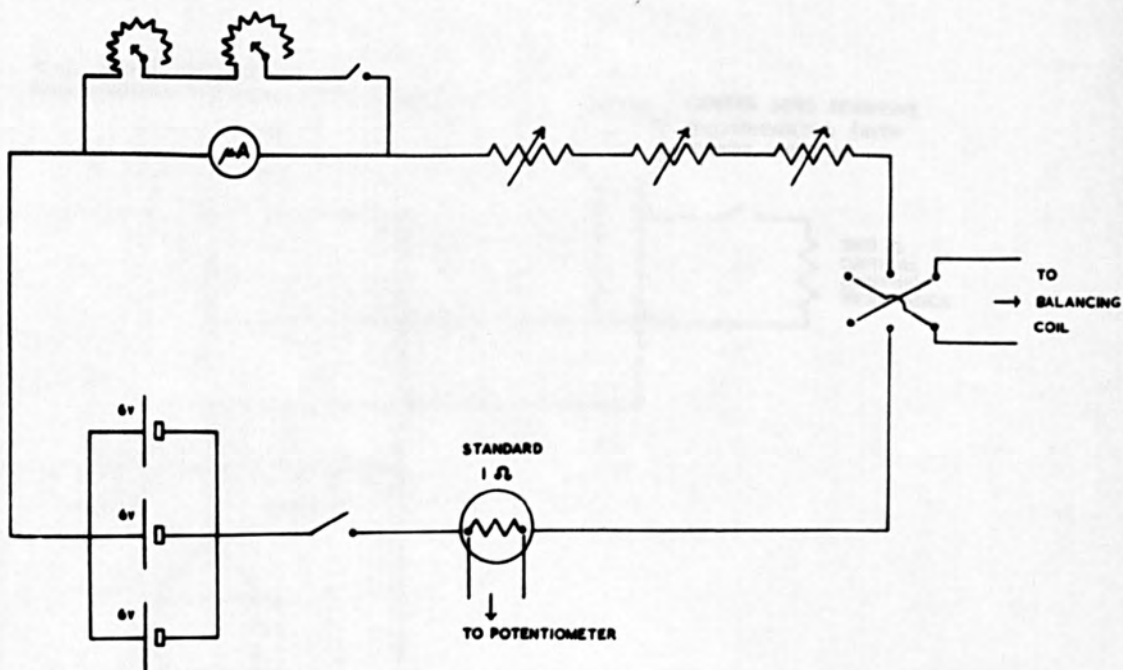


Fig. 9. Control circuit for the restoring coil.

attracting a small permanent magnet, suspended from the beam, with the magnetic field produced by a fixed coil of wire - the restoring coil - energised by an electrical current.

The magnet consisted of a piece of permanent magnetic wire, and was contained in an evacuated silica tube. It was suspended from the counterbalance arm of the beam of the microbalance by a silica fibre, see Fig. 7.

The restoring coil consisted of 1250 turns of 36 s.w.g. wire, wound on a brass former. The coil was clamped firmly around the tube surrounding the counterbalance weight (magnet), using three screws set into each end of the brass former, and was positioned such that the bottom of the magnet was located just inside the coil. Steady electrical power was supplied to the restoring coil by three 6 volt accumulators wired in parallel, and could be adjusted by a series of continually variable resistors (see Fig. 9).

2.3 Movement-Detection System

Deflections of the beam from the balanced position were detected using a photo-electric method. In essential this consisted of reflecting a beam of light from a mirror mounted on the beam of the microbalance, onto a dual photo-conductive cell. The two halves of the latter formed the active arms of an electrical bridge network, shown in Fig. 10, designed so that the two halves of the cell

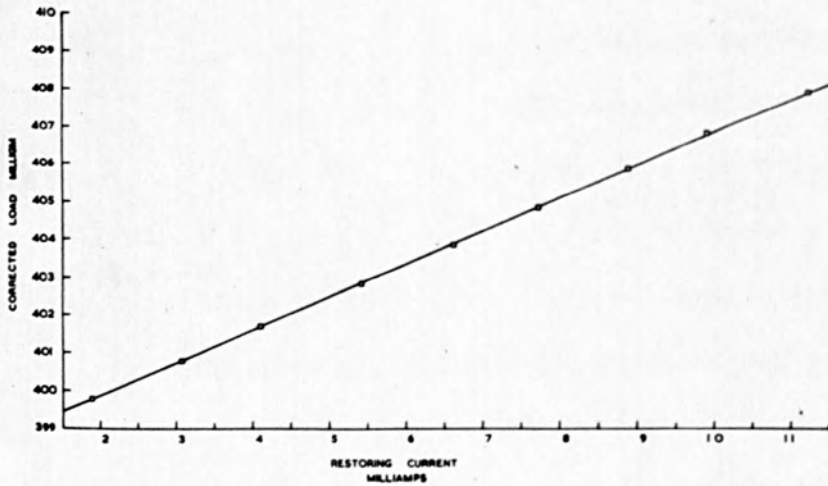


Fig. 11. Calibration curve of the quartz microbalance.

were maintained at a constant bias voltage of 6 volts, irrespective of their resistance. Movement of the beam of the microbalance resulted in the two halves of the photo-conductive cell being differentially illuminated, and hence for them to have unequal resistances. This unbalanced the bridge network and caused a current to flow through a galvanometer, G of Fig. 10, the reading of which gave a direct indication of the deflection of the beam.

2.4 Calibration

The microbalance was calibrated, in vacuo, using micro-chemical rider weights of known value. With a known load hanging from the specimen side of the beam of the microbalance, the current in the restoring coil was adjusted using variable resistors (see Fig. 9) until the galvanometer of the movement-detection system, G of Fig. 10, indicated that the beam was balanced or was oscillating about the mean position of balance. The current in the restoring coil was measured by determining the potential drop across a standard one ohm resistor, connected in the coil circuit (Fig. 9), with a potentiometer. The beam was rebalanced a number of times so that a mean value of the restoring current was obtained.

The calibration obtained in this way is shown graphically in Fig. 11. The calibration data was treated by a least squares analysis⁽⁷⁷⁾, and it was found that the load (y , in milligrams) depended on the restoring current (x , in milliamps) in the following

way:-

$$y = (0.867 \pm 0.003) x + (398.130 \pm 0.0243) \quad \dots \quad (3.1)$$

The sensitivity of the microbalance was, therefore, 0.867 milligram per milliamp. Since the current in the restoring coil could be reproduced, for a particular load, to within ± 0.01 milliamps, the weight of a specimen could be determined with a precision of $\pm 9 \times 10^{-6}$ gm.

3. Reasons for Abandoning the Quartz Microbalance

Although the weight of a specimen could be measured with a precision of $\pm 9 \times 10^{-6}$ gm, changes in weight could only be determined with an accuracy of $\pm 1.8 \times 10^{-5}$ gm, since the error involved when one reading is subtracted from another is twice the error in each reading⁽⁷⁷⁾. With a specimen weighing 0.5 gm this accuracy was equivalent to $\pm 1.8 \times 10^{-5}$ anion vacancies per molecule of specimen, and could have been tolerated for the reduction of rutile in vacuo, although a higher accuracy would have been preferred. However, the accuracy of the measurements would have been lowered even further when the system contained a gas, due to the fact that corrections would have to be made for the buoyancy of the specimen in the gas. Thus the accuracy with which changes in weight could be determined was rather low, especially as preliminary experiments had shown that only small departures from the stoichiometric composition occur in high-purity rutile. The calculated changes in

composition would, therefore, be subject to a large error.

In addition to the low accuracy of the microbalance, oscillations of the beam took over three hours to diminish to a small enough amplitude before a mean position of balance could be obtained. Such a period of time would have been excessively long when only short term experimental runs, of the type envisaged for the determination of a buoyancy correction, were carried out.

At this stage of the studies, however, the author was fortunate in being offered the use of a Sartorius Vacuum Electronic Microbalance*. The instrument had a guaranteed sensitivity of $\pm 10^{-6}$ gm, and had two very attractive features: (i) instantaneous automatic balancing of the beam, and (ii) electronic weight compensation, such that a total change in weight of 11 milligm. could be tolerated with an accuracy of $\pm 10^{-6}$ gm. The first of these features dispensed with manual balancing of the beam and the associated time period required for it to settle down - an unfortunate feature of the quartz microbalance described above. In view of the many advantages gained by using the Sartorius microbalance, it was installed in the apparatus.

It could be argued that steps should have been taken to improve the operation of the quartz microbalance that had been constructed, in an effort to overcome its shortcomings discussed above. In this respect, however, it has been the experience of other

* Manufactured by: Sartorius-Werke A.G., Göttingen, West Germany.

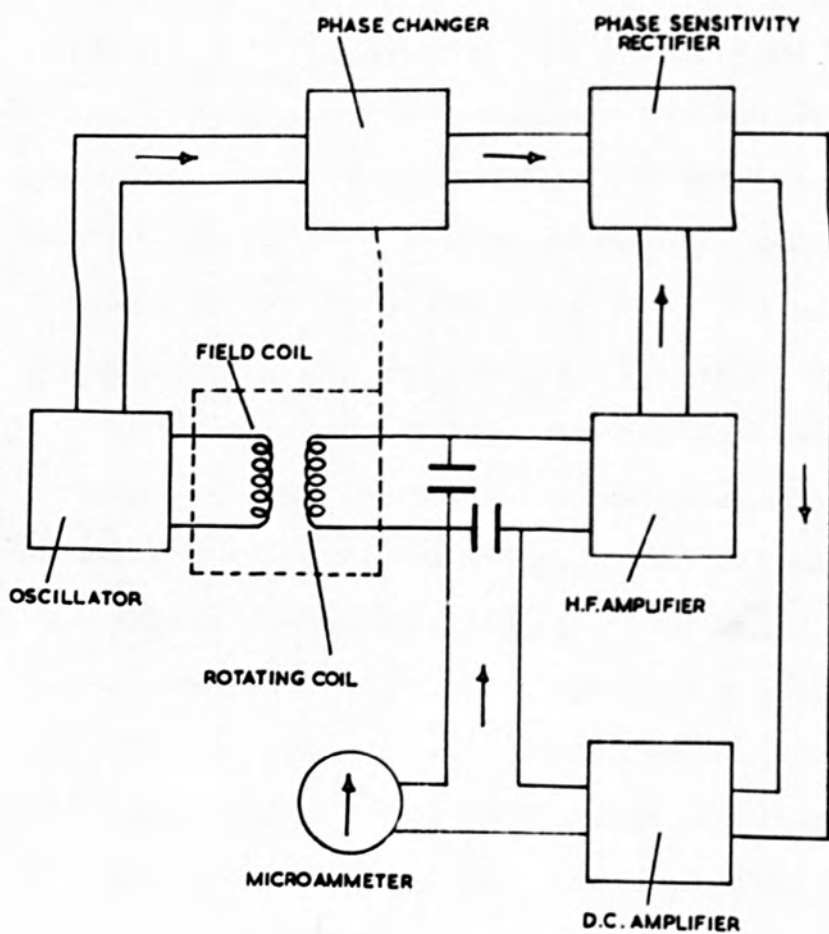


Fig. 12. Block diagram of the electrical circuit of the Sartorius Microbalance (after Gast⁽⁸⁰⁾).

workers^(78,79) using microbalances, that improvements of this type can be extremely time-consuming and unrewarding.

In the next section the Sartorius microbalance will be described, using information given in the handbook of the balance; unfortunately many technical details of the microbalance have not yet been disclosed by the manufacturers.

4. Sartorius Vacuum Electronic Microbalance

The principle of the microbalance was originally proposed by Gast⁽⁸⁰⁾, and can be summarised as follows: A coil of wire attached to the beam of the microbalance is located in close vicinity to a fixed coil of wire energised by a high-frequency current. Movement of the beam alters the position of the coil within the field produced by the fixed coil, causing a high-frequency current to be induced in the moving coil. The magnitude of the current depends on the mechanical shift of the beam, i.e. the change in weight. The beam is then returned to the balanced position by applying an equal, but opposite load to the beam by electromagnetic means.

4.1. Electrical Circuit

The electrical circuit of the power unit of the microbalance is shown schematically in Fig. 12. The fixed field coil was

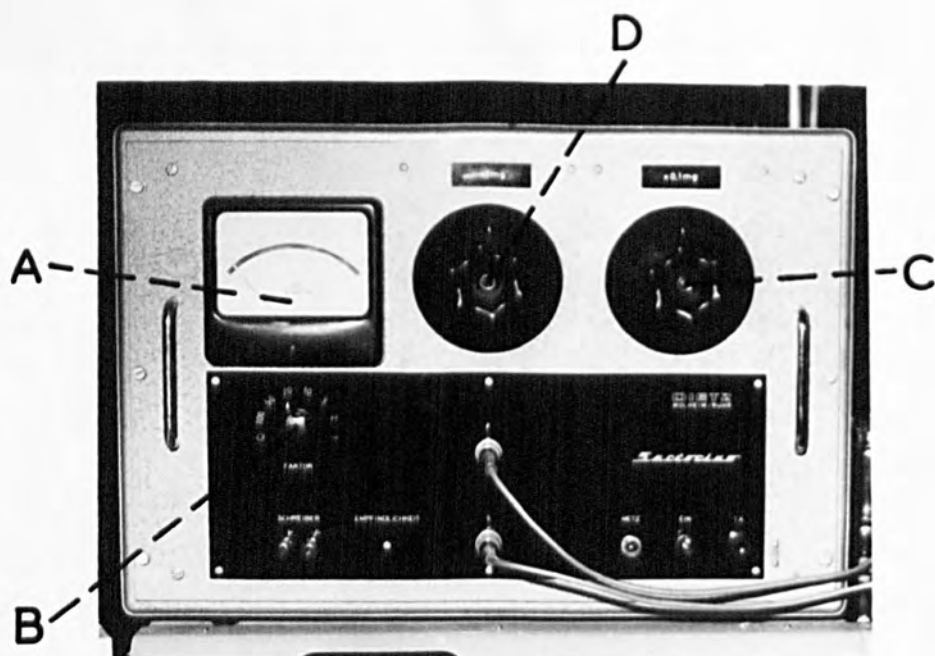


Fig. 13. Power unit of Sartorius Vacuum Electron Microbalance, with electronic weight compensation.

- A microammeter - weight indication meter
- B "Faktor" range switch
- C Decade, 10×0.1 mg.
- D Decade, 10×1.0 mg.

wound on a permanent magnet and was energised by a current from the oscillator at a frequency of 480 kcs. With the rotating coil in the rest position, i.e. with the beam balanced, it was not exposed to the magnetic field produced by the high-frequency current in the field coil. When the coil moved from this position, however, due to a weight change, a high-frequency signal was induced in the rotating coil, the magnitude, phase and polarity of which were dependent on the weight change. This signal was amplified (see Fig. 12) and was compared with the original signal, whose phase had been adjusted using the phase-changer, in a phase-sensitivity-rectifier. The latter consisted, in essential, of an a.c. bridge network, the out-of-balance current arising from the comparison being rectified to a d.c. current. This current was fed back to the rotating coil so as to produce, by interaction with the field of the permanent magnet, an equal but opposite torque to the beam suspension to that produced by the original weight change. The counter-torque thus produced was proportional to the product of the d.c. current and the field intensity of the permanent magnet. Since the latter was known to remain constant over long periods of time, the counter-torque was proportional to the d.c. current alone. A microammeter (A, Fig. 13) was used to measure the d.c. current, and gave a direct indication of weight. The meter was shunted with a series of resistances operated by a "Faktor" switch (B), which

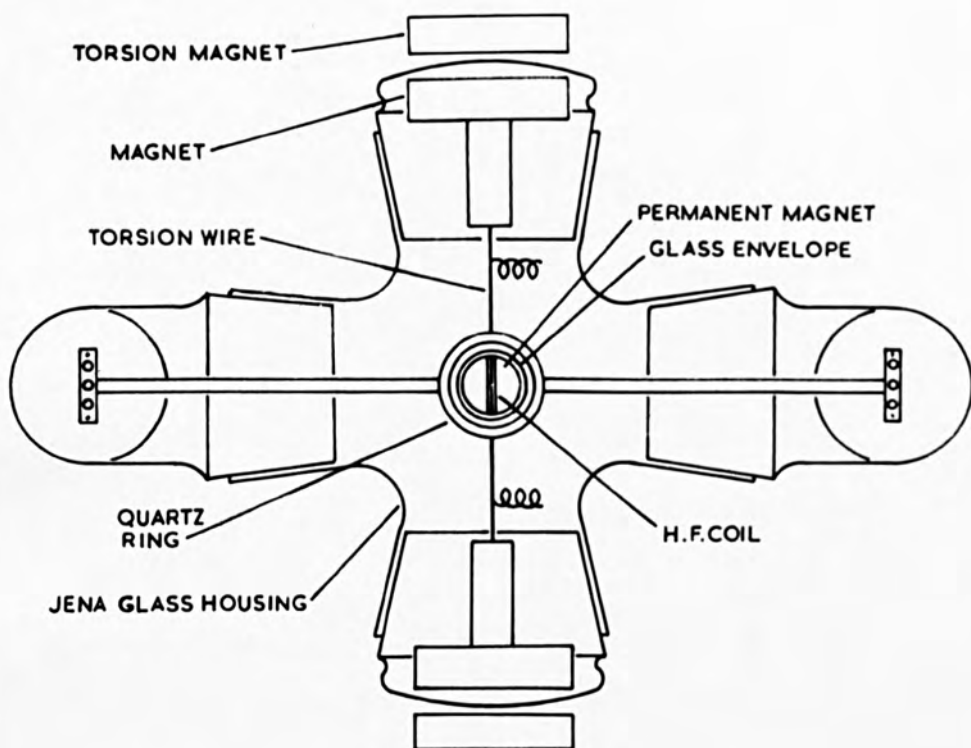


Fig. 15. Sectional plan view of the beam and housing of the Sartorius microbalance.

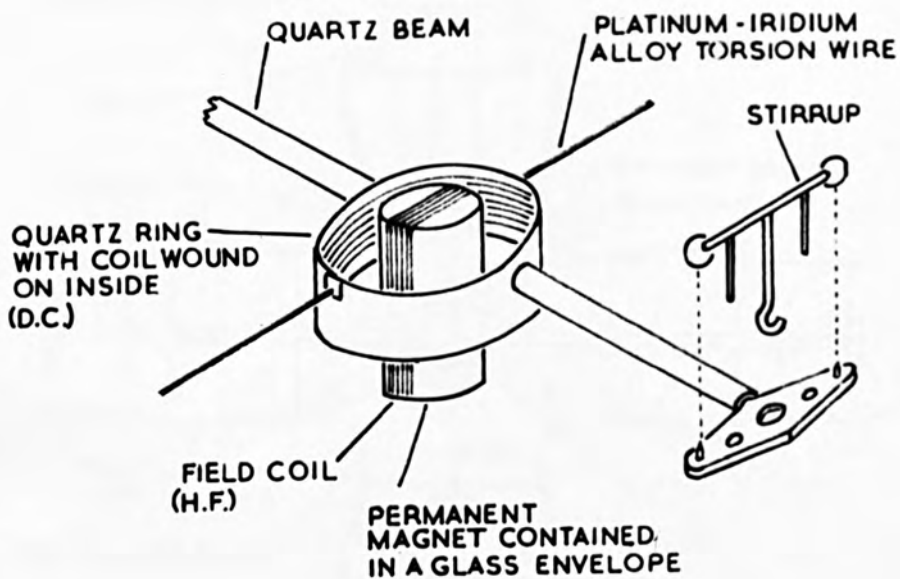


Fig. 14. Diagrammatic view of the beam, and the stirrup of the Sartorius Microbalance.

enabled various weighing ranges to be selected - varying from full scale deflection (f.s.d.) of 10^{-2} gm to 10^{-4} gm, when each scale division was 10^{-6} gm.

Also included in the electrical circuit was a device (not shown in the circuit, Fig. 12) with which weight changes of up to 11 milligm. could be tolerated, at a maximum sensitivity of 10^{-6} gm. The device consisted of two resistance decades, C and D of Fig. 13, energised by a constant voltage (2 volts), one (C) calibrated from 0 to 1 milligm. in steps of 0.1 milligm., the other (D) from 0 to 10 milligm. in steps of 1 milligm. On the most sensitive range of the microammeter a f.s.d. of 10^{-4} gm could be reduced to zero by changing decade C by 0.1 milligm. In principle, therefore, the two decades act as a means of suppressing the zero of the microammeter.

4.2 Microbalance Beam

The beam of the microbalance consisted of two quartz rods joined to the opposite sides of a quartz ring, see Fig. 14. A coil of wire was wound on the inside of the ring and acted as the moving coil of the electrical circuit. Electrical connections were made to the coil using the platinum-iridium torsion wire on which the ring was supported, Fig. 14. The torsion wire could be twisted by rotating the steel magnets (see Fig. 15) to which the wire was attached. In this way differences in weight between the specimen

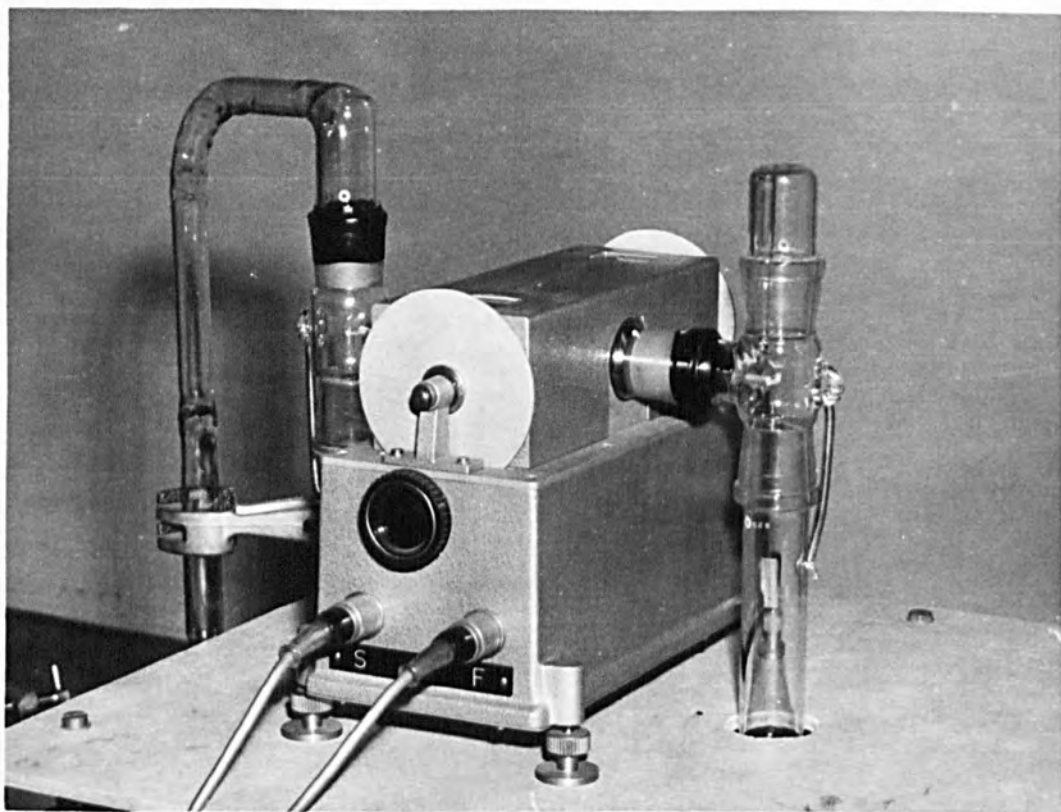


Fig. 16. Photograph of the balance unit of the Sartorius Vacuum Electron Microbalance (about one-third actual size).

and counterbalance of up to 2 milligm. could be tared out.

4.3 Microbalance Housing

The entire weighing mechanism of the microbalance was housed in a glass enclosure (a sectional plan view is shown in Fig. 15), all the parts of which were connected by standard cone joints. The permanent magnet was contained in a separate evacuated glass envelope, located in a recess in the base of the housing, and inside the quartz ring of the beam, see Figs. 14 and 15. The magnets attached to the torsion wire were moved by rotating (multiply polarised) disc magnets mounted outside the microbalance housing (see Figs. 15 and 16). The glass housing was clamped to a supporting base fitted with levelling screws (Fig. 16).

4.4 Specimen Suspension

Both the specimen and counterbalance weight were suspended from stirrups at either end of the beam. Each stirrup consisted of a stainless steel hook joined to two sapphire cups (see Fig. 14) which pivoted on sapphire pins fixed to the flat plates at either end of the beam (Fig. 14).

As it was intended to heat specimens of rutile at temperatures up to 1400°C , neither the silica specimen pans nor the stainless steel suspension wires supplied with the balance could be used. Instead the specimen was contained in a small

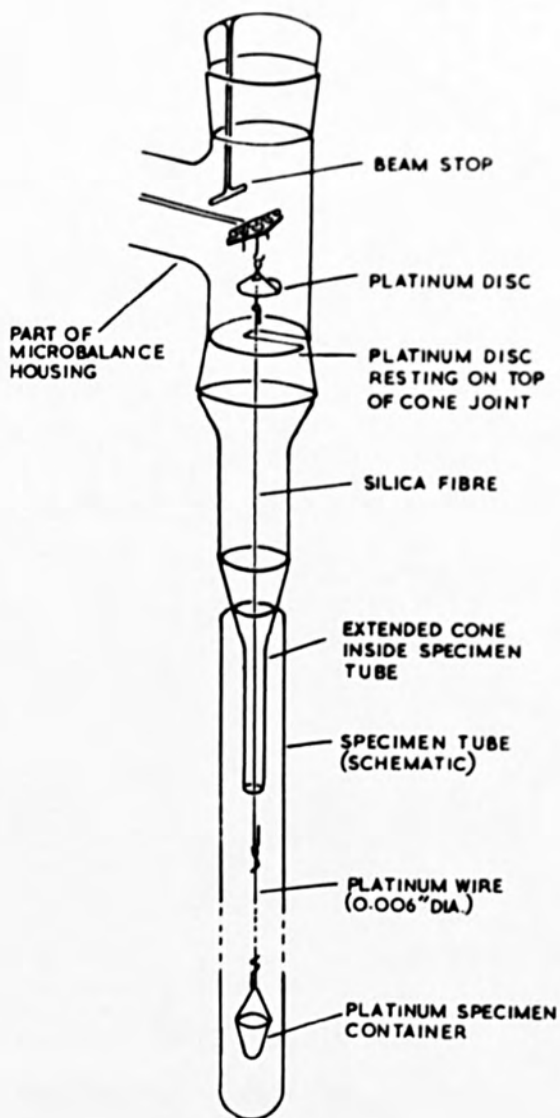


Fig. 17. The method used to suspend the specimen from the stirrup of the microbalance.

platinum crucible which was suspended from the stirrup on the beam in the manner shown in Fig. 17. Platinum wire was used for the lower section of the suspension, where it was subjected to the highest temperatures, and a silica fibre for the upper section. The silica fibre was attached to a small platinum disc suspended from the stirrup, see Fig. 17. Immediately below the disc was another disc of platinum, resting on top of a cone joint of the microbalance housing, the silica fibre of the suspension passing through a slit cut in the disc (see Fig. 17). In this manner the beam was shielded from radiant heat from the furnace, so that spurious effects due to heating of the beam could not arise. A certain amount of protection was also obtained by having a constriction - an extended cone joint, see Fig. 17 - inside the tube surrounding the suspension.

Since pyrex, and especially silica are poor conductors of electricity, they tended to become charged up with static electricity, causing the silica fibre to be attracted to the extended cone joint. In order to avoid this, both the cone extension and the silica fibre were discharged by heating them with a small gas flame, when the apparatus was assembled before an experimental run. By following the above procedure, no effects due to static electricity were encountered.

5. Specimen Tube and Temperature Measurement

As it was proposed to study the reduction of rutile up

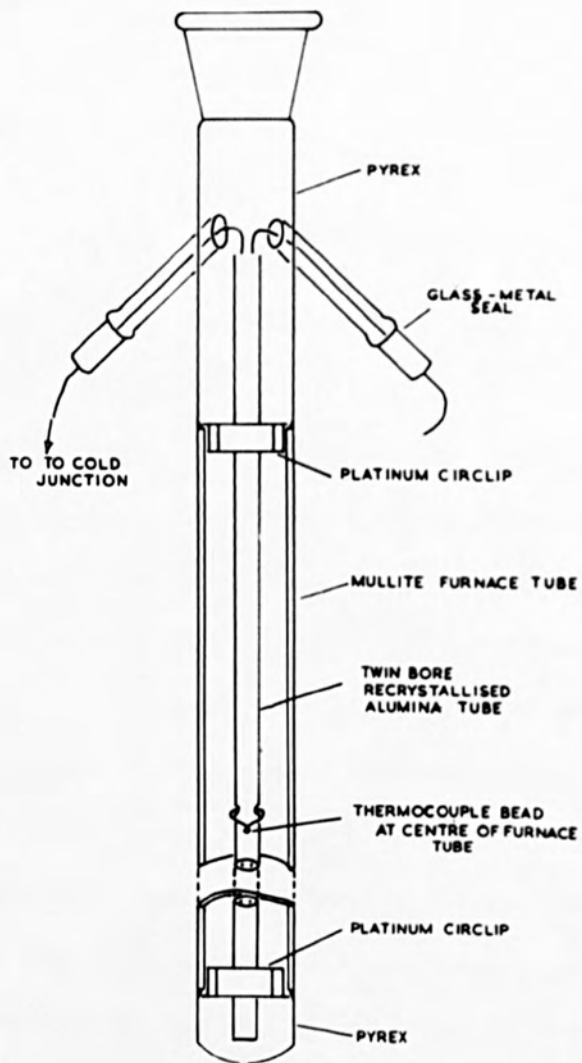


Fig. 18. Sectional view of the specimen tube.

to 1400°C, mullite could be conveniently used for the refractory section of the specimen tube. The main reason for choosing this refractory was that it can be easily joined to pyrex-glass, the constructional material used for the vacuum system of the apparatus. The two ends of the mullite tube were joined to Pyrex-glass tubing, the bottom end being rounded off and the top end joined to a standard cone joint (see Fig. 18), which fitted over the extended cone of the microbalance housing (Fig. 17).

One of the difficulties of microbalance work is the measurement of the temperature of a specimen, since it is impracticable to attach a measuring device to the specimen. At high temperatures a pyrometer method can be used, but for this optical contact has to be made with the specimen. In the present apparatus a platinum/platinum-13% rhodium thermocouple was used to measure the temperature in the specimen tube, in close proximity to the specimen. As the temperature of the centre zone of the furnace was reasonably constant, it is not expected that the temperature measured by the thermocouple will differ to any large extent from the actual temperature of the specimen. Furthermore, by taking temperature readings immediately before and after determining the weight of the specimen, an accurate indication of the mean sample temperature was obtained.

The thermocouple was enclosed in a length of twin-bore recrystallised alumina tubing, the hot junction being exposed in

the manner shown in Fig. 18. The tubing was held against the side of the specimen tube by two platinum circlips sprung into the mullite tube. The leads of the thermocouple were brought out of the specimen tube through two side tubes, fitted with tubular glass-metal joints (see Fig. 18). Each lead passed through a small brass cup which was soldered to the metal part of the joint. The leads were taken to a cold junction, immersed in the usual ice/water mixture, and the temperature difference between the hot and cold junctions was measured using a potentiometer.

The specimen was heated by an electric furnace, the temperature of which was controlled electronically. By using a certain amount of manual control of the input voltage to the furnace, the temperature of the specimen could be maintained, over long periods, to within $\pm 1^\circ\text{C}$ of the required temperature.

6. Vacuum System and Pressure Measurement

The microbalance housing was evacuated, either for studies in vacuo or prior to the admission of oxygen, using an oil diffusion pump backed by a rotary mechanical pump. The latter was supported on antivibration mountings and connected to the oil diffusion pump using a series of flexible metal bellows. Both of these features were incorporated in an effort to reduce the transmission of vibrations along the pumping line to the microbalance. As it was proposed that pressures of less than one atmosphere were to be used for the studies,

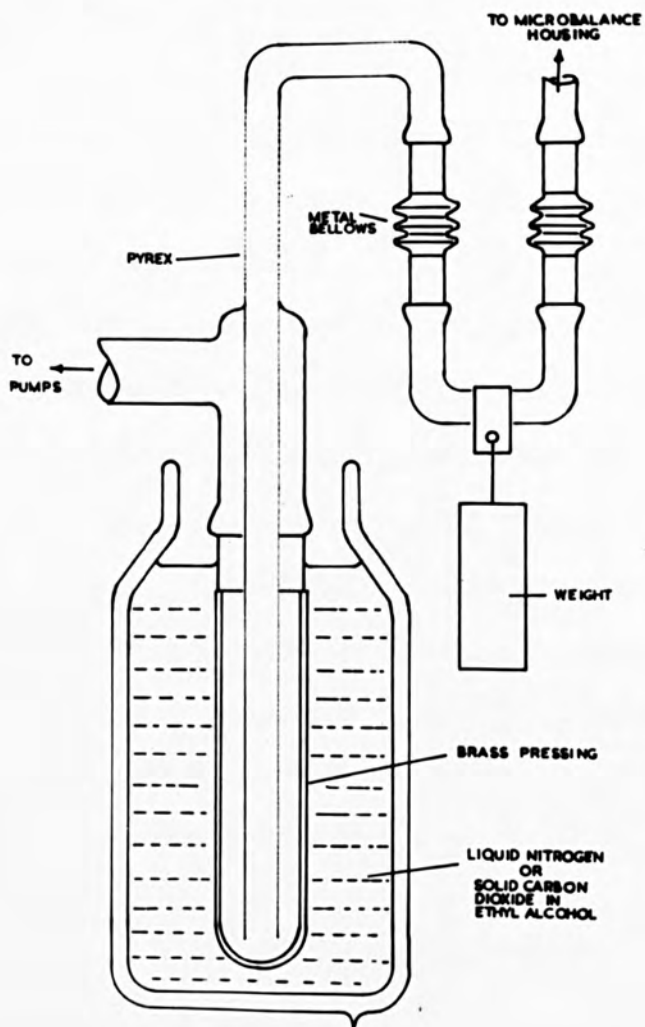


Fig. 19. Sectional view of the cold trap and flexible connection.

the pumping line and pressure-measuring equipment could be conveniently fabricated from Pyrex-glass tubing. The pumping line was connected to the microbalance housing using a flexible coupling. The coupling was U-shaped (see Fig. 19), with two very flexible bellows connected into the upright arms using tubular glass-metal joints. On evacuating the connection, the bellows contracted and in order to restore their flexibility, a suitable load was applied to the lower part of the connection.

Also incorporated in the pumping line was a liquid nitrogen cold trap, used to condense out volatile gases when reductions of rutile were carried out in vacuo. It was inadvisable to construct the trap completely from Pyrex-glass, owing to the disastrous effects that could arise if the glass fractured and the liquid nitrogen entered the vacuum system and hot furnace tube. The trap which was designed (shown on the left of Fig. 19) not only satisfied this requirement but also functioned overnight without the need for topping up with liquid nitrogen. The trap consisted of an annealed brass pressing immersed in liquid nitrogen contained in a vacuum flask, the connection between the brass and Pyrex-glass of the vacuum system being made using a tubular glass-metal joint.

In order to standardise all the vacuum treatments, the specimen tube was never heated without the cold trap being in operation. In this way the possibility of vacuum pump oil decomposing on the hot specimen, which can cause spurious effects⁽⁸¹⁾, was eliminated.

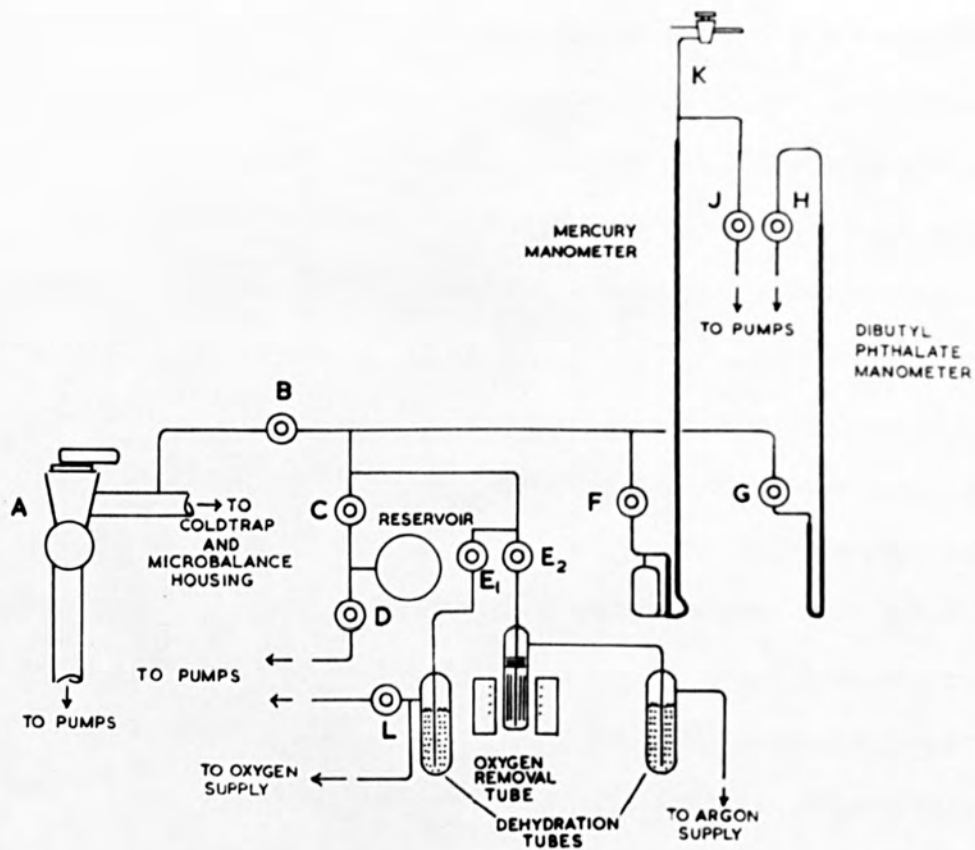


Fig. 20. Schematic diagram of the manometers and part of the vacuum system of the apparatus.

By isolating the microbalance housing from the pumps, i.e. closing tap A of Fig. 20, oxygen could be admitted to the system. Prior to the admittance of the oxygen, however, the refrigerant in the cold trap had to be changed to a solution of solid carbon dioxide ("Drikold") in absolute alcohol. This change was necessitated by the fact that the temperature of liquid nitrogen (-195.7°C) is below the critical temperature of oxygen (-119°C). The temperature of the solid carbon dioxide/alcohol solution (-85°C) was not low enough to cause liquefaction of the oxygen in the trap, but was still sufficiently low to condense out volatile vapours. The time taken to change over the refrigerant was reduced to a minimum by simply replacing the vacuum flask containing liquid nitrogen with one containing a solid carbon dioxide/alcohol solution.

The pressure of oxygen in the system was measured by a manometric method. Two manometers one containing mercury, the other dibutyl phthalate were incorporated in the vacuum system (see Fig. 20), and were used in the pressure ranges 760-25 and 25-0.5 millimetres of mercury respectively. The difference in levels of the liquids in the two arms of the manometer was measured using a cathetometer, reading to 0.02 millimetres.

The mercury manometer was filled under vacuo, so that there was no possibility of trapped air being present, and the surfaces of the mercury were covered with a small amount of dibutyl phthalate. The presence of the latter not only prevented oxidation

of the mercury when oxygen was used in the system, but also reduced the lower pressure limit of the system from 2.3×10^{-3} millimetres of mercury, the vapour pressure of mercury, to 7.8×10^{-5} millimetres of mercury, the vapour pressure of dibutyl phthalate. In addition the dibutyl phthalate served to lubricate the glass-mercury interface, so reducing errors due to surface tension effects⁽⁸²⁾. To ensure continuous lubrication, the mercury menisci were momentarily disturbed before taking a pressure reading, by admitting a small volume of air into the continuously pumped rising arm side of the manometer. The small volume of air was admitted using a three-way tap, K Fig. 20, and was arranged to depress the mercury menisci by about 10 millimetres. When measuring the pressure of gas in the system with the mercury manometer, a correction had to be made for the weight of dibutyl phthalate on each side of the manometer.

The dibutyl phthalate manometer was filled by direct distillation, in vacuo, of the liquid from a reservoir on the evacuated side of the manometer into the evacuated tubes of the latter.

Oxygen gas was supplied to the apparatus from a cylinder, after first removing water vapour with silica gel. The gas line was evacuated, via tap L (Fig. 20), prior to the admission of oxygen, so that any air present was removed.

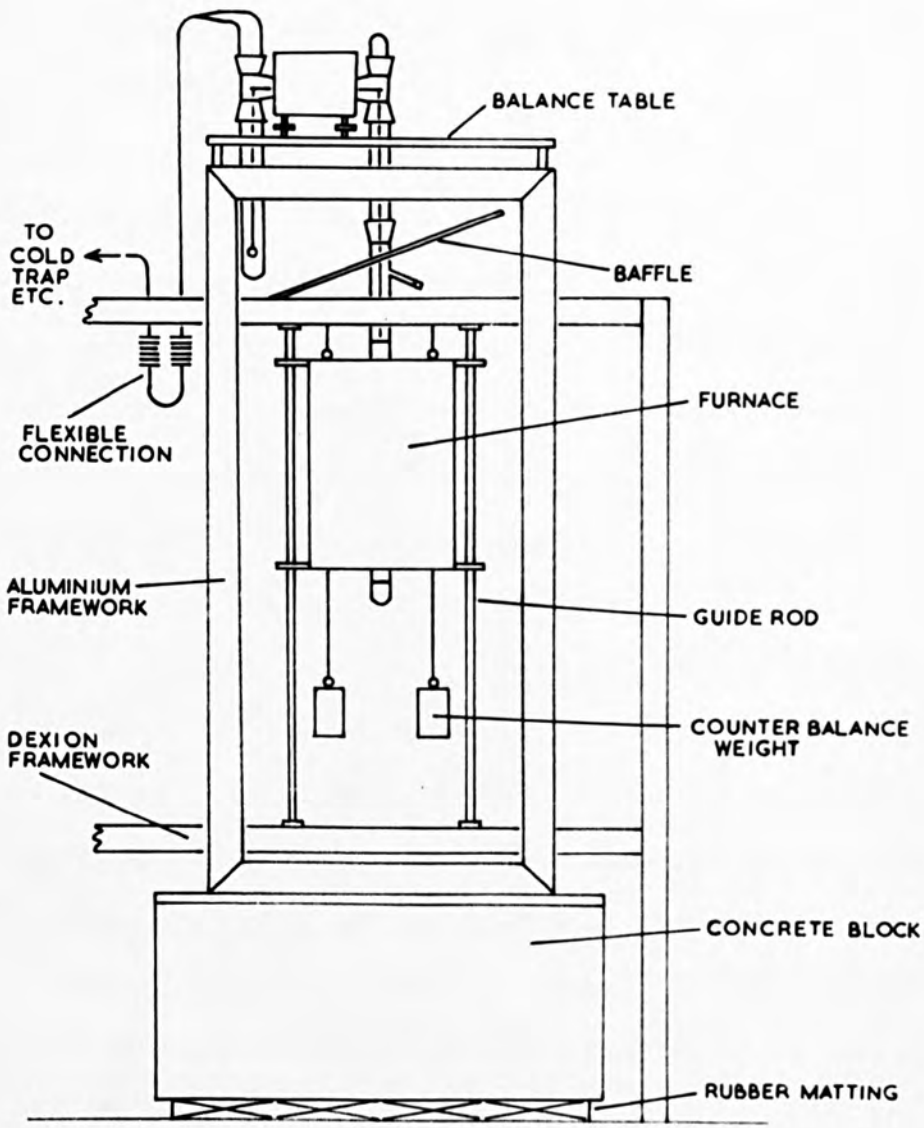


Fig. 22. Arrangement of supporting rigs for the microbalance and furnace.

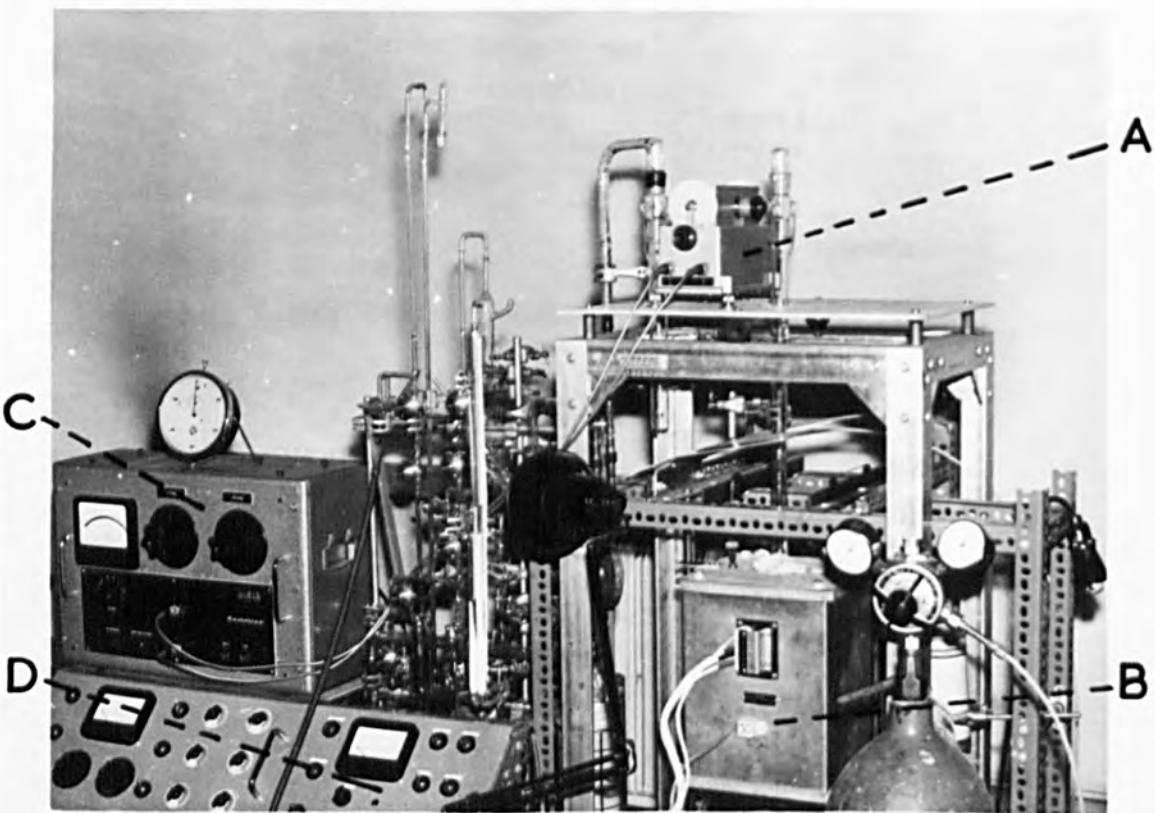


Fig. 21. A photograph of the apparatus, showing the two separate units:

- A Balance unit
- B Furnace
- C Power unit
- D Main switchboard

7. General Assembly

The apparatus was constructed in two separate units, see photograph in Fig. 21; one unit containing the vacuum system and controls, the other supporting the microbalance.

The microbalance, A, was clamped to the balance table which was mounted above a framework constructed from aluminium angle, see Fig. 22. The framework was bolted to a heavy concrete block standing on antivibration matting, and by using this type of support, the microbalance was found to suffer little from vibrations from external sources. The furnace, B, Fig. 21, was counterbalanced, see Fig. 22, so that it could be moved vertically, in order to facilitate the detachment of the specimen tube from the microbalance housing without fouling either the suspension or specimen. The furnace was located between two guide rods bolted to an extension of the Dexion framework, see Fig. 22, containing the main controls of the apparatus. By mounting the furnace in this way, it could be moved into the working position without disturbing the microbalance to any great extent.

The main pumping line and manometers, together with the various controlling and measuring units were built into a separate structure, shown on the left of Fig. 21. The power unit (C) for the microbalance was arranged so that the weight indication meter was at eye level. The temperature controller and variable power

supply for the furnace were positioned in one panel below the main switchboard (D).

In practice it has been found that the apparatus is easily operated, and manipulation of the taps of the vacuum system causes only a small level of vibration to be transmitted to the microbalance.

8. Corrections to Meter Readings

The change in weight of a specimen was not obtained by subtracting readings of the meter before and after heat-treatment, because corrections arising from the following sources had to be applied.

8.1 Scale Reading

The calibration of the microbalance that had been carried out by Sartorius was accepted since each balance undergoes a stringent calibration, using test weights more accurately known than those available to the author, followed by four weeks continuous operation before despatch. It was noted, however, that 100 scale divisions on the most sensitive scale (f.s.d. of 10^{-4} gm) was not equal to one step of the 0.1 milligm. decade. That is, if the meter gave a deflection of 10^{-4} gm, on changing the decade by 0.1 milligm. the meter reading did not fall to zero, but slightly lower. In order to determine the exact difference between the two, a load was applied to the beam and the various scale readings compared,

see Table IV:

TABLE IV

Decade milligm.	Scale Reading	Faktor	Total Load $\times 10^{-6}$ gm.
2.3	1	x1	2301
2.3	0.5	x2	2301
2.2	52	x2	2304
2.2	20.8	x5	2304
2.1	41.4	x5	2307

From Table IV it is evident that 3×10^{-6} gm had to be subtracted from the total load each time the decade was decreased by 0.1 milligm., and vice versa when it was increased.

The above error in the meter reading has arisen because the scale of the microammeter was not exactly matched to the decade resistances⁽⁸³⁾, which have been very accurately calibrated. However, by using the correction described, the mis-match between the two was overcome.

8.2 Temperature Effects

The balance reading was found to increase by only 2×10^{-6} gm when the empty specimen container was heated, in vacuo,

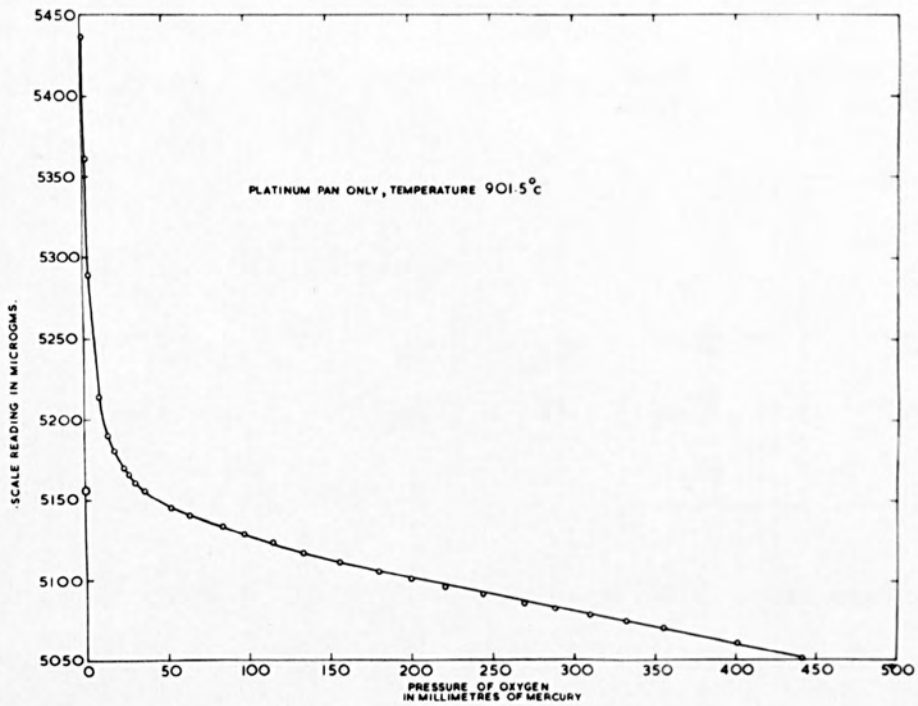


Fig. 23. Balance reading as a function of the pressure of oxygen in the system.

from 350 to 1200°C. On cooling, the reading decreased by 2×10^{-6} gm. These changes only introduced a small error in any weight change, and proved that the heat baffles described in Section 4.4 worked very efficiently.

8.3 Buoyancy Effects

As it was intended to study how departures from the stoichiometric composition depended on the pressure of oxygen, it was necessary to observe the effects of admitting gas to the system on the balance reading. With an empty specimen pan suspended from the balance, and maintained at a constant temperature, oxygen was admitted to the system to give various pressures. When equilibrium conditions had been attained, the balance reading was noted; the data obtained is shown graphically in Fig. 23. Above a pressure of about 70 millimetres of mercury the balance reading was found to be directly proportional to pressure. Such a relationship would be expected since the balance reading, by indicating the apparent weight of the pan, gives a measure of the density of the gas, which is known from the Gas Laws to be directly proportional to its pressure.

The non-linear behaviour of the data below a pressure of 70 millimetres of mercury (see Fig. 23) can be explained by the fact that the properties of gases at low pressures (i.e. densities) are different to those at normal pressures⁽⁸⁴⁾. This difference

arises in the following way: At normal pressures the properties of a gas depend essentially on the frequency and character of the intermolecular collisions. However, when the pressure within an experimental system is decreased, collisions between gas molecules are less important than collisions between them and the walls of the system⁽⁴⁸⁾. In effect, therefore, each gas molecule begins to act independently of all the others in giving rise to the properties of the gas.

At low pressures the most important property of a gas is its ability to creep along the surface of any body in contact with it, in regions where a temperature gradient exists. In the present experimental arrangement this property undoubtedly caused a flow of gas along the sides of the specimen tube towards its hottest section. In order to balance out any pressure gradients thus formed, gas would also have to flow in the opposite direction in the centre of the tube, resulting in the pan being subject to an upthrust. Of greater importance, however, would be the creep of gas around the pan, which by reason of its geometry - a cup shape - would also cause an upthrust⁽⁸⁴⁾. The force causing the upthrust has the same origins as the forces used to revolve the vanes of the Crookes radiometer⁽⁸⁵⁾. Treatments of the radiometric force suggest that it is inversely proportional to pressure, and has a maximum effect at a pressure of 1 millimetre⁽⁸⁴⁾. It is interesting to note that the curve in

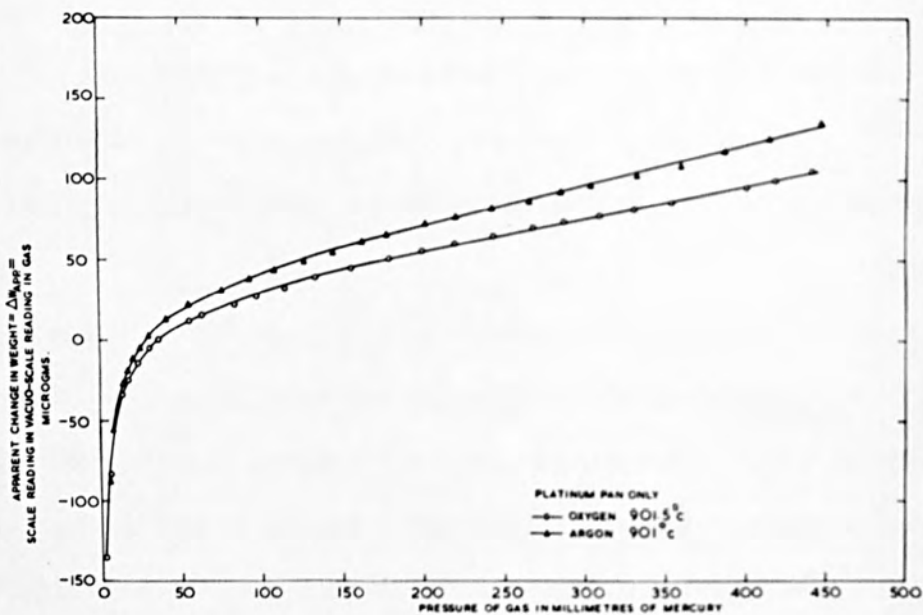


Fig. 24. Apparent change in weight of a platinum specimen pan as a function of the pressure of oxygen and argon in the system.

Fig. 23 is of a reciprocal nature below a pressure of 70 millimetres, and also that at 1 millimetre pressure an upthrust equivalent to 3×10^{-4} gm was experienced by the pan (weight 0.5 gm).

It was considered that effects arising from buoyancy in oxygen could be calculated by comparison with another gas, the choice of which was limited to one that was inert to rutile. Argon was the obvious choice in this respect, and the experimental procedure described above was repeated at the same temperature using argon in the system. The data obtained, together with that for oxygen, is plotted in Fig. 24, in which the ordinate is the apparent gain in weight (ΔW_{app}). Above a pressure of 70 millimetres of mercury, if the value of ΔW_{app} at a chosen pressure of argon is multiplied by the ratio of the molecular weights of oxygen and argon (0.8), the value of ΔW_{app} at the same pressure of oxygen is obtained. This type of relationship between the two sets of data was expected, since the densities (i.e. buoyancies) of two different perfect gases at the same temperature and pressure are proportional to their molecular weights⁽⁸⁴⁾. No relationship of this type was found applicable below a pressure of 70 millimetres of mercury, which was not surprising since the detailed effects of surface in various gases at low densities are, as yet, unknown. The data plotted in Fig. 24 does not coincide at low pressures. Replotting of the low pressure data on an enlarged scale, justified because the measurements of pressure were made using the dibutyl phthalate

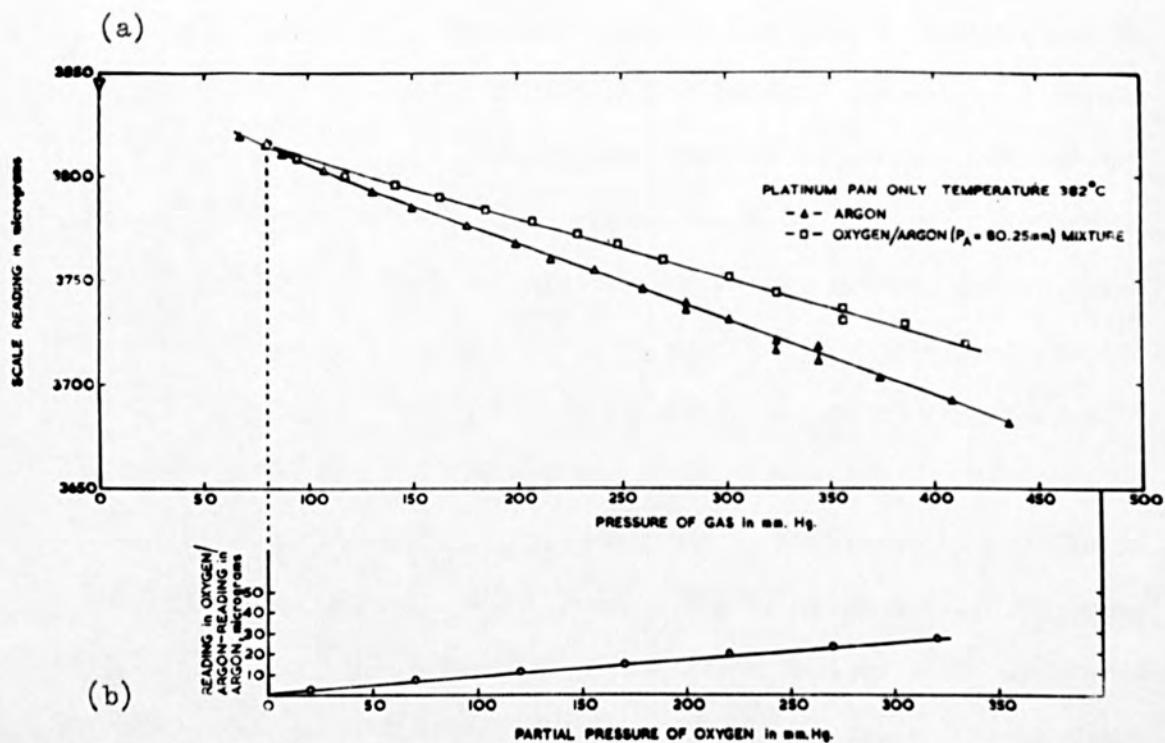


Fig. 26 (a) Variation of scale reading with pressure of argon, and oxygen in oxygen/argon mixture, and
 (b) difference between curves of (a) plotted against partial pressure of oxygen.

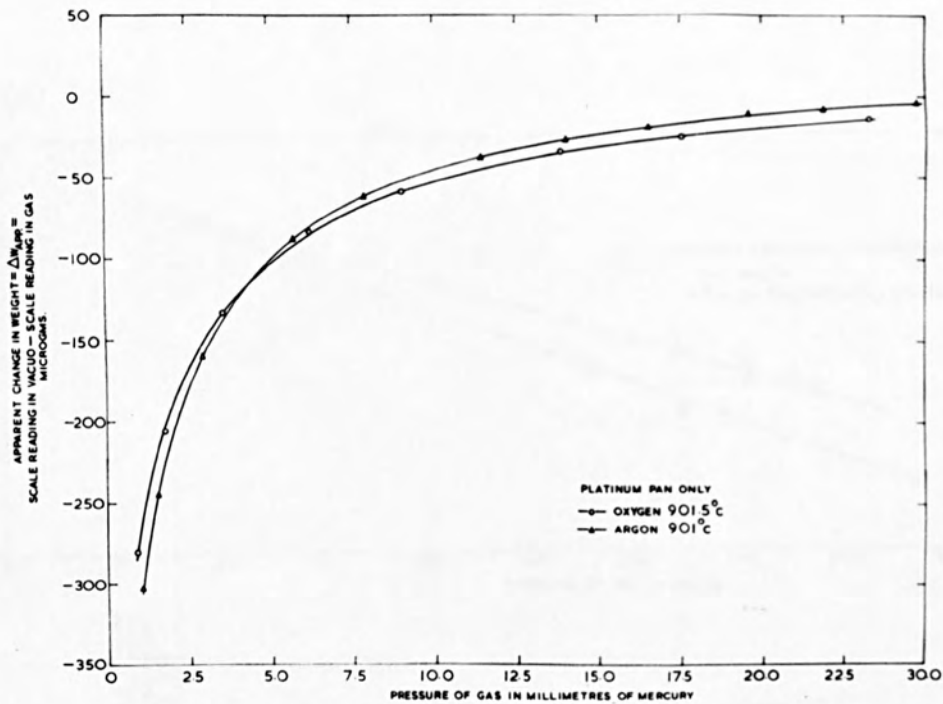


Fig. 25. Low pressure part of Fig. 24 plotted on an enlarged pressure scale.

manometer, magnifies the difference in behaviour of oxygen and argon, see Fig. 25.

In order to be able to cover the range of oxygen pressures below 70 millimetres of mercury, and yet be able to correct for buoyancy, it was decided to have a partial pressure of argon of 70 millimetres of mercury in the system during studies in oxygen. The effects due to buoyancy in the argon-oxygen mixture would then have to be calculated from an initial experiment in argon alone. The method was checked before use; after taking balance readings in argon at various pressures, the pressure in the system was reduced to about 70 millimetres of mercury, and oxygen was added to various pressures. The data obtained is plotted in Fig. 26(a), and in Fig. 26(b) the difference between the two curves of Fig. 26(a) is plotted against the partial pressure of oxygen in the system. The slope of the line in Fig. 26(b) has been checked at various temperatures and has been found to have an average value of 0.08×10^{-6} gm/millimetre of oxygen. Thus at a partial pressure of P_o millimetres of oxygen, the buoyancy of a specimen could be calculated by adding $0.08 P_o \cdot 10^{-6}$ gm to the balance reading obtained at an equivalent pressure of argon. In this way it was possible to correct for the buoyancy of a specimen in an oxygen/argon mixture with an accuracy varying from $\pm 2 \times 10^{-6}$ gm to $\pm 4 \times 10^{-6}$ gm at low and high pressures respectively. The presence of the argon in no way affected either the kinetics or the extent

of the departure from the stoichiometric composition⁽⁸⁶⁾ in rutile. Traces of oxygen and water vapour were removed from the high-purity argon, using heated copper foil and silica gel respectively (see Fig. 20).

The only disadvantage in using a partial pressure of argon of 70 millimetres of mercury in the system was that small partial pressures of oxygen could not be measured very accurately using the mercury manometer. In order to cover this low pressure range, which later proved to be of extreme interest, a novel arrangement was devised whereby the dibutyl phthalate manometer was used, with gas isolated in its normally evacuated arm. However, the displacement of the dibutyl menisci was then not equal to the partial pressure of oxygen in the system, because the gas in the other arm of the manometer had been compressed. The way in which the displacement was adjusted to give the correct partial pressure of oxygen is given in Appendix II.

Effects due to convection of gas in the hot furnace tube only occurred at pressures above about 300 millimetres of mercury. By observing the changes of the balance reading (not more than $\pm 6 \times 10^{-6}$ gm), an average reading at a particular pressure was obtained.

9. Operation of the Apparatus

The specimen pan was loaded with a dehydrated sample of rutile (details of sample pre-treatment are given in the next section) of known weight (W), and the beam nearly balanced by adjusting the counterbalance load. Normally it was arranged that

about 2 millim. of the decade resistances were required to give a scale reading, so that apparent increases in weight of the specimen could be accommodated when argon was admitted to the system.

After joining the specimen and counterbalance tubes to the microbalance housing, the system was evacuated and, when the pressure had fallen to about 10^{-5} millimetres of mercury, was degassed by heating the glass-ware with a small gas flame. The specimen was then maintained at a temperature of 350°C for 12 hours after which the balance reading (R_1) was noted; R_1 represents the weight of the specimen when of the stoichiometric composition. The temperature of the specimen was subsequently increased to the desired value, and when no further change in weight occurred, generally after a period of 12 hours, the balance reading (R_2) was noted. The loss in weight of the specimen ($R_2 - R_1$) was equal to the amount of oxygen lost from the specimen, and the concentration of anion vacancies per molecule of material, $[\text{AV}]$, was calculated from the following equation:-

$$\begin{aligned}
 [\text{AV}] &= \frac{\text{Molecular Wt. of Rutile}}{\text{Atomic Wt. of Oxygen}} \times \frac{(R_2 - R_1)}{W} \\
 &= \frac{79.9 (R_2 - R_1)}{16 W} \qquad (3.2)
 \end{aligned}$$

$$\text{i.e. } [\text{AV}] \approx \frac{5(R_2 - R_1)}{W} \qquad (3.3)$$

When it was necessary to study the dependence of the concentration of anion vacancies on the pressure of oxygen, the vacuum reduction of the sample was interrupted at the desired temperature, and argon was admitted to the system. The balance reading was noted as a function of the pressure of argon, after which the system was partially evacuated to a pressure P_A millimetres of mercury, and argon admitted to both sides of the dibutyl manometer. Oxygen was then admitted to the system to the required partial pressure (P_O) and the specimen left to reach equilibrium - generally a time of between 12 and 24 hours was required. When the balance reading no longer changed, it was noted (R_{P_O}). The balance reading (R_A) corresponding to a pressure of argon of ($P_A + P_O$) was interpolated from the data already obtained and by adding $0.08 P_O \times 10^{-6}$ gm to it, the weight (R_{P_O}) of the non-stoichiometric sample in the oxygen/argon mixture, prior to oxidation, was obtained. The concentration of anion vacancies at P_O , $[AV]_{P_O}$, in the sample was calculated from equation (3.2) and the weight uptake of oxygen:-

$$\begin{aligned}
 [AV]_{P_O} &= [AV]_{\text{in vacuo}} - \text{oxygen uptake} \\
 &= \frac{79.9}{16} \frac{(R_2 - R_1)}{W} - \frac{79.9}{16} \cdot \frac{R_{P_O} - R_{P_O}}{W}
 \end{aligned}$$

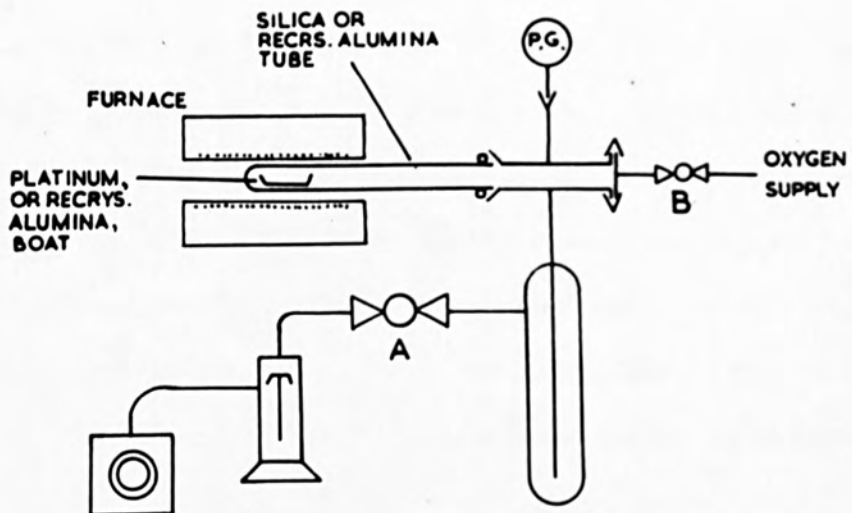


Fig. 27. Schematic diagram of the vacuum system of the subsidiary high-temperature furnace.

$$\begin{aligned}
&= \frac{79.9}{16 W} \left(R_2 - R_1 - R_{P_o} - R_{P_o} \right) \\
&= \frac{79.9}{16 W} \left(R_2 - R_1 - R_A - 0.08 \cdot P_o \cdot 10^{-6} - R_{P_o} \right) \quad (3.4)
\end{aligned}$$

10. Specimen Source and Pre-treatment

Interest was mainly centred on rutile powder of very high purity (details of impurities are given in Appendix III). The properties of this material were compared with those of "Purified" and "Technical"* grades of titanium dioxide, and single crystals† of rutile, all of which were purchased commercially.

The treatment given to the powders prior to installation in the apparatus was carried out in a subsidiary vacuum furnace, shown schematically in Fig. 27. The treatment consisted of heating the sample for 12 hours at 1050°C, in vacuo, in order to expel adsorbed water vapour and also to ensure that all of the titanium dioxide was in the rutile form. The powders were reduced as a result of this treatment, and they were oxidised back to the stoichiometric composition by admitting dry oxygen at a pressure of one atmosphere to the furnace. The temperature of the latter was then slowly reduced, over a period of days, to 400°C.

A sample of "Purified" titanium dioxide doped with one

* Hopkin and Williams Ltd., Chadwell Heath, Essex.

† S.A. Minerals Ltd., Switzerland.

weight percent of niobium oxide was prepared* by high-frequency induction melting. As the material was drastically reduced as a result of melting, an oxidation treatment, commencing at a temperature of 1300°C and cooling to 500°C over a period of a month, was given to part of the material in the subsidiary furnace.

11. Estimation of Errors

An estimation of the overall accuracy of the concentration of oxygen vacancies was made using equations (3.2) and (3.4) above. The accuracies of the various factors in these equations are listed below:

Balance Readings, R_1, R_2 , etc.	$\pm 1 \times 10^{-6}$ gm (in a reading of about .3 gm)
Specimen Weight, W	$\pm 1 \times 10^{-4}$ gm (in 0.5-1gm)
Buoyancy Correction to R_A	$\pm 2 \times 10^{-6}$ gm
Pressure, P_o	± 0.04 mm

This gives an accuracy of better than 2% for the concentration of anion vacancies in a specimen reduced in vacuo, and better than 4% when oxygen was present in the system.

* The author is indebted to Drs. P. Chester and J. Holt of the Solid State Division, Central Electricity Generating Board Research Laboratories, Leatherhead, for kindly supplying this material.

IV EXPERIMENTAL METHODS USED FOR THE DILATOMETRIC AND DENSITY STUDIES OF NON-STOICHIOMETRIC RUTILE

1. Dilatometric Studies

1.1. Introduction

In Part II (Sec. 2) it was shown that cation interstitials might possibly be formed as defects in rutile on departure from the stoichiometric composition⁽²²⁾. The method by which interstitials are formed was not discussed by Hurlen⁽²²⁾, but as anion vacancies were not included in either defect reaction (2.7) or (2.8) it must be concluded that, although anion vacancies are initially present in non-stoichiometric rutile, they are subsequently removed by some process. This could occur by a collapse of the lattice about the vacancies, and will be discussed more fully at a later stage. If a collapse of the lattice does occur in order to form this type of cation interstitial, the dimensions of a sample of rutile would be expected to decrease along certain crystallographic directions on departure from the stoichiometric composition.

If anion vacancies are formed as defects, however, an expansion of the lattice, and hence an increase in the dimensions of a sample of rutile, would be expected to occur, due to the electrostatic effects arising from the presence of

vacancies in an ionic solid^(49,86).

Thus a careful study of the changes in length of a single crystal sample of rutile as it departs progressively from stoichiometric composition could aid in determining the type of defect formed. It was for this reason that the dilatometric studies described below were undertaken.

1.2. Apparatus

The design and construction of the sensitive dilatometer used for the present studies has been described in detail by Basterfield⁽⁸⁷⁾, and so only a brief description of the main features of the apparatus will be given.

The dilatometer and associated equipment was originally designed to study the dilation of some early transition elements on absorption of hydrogen. As these elements are very prone to oxidation and have poor creep properties at high temperatures⁽⁸⁷⁾, great attention was paid in designing the apparatus to ensure that: (i) a vacuum of 5×10^{-5} mm of mercury could be maintained at all temperatures up to 1000°C , (ii) only the smallest possible load was applied to a specimen in order to maintain contact between it and the measuring device. Both of these features were of importance in the present study since the vacuum conditions under which a sample of rutile is reduced must be carefully controlled,^(58,81)

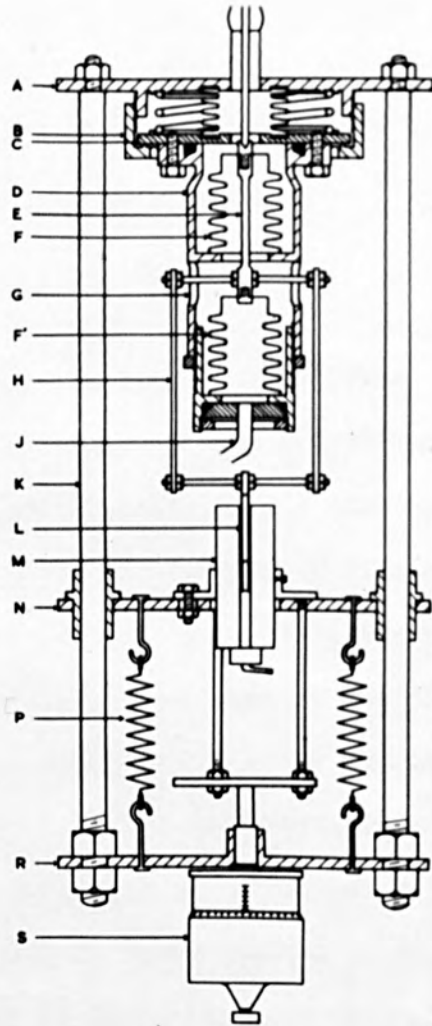


Fig. 29. Sectional view of the balanced-bellows arrangement used for transmitting movement of the push-rod out of the vacuum system to the measuring device (after Basterfield⁽⁸⁷⁾).

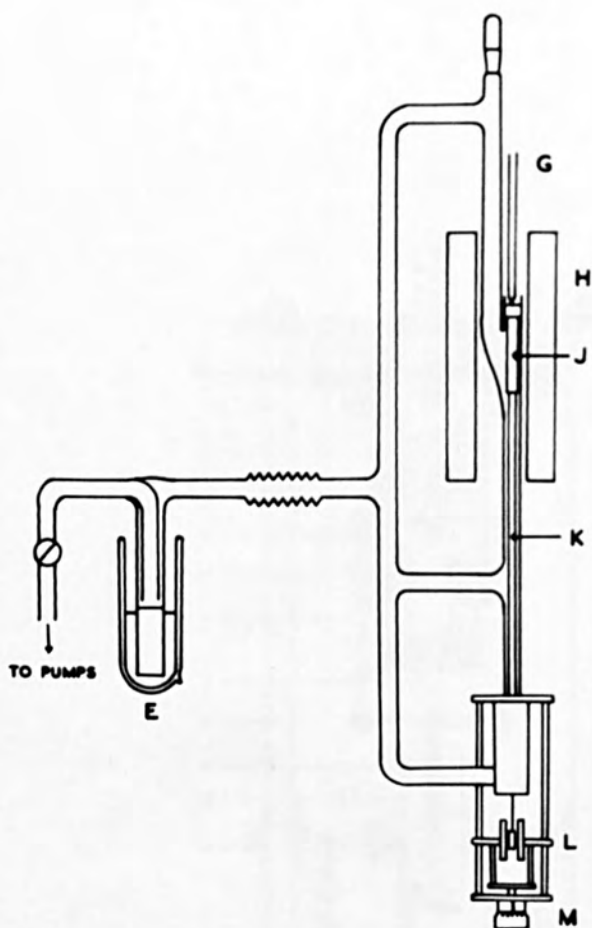


Fig. 28. Schematic diagram of the high-temperature, vacuum dilatometer (after Basterfield⁽⁸⁷⁾).

- E ... Cold trap
- G ... Thermocouple
- H ... Furnace
- J... Specimen
- K ... Push-rod
- L ... Transducer
- M ... Micrometer

and non-stoichiometric rutile has poor creep properties⁽⁸⁸⁾.

A schematic diagram of the dilatometer is shown in Fig. 28. A specimen (J) was located in a silica tube surrounded by a furnace (H), the thermal gradient of which was constant over the length of a specimen to within $\pm 0.5^\circ\text{C}$. The specimen was held in a vertical position by a silica push-rod (K), which was used to transmit changes in length of the specimen to the measuring device (L). Movement of the push-rod was transmitted out of the vacuum system to the measuring device using a balanced-bellows arrangement shown in detail in Fig. 29. The push-rod, shown at the top of Fig. 29, was located in a recess on the face of a flexible metal bellows (F) which was connected to an exactly similar bellows (F') using a tie-rod (E). The bellows arrangement was constructed so that the outside of F, and inside of F', formed part of the vacuum system. On evacuation of the arrangement, although F tended to expand and F' tended to contract, the net movement was zero due to the restricting influence of the tie-rod.

Changes in length of the specimen and hence movement of the tie-rod were transmitted to the measuring device via a yoke arrangement (H). A ferromagnetic armature (L) fixed to H was located inside the measuring device (M) - a differential transducer comprising of an electrical bridge network energised by an a.c. current. Movement of the armature arising from changes

in length of a specimen, altered the inductance of the arms of the bridge circuit and caused it to become unbalanced. The out-of-balance current flowing across the bridge network was measured using a meter, the readings of which could be directly related to the length changes of the specimen.

The measuring device was calibrated⁽⁸⁷⁾ by moving the transducer by known amounts, using a micrometer (S, Fig. 29 and M, Fig. 28), and observing the changes in meter reading. The data obtained in this way was treated by a least squares analysis⁽⁷⁷⁾.

1.3. Preparation of Specimens

The two samples studied were cut from single crystal boules of rutile, which had been grown commercially by the Verneuil⁽⁵⁶⁾ flame fusion process⁽⁵⁵⁾. The boules were oriented prior to cutting by a Laue back-reflection technique, and were subsequently cut using an annular diamond saw⁽⁸⁹⁾. The dimensions of the samples were $1" \times 1/8" \times 1/8"$ with plane cut ends, the length of one specimen being parallel to the a crystallographic direction, the other being parallel to the c direction. After the samples had been cut they were ground and polished using normal metallographic methods.

1.4. Experimental Procedure

In the dilatometric studies of both specimens readings of the measuring device were taken at temperature intervals of about 50°C. Up to a temperature of 550°C readings were taken after thermal equilibrium had been maintained for 30 minutes. At temperatures above 550°C readings were taken only after a period of 24 hours had elapsed, so that sufficient time was allowed for chemical equilibrium to be reached.

2. Density Measurements

In Part II (Sec. 3.6) it was shown that all existing data regarding the effects of departure from the stoichiometric composition on the density of rutile is contradictory, and so cannot be used with confidence when discussing the defect structure of rutile. It was decided, therefore, to measure the density of a few single-crystal samples of rutile with a known composition, so as to give a more reliable indication of how the density of rutile changes on departure from the stoichiometric composition.

A hydrostatic weighing method was used, being chosen for its simple experimental requirements and potential high-accuracy⁽⁷¹⁾. The principle of the method was to weigh a sample in air and then completely immersed in dibutyl phthalate - a liquid with an accurately known density (determined by the

National Physical Laboratory). When submerged in the liquid, the sample was supported by a platinum cradle suspended from the beam of a balance. All weighings, accurate to within 1 and 3×10^{-5} gm, were carried out using a semi-microbalance (Stanton S.M.12).

1. Variation of Non-Stoichiometry with Oxygen Pressure

1.1. Pressure Range

Information about departures from the stoichiometric composition had already been reported at relatively high partial pressures of oxygen (23-760 mm of mercury)⁽¹⁹⁾, and the present studies were restricted, therefore, to pressures of oxygen below 30 mm of mercury. As it was originally intended to carry out studies using rutile of very high-purity, a preliminary study was made of the maximum departure from stoichiometric composition which could be produced by heating such a sample at various temperatures in a high vacuum ($\sim 10^{-5}$ mm of mercury).

1.2. Vacuum Reduction

The fractional losses in weight, and corresponding values of $[\Delta V]$, obtained on heating a sample of high-purity

V EXPERIMENTAL RESULTS

In the following sections where the variation in non-stoichiometry of rutile is described, the composition of a sample of rutile is expressed in terms of the concentration of anion vacancies per molecule of rutile and is represented by the symbol [AV].

1. Variation of Non-Stoichiometry with Oxygen Pressure

1.1. Pressure Range

Information about departures from the stoichiometric composition had already been reported at relatively high partial pressures of oxygen (23-760 mm of mercury)⁽¹⁹⁾, and the present studies were restricted, therefore, to pressures of oxygen below 30 mm of mercury. As it was originally intended to carry out studies using rutile of very high-purity, a preliminary study was made of the maximum departure from stoichiometric composition which could be produced by heating such a sample at various temperatures in a high vacuum ($\sim 10^{-5}$ mm of mercury).

1.2. Vacuum Reduction

The fractional losses in weight, and corresponding values of [AV], obtained on heating a sample of high-purity

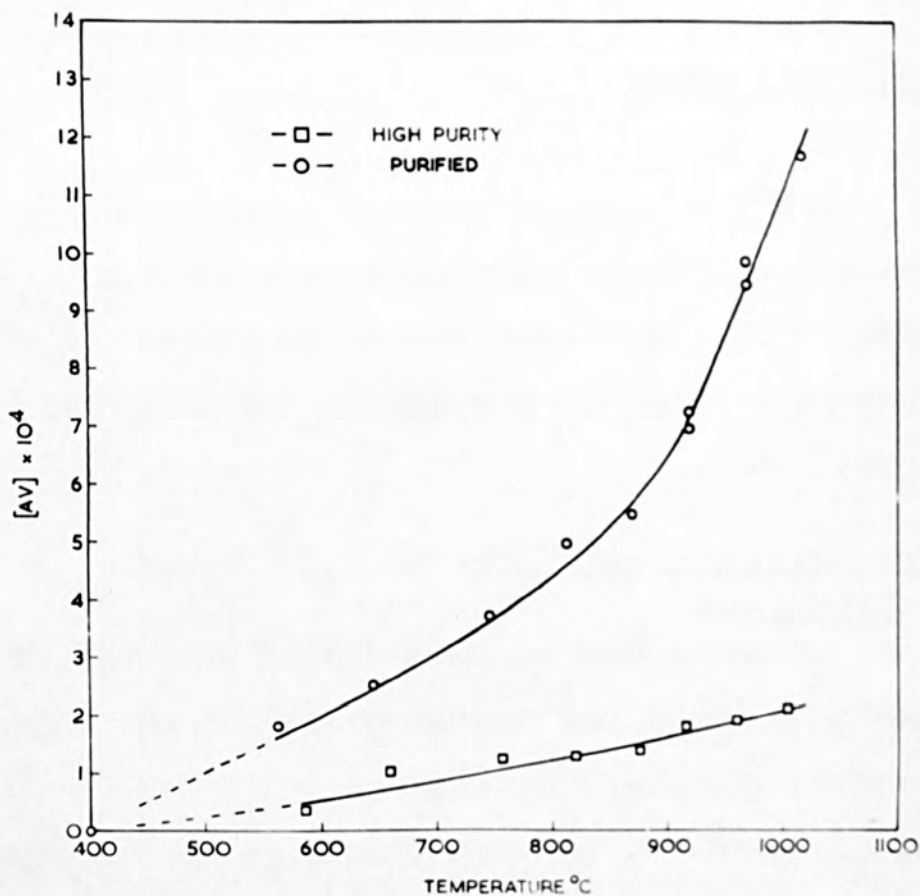


Fig. 30. Variation of [AV] with temperature in the high-purity and purified rutile. Reduction in vacuo.

rutile in a vacuum at various temperatures are given in Appendix IV, and are shown graphically in Fig. 30. The departures from stoichiometric composition were, at all temperatures, smaller than those previously reported for rutile^(19,73). Furthermore, departures from the stoichiometric composition occurred at temperatures below 600°C, although it had been previously reported not to occur until about 875°C⁽⁷³⁾.

A sample of less-pure rutile, the so-called purified rutile, of which details of the major impurities present are given in Appendix III, was reduced in a manner similar to that used for high-purity rutile, and the variation of [AV] with temperature is also shown in Fig. 30. At every temperature the extent of departure from stoichiometric composition was greater in purified rutile than in high-purity rutile.

Since losses in weight, and hence values of [AV], obtained on heating a sample of high-purity rutile, in vacuo, were very small compared with the sensitivity of the microbalance, it was concluded that no accurate measurements of weight change as a function of oxygen pressure could be made using this material. It was decided, therefore, to use purified rutile for studies of the effect of oxygen pressure on composition, since the larger values of [AV] obtained on reducing a sample of this material in a vacuum, would lead to correspondingly larger increases in weight on re-oxidation.

1.3. Treatment of Results

In Sec. 2 (Part II) it was shown that the creation of various types of defect in non-stoichiometric rutile leads to a relationship of the type:

$$[AV] = kp^n \quad (5.1)$$

Thus by plotting the logarithm of the experimental values of $[AV]$ found at a constant temperature against the logarithm of the oxygen pressure, the value of n is given by the slope of the line.

1.4. Temperatures below 1000°C

Isothermal studies of the variation of $[AV]$ with oxygen pressure were carried out, using one sample of purified rutile at temperatures of 850°, 900°, 950° and 1000°C, and another, taken from the same stock but subjected to a separate dehydration treatment, at a temperature of 970°C. The fractional increases in weight of the vacuum-reduced samples of known initial departure from stoichiometric composition as a function of oxygen pressure are given in Appendix IV. Over the whole range of temperatures investigated the values of $[AV]$ never exceeded 10^{-3} , whereas results reported previously by Buessem and Butler⁽¹⁹⁾

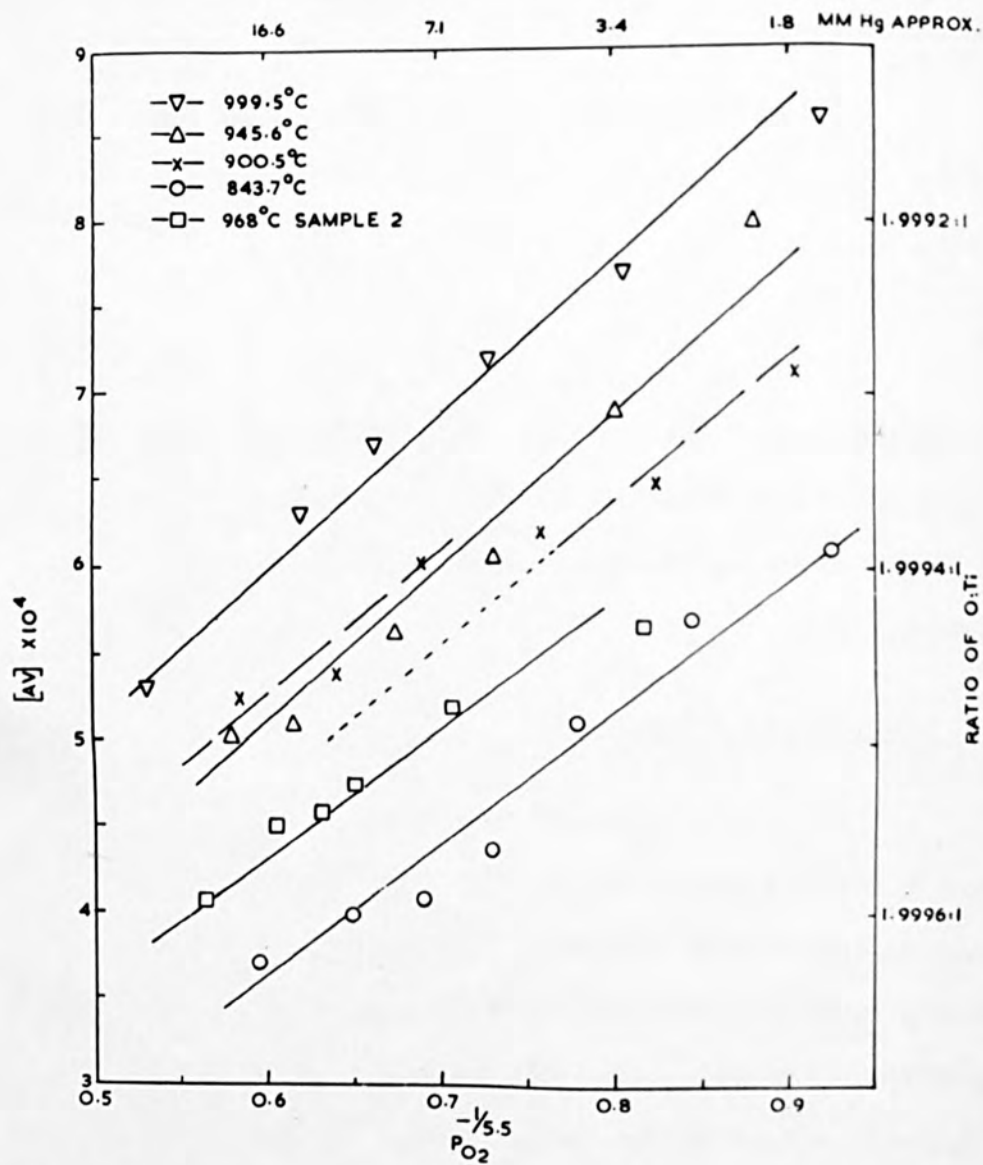


Fig. 37. Isothermal variation of [AV] as a function of oxygen pressure raised to a power equal to the mean value of the slope of the lines in Figs. 32 to 36.

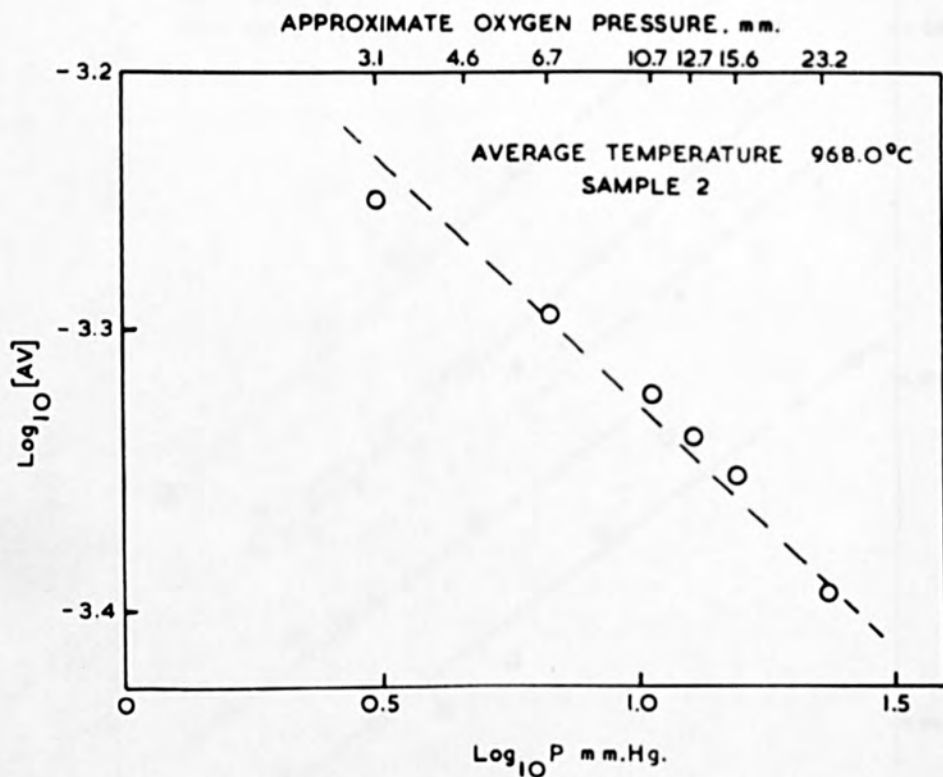


Fig. 36. Sample of purified rutile, from same stock as that studied at other temperatures but subjected to a different dehydration treatment, at a nominal temperature of 970°C. Slope (by least-squares analysis) of -0.16.

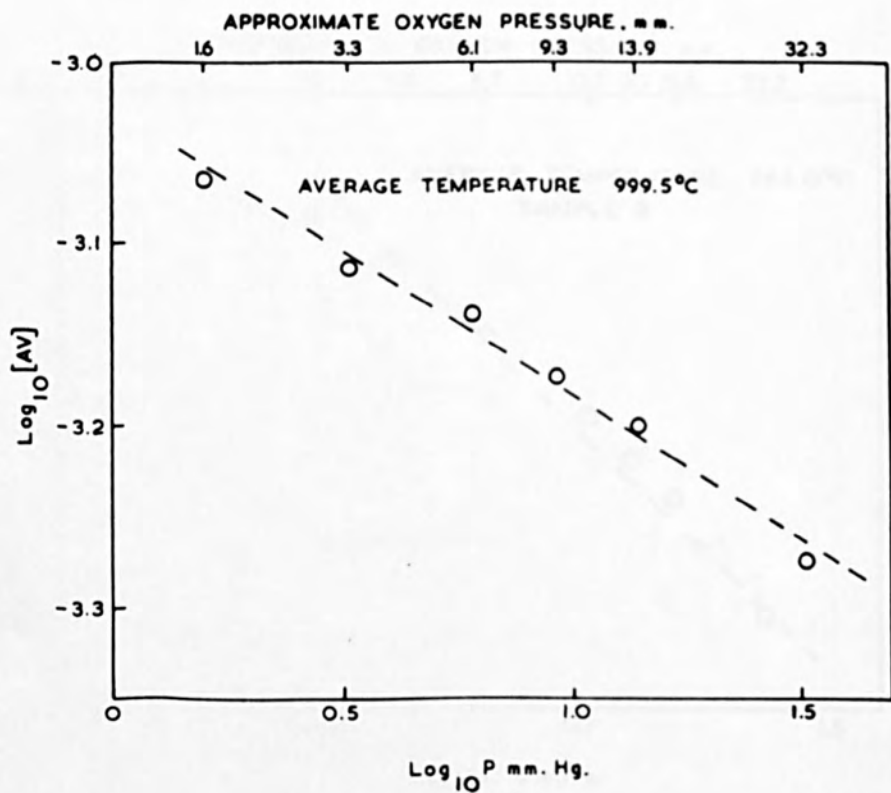


Fig. 35. Sample of purified rutile at a nominal temperature of 1000°C. Slope (by least-squares analysis) of -0.17.

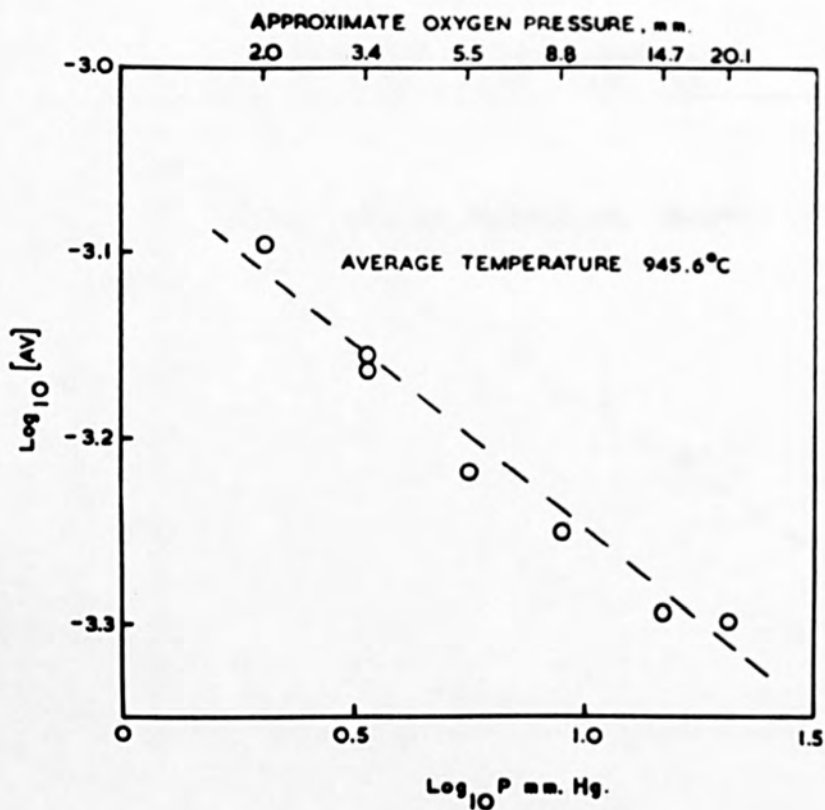


Fig. 34. Sample of purified rutile at a nominal temperature of 950°C. Slope (by least-squares analysis) of -0.22.

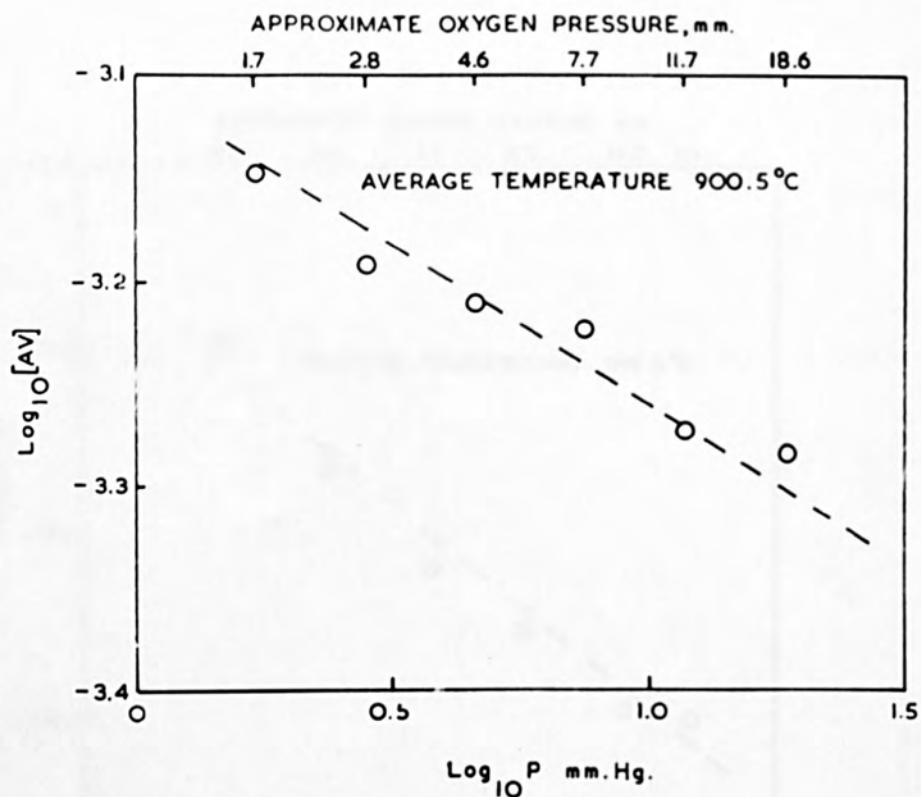


Fig. 33. Sample of purified rutile at a nominal temperature of 900°C. Slope (by least-squares analysis) of -0.13.

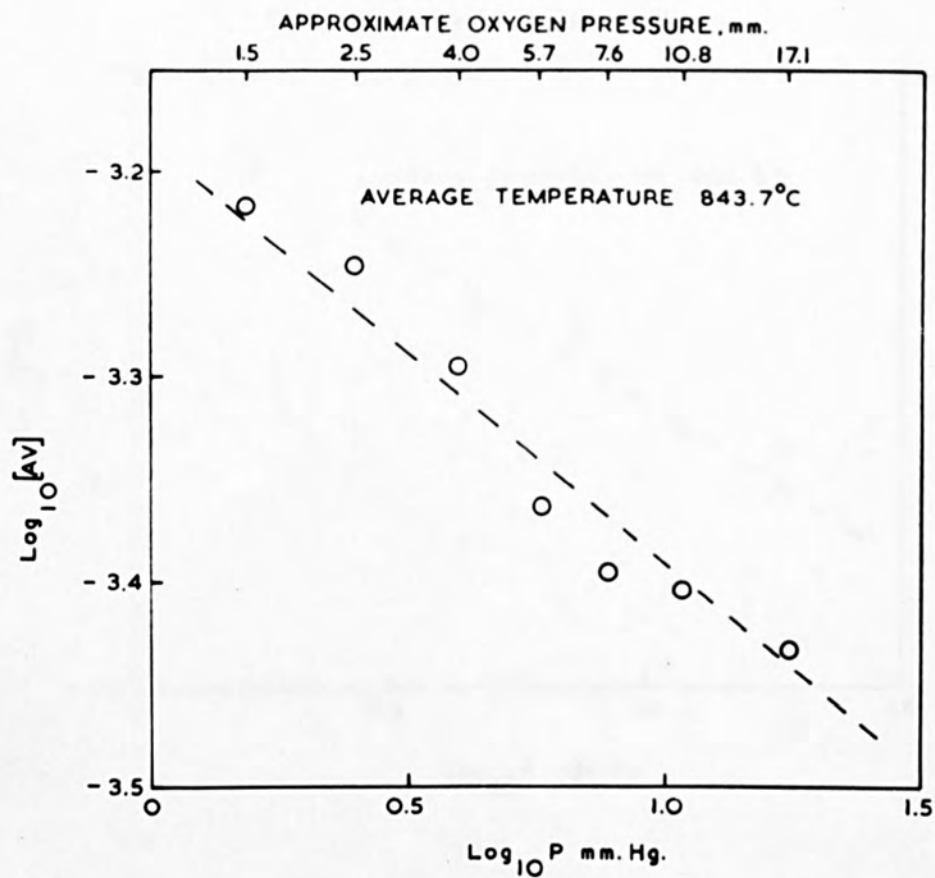


Fig. 32. Sample of purified rutile at a nominal temperature of 850°C. Slope (by least-squares analysis) of -0.23.

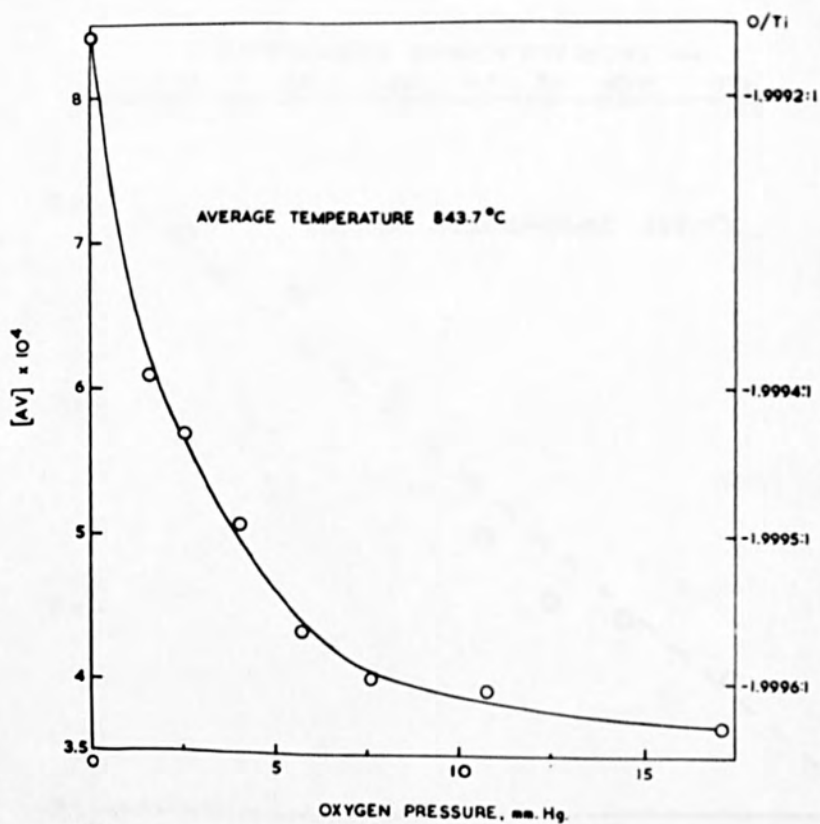


Fig. 31. Variation of [AV] with oxygen pressure in a sample of purified rutile at a nominal temperature of 850°C.

gave values of [AV] which were an order of magnitude greater than this. In these isothermal studies the composition of the samples varied with oxygen pressure in a way similar to that shown in Fig. 31. Since we are concerned with a power relationship between [AV] and p , the results obtained at each temperature are shown in Figs. 32 to 36, plotted on a logarithmic scale. The slopes of the lines in Figs. 32 to 36 were determined by a least-squares analysis, and were found to be:

TABLE V.

Temperature, °C	850	900	950	970	1000
Slope, \underline{n}	-0.23	-0.13	-0.22	-0.16	-0.17

The average value of the slope is -0.182, that is $-1/5.5$.

In Fig. 37 the experimental results have been re-plotted as a function of $p^{-1/5.5}$. Although the points for each isothermal run are somewhat scattered, the curves representing temperatures of 850°, 950° and 1000°C are self-consistent, in that the departure from stoichiometric composition at a given oxygen pressure increases with temperature. Also the slopes of these curves are closely similar. The curve for a temperature of 900°C, although obtained with the same sample, does not appear to show the same type of behaviour at high pressures, (i.e. on the

left-hand side of Fig. 37). Although this anomalous behaviour may be real, it is much more likely that a change in zero of the microbalance took place during the course of the experiment at 900°C. The data obtained at 900°C at high and low pressures would then have to be considered to lie on two parallel lines with a separation of about 5×10^{-5} [AV] (see Fig. 37). This separation corresponds to a change in zero of 5×10^{-6} gm occurring at 7.66 mm of mercury during the experimental run at 900°C. If such a zero-change has occurred, the value of \underline{n} at this temperature given in Table V will be in error. If this particular value of \underline{n} is neglected, the mean value of \underline{n} calculated from the remaining data is $-1/5.13$.

The curve in Fig. 37 representing the behaviour of sample 2 at 970°C lies below that given by the other sample at a temperature of 950°C. This surprising difference in behaviour of the two samples probably arises because of differences introduced during the dehydration treatments which have resulted in the two samples being contaminated to different degrees. This question of the effect of impurities on non-stoichiometric behaviour of rutile will be discussed later.

The wide spread of the values of the slope given in Table V, even when that at 900°C is excluded for the reasons given above, was greater than might have been anticipated when

originally designing the apparatus on the basis of previously obtained results of other workers. This is entirely due to the unexpectedly small magnitude of departure from stoichiometric composition associated with the relatively pure material used in this work, compared with the materials used by earlier workers. Although great care was taken in eliminating inaccuracies which can arise in microbalance work at low pressures, the overall sensitivity of the microbalance was $\pm 3 \times 10^{-6}$ gm, whereas the changes in weight of a sample due to uptake of oxygen at very low pressures lay between 2 and 4×10^{-5} gm. Thus the values of [AV] at low oxygen pressures are subject to a considerable error. Furthermore, the measurement of low gas pressures involves difficulties because of errors in measuring small manometric displacements, and because of variation in the level of refrigerant in the cold-trap causing changes in both the pressure of oxygen and argon in the system.

1.5. Temperatures above 1000°C

At 1050°C and at higher temperatures, the weight of a non-stoichiometric sample of rutile was found to increase at low pressures of oxygen, due to uptake of oxygen, but to decrease at high pressures. This effect was obviously spurious since the values of [AV] must progressively become smaller as

the pressure of oxygen is increased, and can only be explained on the basis of a loss in weight of the platinum specimen pan. Volatilisation of an empty platinum pan was found not to occur in a high vacuum or in argon even at a temperature of 1250°C, but did take place in an oxygen atmosphere. It has been reported that platinum forms a volatile oxide in air at a temperature of 1200°C⁽¹⁰¹⁾, and it would seem likely that, even at temperatures as low as 1050°C, platinum slowly oxidises.

Since it is not possible to use platinum at high temperatures, an attempt was made to obtain isothermal data at 1050° using a specimen container made of silica. At this temperature the weight change did not show a systematic increase with increasing oxygen pressure, probably because of volatilisation of the silica specimen container.

To date it has not been possible to obtain a ceramic container capable of being used at temperatures above 1000°C, with dimensions such that its weight, combined with the weight of a sample, does not exceed the maximum loading of the microbalance. In the absence of a suitable specimen container, no isothermal data could, therefore, be obtained at temperatures above 1000°C.

2. Maximum Extent of Non-Stoichiometry in Rutile

In Sec. 1.2 it has been shown that departures from stoichiometric composition obtained on reducing a sample of high-purity rutile at various temperatures in a vacuum are very small. Larger departures are obtained, however, by using a sample of less-pure (purified) rutile, although even in this material the extent of departure from stoichiometry in oxygen at various pressures was still smaller than that previously reported. These results would seem to indicate that under the same conditions of temperature and oxygen pressure, the extent of departure from the stoichiometric composition in rutile is controlled by the presence of impurities. It was not possible to carry out a systematic investigation of the effects of impurities on the non-stoichiometric characteristics of rutile, since no facilities were available for preparing samples of rutile containing controlled amounts of known elements. However, it was thought that additional information on the effects of impurities could be obtained by studying the maximum extent of non-stoichiometry in other types of rutile which were available, and have already been mentioned in Sec. 10 (Part III).

Samples of a technical grade of rutile, a purified rutile to which has been added 1 wt.% of niobium pentoxide, and

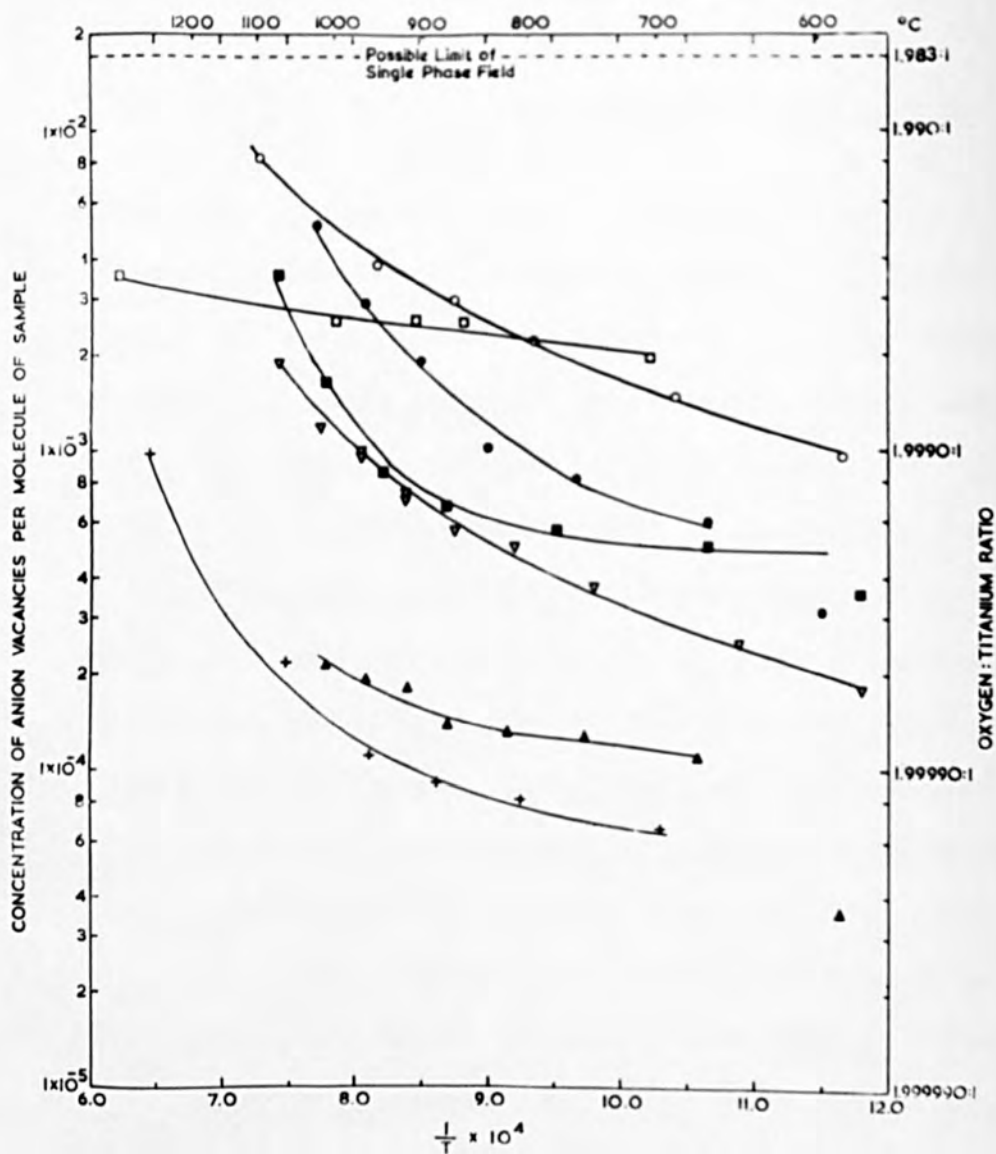


Fig. 38. Variation of $\log_{10} [AV]$ in a sample as a function of the absolute temperature of reduction in vacuo.

- | | | | |
|---|----------------------------------|---|-------------------------------|
| ▲ | High-purity rutile | ● | Niobium-doped rutile |
| □ | High-purity rutile (as-received) | + | Single-crystal rutile |
| ▽ | Purified rutile | ○ | Crushed single-crystal rutile |
| ■ | Technical rutile | | |

a single-crystal of rutile were reduced in a high vacuum in the manner described earlier. The values of $[AV]$ obtained at various temperatures are given in Appendix IV. The logarithm of the values of $[AV]$ obtained in each sample have been plotted against the reciprocal of the absolute temperature, at which the sample was reduced in Fig. 38. Although linear relationships were not found, the trend of the results shown in Fig. 38, excluding the behaviour of the single-crystal sample of rutile, indicates that, at a given temperature, the departures from stoichiometric composition are progressively larger the greater the impurity content of a sample. The data obtained using the single-crystal sample of rutile is anomalous, and the deviation is thought to be due to lack of equilibrium because of slow diffusion in the solid sample. This is borne out by the fact that large values of $[AV]$ were obtained when a single crystal was first crushed to a fine powder (see Fig. 38).

3. Dilatometric Studies

3.1. Treatment of Results

The fractional expansion of specimens of single-crystal rutile heated in vacuum is made up of two components, the normal thermal expansion of the material, and the change of dimensions brought about by departure from stoichiometric composition.

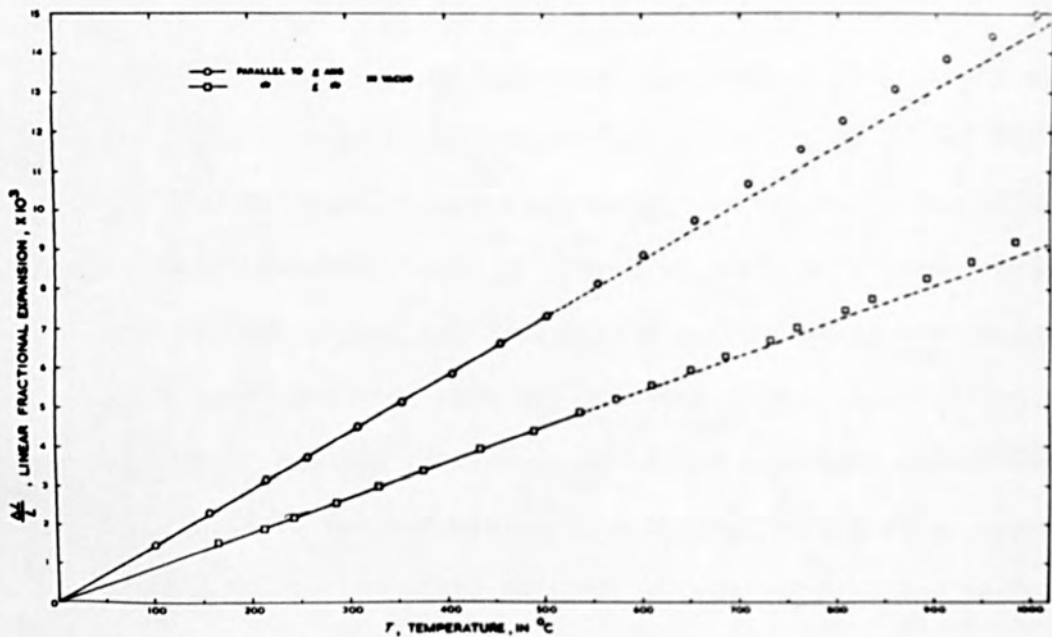


Fig. 39. Temperature variation of the fractional expansion of samples of rutile cut parallel to the a and c axes.

In order to assess the magnitude of the second contribution to the change in length, it is necessary to subtract from the results the thermal contribution.

The fractional expansion of the specimens increased linearly with temperature up to 550°C, that is to say, up to temperatures where departures from the stoichiometric composition were negligibly small. The values of fractional expansion of each specimen at temperatures below 550°C were, therefore, treated by a least-squares analysis, to obtain accurate values of the coefficient of linear thermal expansion in the a and c directions. Using these coefficients, the thermal contribution to the fractional expansion of each specimen was calculated over the whole temperature range of the experiments. The experimental and calculated values of the fractional expansions of the samples along the a and c directions of rutile are given in Appendix V.

3.2. Data Obtained Parallel to the a Axis

The variation with temperature of the fractional expansion of the sample cut parallel to the a axis is shown in Fig. 39. The coefficient of linear thermal expansion between 0° and 550°C. was calculated to be $1.45 \times 10^{-5}/^{\circ}\text{C}$. At temperatures above 550°C the measured fractional expansions were greater than those

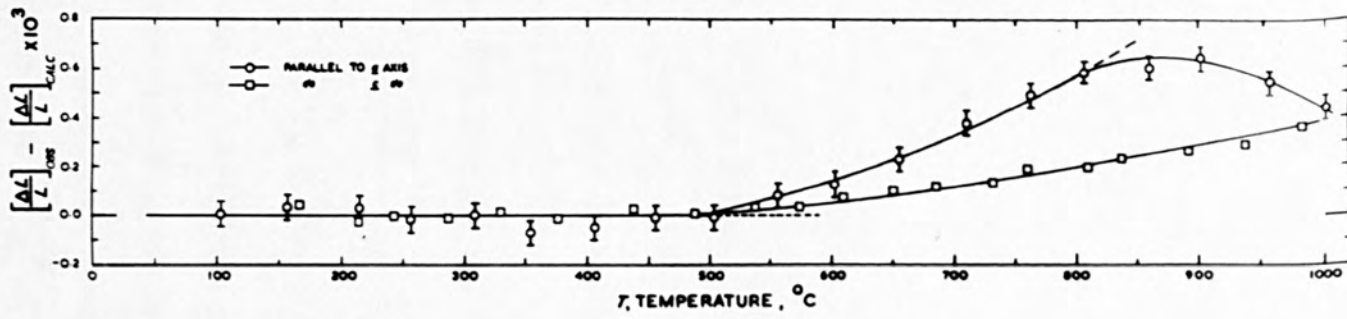


Fig. 40. Temperature variation of the difference between the experimental and calculated values of the fractional expansion the samples of rutile cut parallel to the a and c axes.

calculated from the coefficient of thermal linear expansion which are shown as a broken line in Fig. 39. In Fig. 40 the difference between the experimental and calculated values have been plotted against temperature. The experimental values of the linear fractional expansion were found to increase progressively above the calculated values as the temperature increased from 550° to a temperature between 800° and 850°C . Above this temperature the experimental values of the linear fractional expansion began to approach the calculated values, which would indicate that the contribution to the expansion due to departure from stoichiometric composition was diminishing with increasing extent of departure. This effect could have been brought about by mechanical creep of the specimen under the load of the dilatometer push-rod. However, this possibility is ruled out by the fact that above 850°C , the dilatometer readings were observed to change only in the first 3 hours of an experiment, no further significant changes occurring in the following 21 hours. If the specimen had contracted due to a creep process, then a continuous change in dilatometer reading would have been observed during the whole 24 hours at which the specimen was maintained at a constant temperature.

3.3. Parallel to c Axis

In Fig. 39 the variation with temperature of the fractional expansion of the specimen cut parallel to the c axis is also shown. The coefficient of linear thermal expansion between 0° and 550°C was calculated to be $0.90 \times 10^{-5}/^{\circ}\text{C}$. At all temperatures above 550°C the experimental values of the fractional expansion were found to increase progressively above the values calculated assuming only linear thermal expansion of a sample had occurred. In Fig. 40 the difference between the experimental and calculated values of the linear functional expansion along the c axis is plotted against temperature, and indicates that there is a continuous increase in length as the departure from stoichiometric composition increases.

4. Density

The densities of three samples of single crystals of rutile taken from the same stock as used for the dilatometric work were measured, to an accuracy of $\pm 5 \times 10^{-4}$ gm/cc. The values obtained at known departures from stoichiometric composition are presented in Table VI.

TABLE VI

Composition [AV]	Density gm/cc	Temperature °C
0 (stoichiometric)	4.2502	22.3
7.8×10^{-5}	4.2489	22.6
1.62×10^{-3}	4.2518	22.3

The density of the stoichiometric sample of rutile agrees favourably with the value of 4.2498 gm/cc (at 20°C) reported by Straumanis et al.⁽¹³⁾. Although the information is sparse the results indicate that as departures from the stoichiometric composition became progressively larger, the density of rutile initially decreases, but subsequently increases.

VI DISCUSSION

The results presented in Part V can be conveniently divided into two groups, one concerned with the defect structure of non-stoichiometric rutile, the other concerned with the effects of impurities on the maximum extent of non-stoichiometry in rutile. The results will, therefore, be discussed separately, according to this division.

1. Defect Structure of Non-Stoichiometric Rutile

1.1. Variation of Non-Stoichiometry at Low Oxygen Pressures

The isothermal studies on the variation in stoichiometry of rutile as a function of oxygen pressure were carried out at relatively low partial pressures of oxygen (< 30 mm of mercury), and were restricted to temperatures between 850° and 1000°C . In this low-pressure region the departures from ideal composition in the samples of rutile were found to vary with oxygen pressure raised to the power $-1/5.13$. This value lies within the range of values quoted by Hauffe et al.⁽³⁰⁾ (see page 16), and is very close to $-1/5$ reported by Assayag et al.⁽¹¹⁾. The value of $-1/5.13$ disagrees with $-1/6$ quoted by Buessem and Butler⁽¹⁹⁾, who carried out similar types of isothermal studies

to those described above, only at even higher partial pressures of oxygen (23-760 mm of mercury). These workers did, however, find that at low partial pressures of oxygen the non-stoichiometry of rutile deviated from a one-sixth-power type of relationship (see Fig. 4). No attempt was made to explain the deviation, but it is possible that it is due to the beginning of a change-over in power of the oxygen pressure from $-1/6$ to $-1/5.13$. It seems probable, therefore, that the change in power of the oxygen pressure relationship at low partial pressures of oxygen (corresponding to large departures from the stoichiometric composition) denotes an alteration in the defect structure of rutile.

From a knowledge of the way in which the composition of rutile varies with oxygen pressure, it is possible, by considering equations (2.11) to (2.16.2), to suggest which type of defects are most likely to be present in the material. However, none of the defects discussed in Sec. 2 (Part II) resulted in the power of the oxygen pressure being equal to $-1/5.13$. It is to be expected, therefore, that a combination of defects, which individually give rise to a one-sixth-, one-fifth- or one-fourth-power type relationship, will be present in non-stoichiometric rutile. Defects which give rise to:

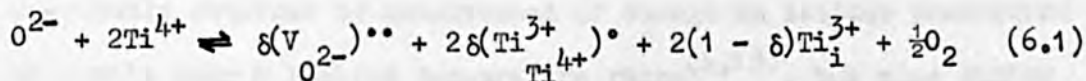
(i) a one-sixth-power type relationship are anion vacancies

together with either free electrons in a conduction band (equation (2.12)), or trivalent titanium ions at normal cation sites (equation (2.11)).

(ii) a one-fifth-power type relationship are interstitial tetravalent titanium ions together with free electrons in a conduction band ($n = 4$ in equation (2.16.1)).

(iii) a one-fourth-power type relationship are either equal numbers of anion vacancies each with a single associated electron and trivalent ions at normal cation sites (equation (2.15), or trivalent titanium ions in interstitial positions (equation (2.16.2)) possibly with free electrons in a conduction band ($n = 3$ in equation (2.16.1)).

As an example of how a combination of defects leads to the non-stoichiometry of rutile varying with oxygen pressure raised to a power between $-1/4$ and $-1/6$, consider the formation of anion vacancies together with trivalent titanium ions at normal cation sites and in interstitial positions. The reaction representing the formation of these defects can be compiled from equations (2.3) and (2.8):



where δ has a value between 0 and 1 only. By treating (6.1) in the manner described in Sec. 2 (Part II) it can be shown that:

$$[(V_{O_{2-}})^{\bullet\bullet}] \propto p_{O_2}^{-\frac{1}{2}} (\delta + 2) \quad (6.2)$$

Defect reactions similar to (6.1) can also be compiled for the other defects discussed above, and relationships of the type (6.2) are obtained.

Using only the data obtained from isothermal studies of the above type it is impossible to be more specific regarding the defect structure of non-stoichiometric rutile. The additional work on dilatometry and density measurements was undertaken in order to obtain information which would help in deciding between the alternative defect structures deducible from the oxygen-pressure work.

1.2. Dilatometric Effects of Departures from Stoichiometric Composition

Normal thermal expansion of rutile occurred in both the a and c directions up to 550°C. The values of the coefficient of linear thermal expansion in the a (α_a) and c (α_c) directions were found to be 1.45 and $0.90 \times 10^{-5}/^\circ\text{C}$ respectively. These values not only differ in magnitude from those which have been previously obtained by measurement of change in lattice parameters of rutile over a limited temperature range^(4,13), but also differ in relative magnitude since, whereas the previous workers reported that α_c was greater than α_a , in our case the reverse was found.

Bearing in mind the difficulties involved in measurement of thermal expansion by X-ray methods, and the fact that the present work was carried out on single crystals in an accurate dilatometer, it is felt that our values are likely to be more reliable. On the question of whether α_a would be expected to be either greater or smaller than α_c , it may perhaps be relevant to note that, in anisotropic solids, the coefficient of linear thermal expansion is, in general, least in the direction of closest packing of ions or atoms. In zinc and cadmium α_c is greater than α_a , and in both elements $c/a > 1$, that is the a direction is more closely packed than the c direction. Therefore in rutile where $\frac{c}{a} < 1$, the c direction is more closely packed than the a direction, and hence α_a would be expected to be greater than α_c .

Since it has been found in the present studies that a sample of rutile loses oxygen on heating in a vacuum at a temperature as low as 600°C, the dilatometric specimens would be expected to begin to depart from the stoichiometric composition at about this temperature. Between 550° and 850°C the fractional increases in length in both a and c directions were found to be greater than those expected from extrapolation of the normal thermal expansion effects which occurred at lower temperatures. A similar type of increase in the deviation from linear expansion has been observed in metals at high-temperatures⁽⁹¹⁾, and is attributed to the effect

of the presence of thermal vacancies leading to an abnormal expansion⁽⁹²⁾. In a purely ionic solid such as rock salt, the creation of an anion vacancy leads to a larger fractional volume expansion than that produced by a vacancy in a metal⁽⁹²⁾, because of the electrostatic effects arising from the removal of a negatively charged atom. The removal of an anion (Cl^-) causes the six cations (Na^+) surrounding the anion vacancy to repel each other^(49,92). In rutile the electrostatic consequences of an anion vacancy would be expected to be of this form, but might be complicated by the more complex crystal structure of rutile. The abnormal expansion in rutile would be larger than that observed in rock salt since, in addition to thermal vacancies, anion vacancies are being created as the result of departure from stoichiometry attendant on the loss of oxygen. Thus it seems likely that the additional expansion of the rutile samples in the temperature range of 550° to 850°C arises from the creation of anion vacancies in the lattice.

Above temperatures of 850°C the thermal expansion of rutile in the a and c directions behaved differently. The fractional expansion in the c direction continued to increase progressively above that expected from a normal linear thermal expansion, whereas in the a direction the extent of the abnormal expansion began to decrease with increasing temperature.

A possible explanation of the contraction observed in the a direction at high temperatures is that when the concentration of anion vacancies has increased to a sufficiently high value, they begin to cluster. When the cluster reaches a certain critical size it collapses, annihilating the vacancies, and also giving rise to cation interstitials. The production of interstitials in this way provides a mechanism for their formation in non-stoichiometric material as envisaged by Hurlen⁽²²⁾ (see equations (2.7) and (2.8)). The manner in which anion vacancies cluster and subsequently collapse must now be discussed in greater detail.

1.3. Methods of Creating Cation Interstitials

Any proposed mechanism for the formation of cation interstitials in non-stoichiometric rutile by a collapse of clustered anion vacancies must be consistent with the observed contraction in the a direction and must lead to no contraction in the c direction.

1.3.1. Interstitial Sites in Rutile

The crystal structure of rutile can be described (see Part II, Sec. 1.1) as a body-centred tetragonal array of cations at $(0,0,0)$ and $(\frac{1}{2},\frac{1}{2},\frac{1}{2})$, with anions situated at $\pm(x,x,0)$

and $\pm (\frac{1}{2}+x, \frac{1}{2}-x, \frac{1}{2})$. Thus each cation is co-ordinated with six anions. In rutile not all interstitial sites surrounded by an octahedral array of anions are occupied, those centred on $\{\frac{1}{2}, 0, 0\}$ and $\{\frac{1}{2}, 0, \frac{1}{2}\}$ are vacant. In the following discussion we will be concerned with the possible filling of these vacant octahedral sites with a cation. Tetrahedral interstitial sites also exist in the oxygen sub-lattice, but since these sites are not occupied by cations in stoichiometric rutile, it is felt to be unlikely that they will provide sites for displaced cations produced by the collapse of anion vacancies.

1.3.2. Possible Sites for Clustering Anion Vacancies

Assuming that anion vacancies cluster when their concentration reaches a sufficiently high value, and assuming that such clusters are in the form of discs, lying on particular planes in the lattice, the question arises - on which planes will vacancies preferentially cluster? In discussing this problem, we will use as criteria the restrictive conditions that clustering will only occur on those planes of anions which do not contain cations, and that after the collapse of such clusters, the cations adjacent to the plane of the collapsed disc should occupy octahedral sites. The reason why it is assumed that anion vacancies cluster on a plane rather than as a three dimensional cavity is that the

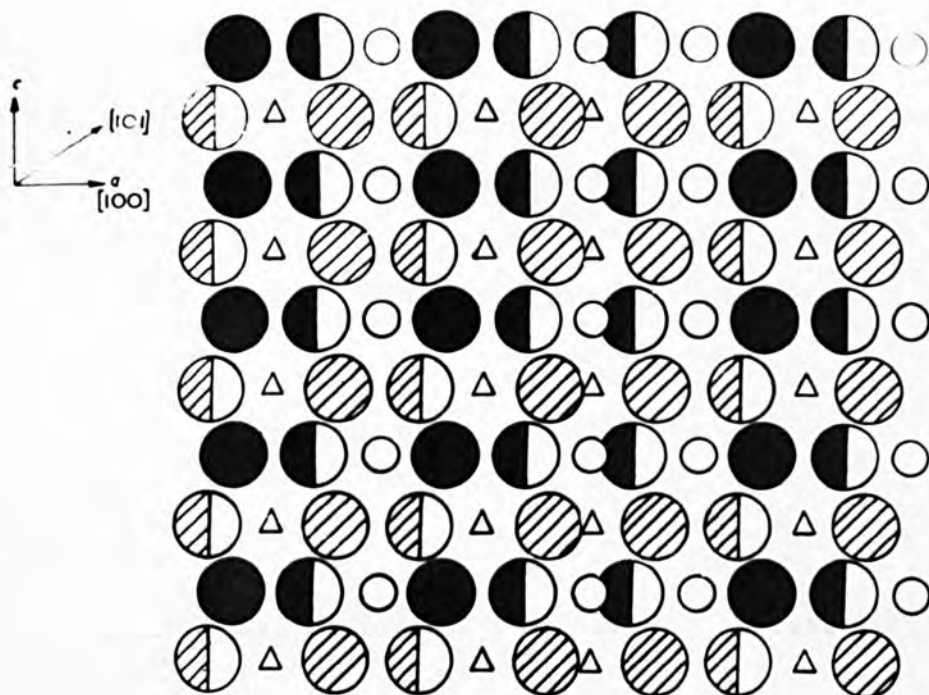


Fig. 42. Effect of removing the double plane of anions XX from Fig. 41 and moving the left-hand-side by $\frac{1}{2}[100]$. The cations on the left of XX now occupy interstitial positions sited at $(\frac{1}{2}, 0, 0)$ relative to the cations on the right. These interstitial sites are not indicated in Fig. 41(b), but are situated between the full and half-full circles.

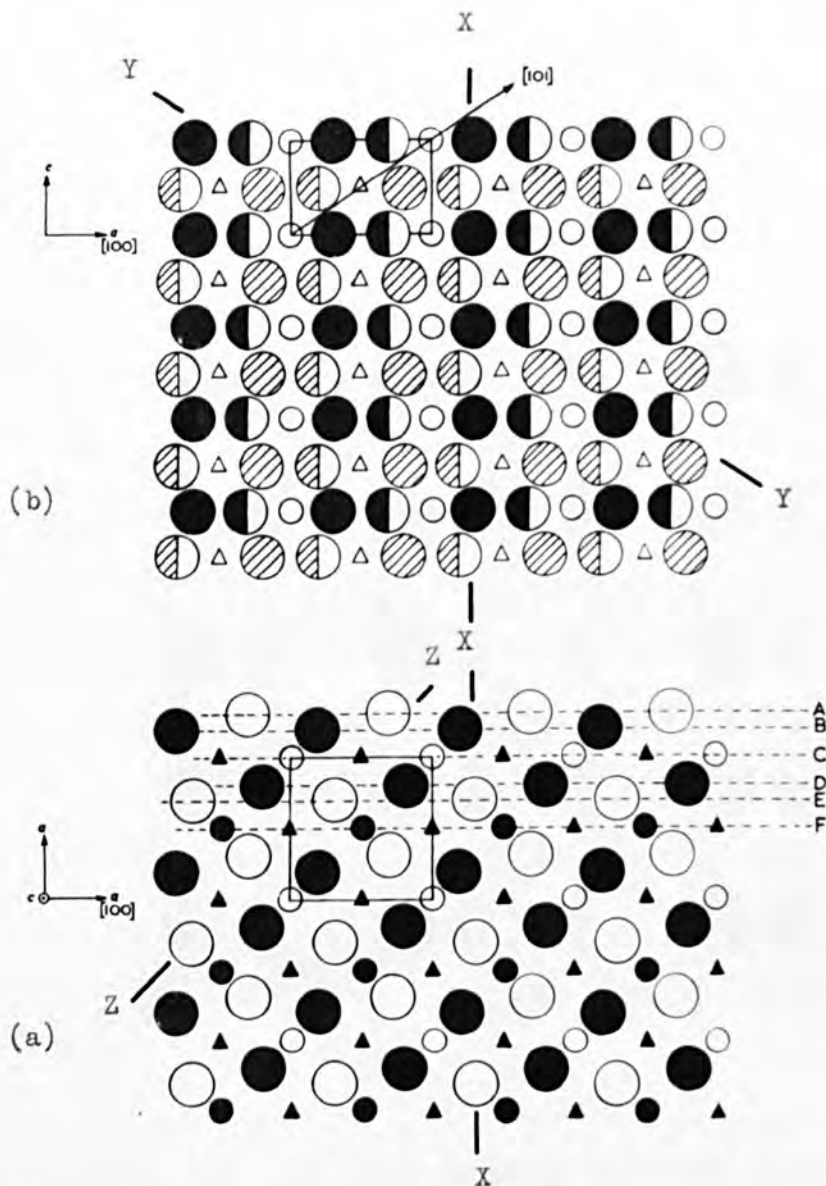


Fig. 41. Ionic arrangement of rutile:

(a) projected on an (001) plane. Large and small circles represent anions and cations respectively. All open circles lie in the same plane, which is separated by $\frac{1}{2}c$ from the plane containing closed circles. Triangles indicate unoccupied interstitial sites.

(b) projected on an (010) plane. Anions in planes A, B, D and E of (a) are projected on plane C, but interstitial positions and cations in plane F are not projected on C. Full and half-full circles represent anions in planes E and A. Shaded and half-shaded circles represent anions in planes D and B. Triangles represent unoccupied interstitial sites of the $(\frac{1}{2}, 0, \frac{1}{2})$ type relative to cations in plane C.

formation of a cavity would involve the diffusion of cations, whereas condensation on a plane need not involve cation migration.

In the rutile structure there exists three types of plane which contain only anions. These can be considered as either slightly corrugated single planes or as closely separated double planes of anions, lying parallel to $\{100\}$, $\{110\}$ and $\{101\}$ planes. It is necessary now to consider the consequences of vacancy collapse on each of these planes. This can be most conveniently done in terms of the projections of the rutile structure on (001) and (010) planes as shown in Fig. 41.

The clustering of anion vacancies on an $\{100\}$ plane is equivalent to removing the double plane of anions XX shown in Fig. 41. After removal of the plane, the ions on the left hand side of XX could close up, as a whole, by movement of one side relative to the other, either in a $[100]$ or a $[101]$ direction, in each case by a displacement equal to a half lattice vector. Movement of $\frac{1}{2}[100]$ corresponds to placing cations in the plane immediately to the left of XX into the octahedral interstitial positions sited at $(\frac{1}{2}, 0, 0)$. These interstitial positions have not been indicated in Fig. 41(b), but are located between the full and half-full circles which are close neighbours immediately to the right of XX. The resulting ionic arrangement would be that shown in Fig. 42. In the diagram the cations which were

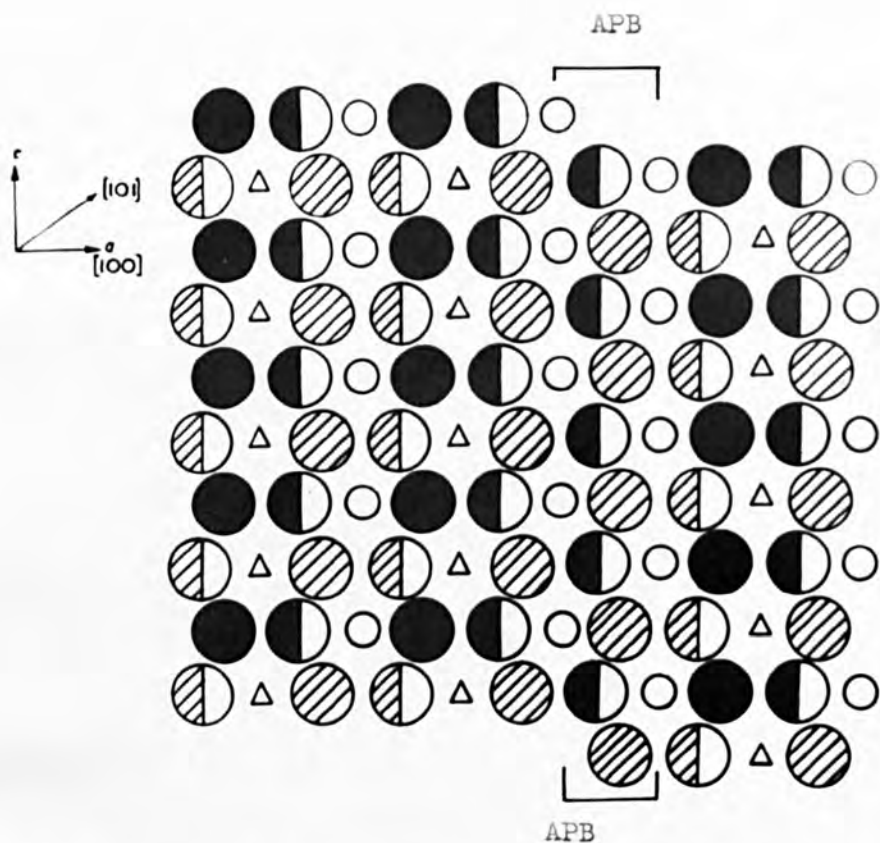


Fig. 43. Effect of removing the double plane of anions XX from Fig. 41, and moving the left-hand-side of XX relative to the right-hand-side by $\frac{1}{2}[101]$. A fault or antiphase boundary (APB) is produced in a (100) plane. Cations on the left of the APB occupy interstitial positions of the $(\frac{1}{2}, 0, \frac{1}{2})$ type relative to cations on the right. The APB consists of a doubly occupied plane of cation interstitials.

originally adjacent to XX are shown as apparently overlapping certain anions, but this is only because these anions and cations are not coplanar on the (010) plane. The geometric arrangement of the six anions about the displaced cations is not octahedral. The anions form a slightly distorted triangular prism about each cation. The lack of spherical symmetry in this prismatic arrangement would be expected to be highly unstable, and no such arrangement has ever been observed in any type of solid⁽⁹³⁾. Thus we must conclude that it is highly unlikely that the vacancies would collapse by a shear of $\frac{1}{2}\langle 100 \rangle$ about a cluster of anion vacancies on $\{100\}$ planes.

The other possibility is a collapse displacement of $\frac{1}{2}[101]$ after the removal of the double plane of anions XX shown in Fig. 41. Movement in this direction corresponds to displacing cations originally in the plane immediately to the left of XX in Fig. 41 into the octahedral interstitial positions of $(\frac{1}{2}, 0, \frac{1}{2})$ type, represented by the triangles in Fig. 41. The resulting ionic arrangement is shown in Fig. 43. In the diagram it can be seen that each cation is always surrounded by six anions in an octahedral array. The shape of the octahedron of anions surrounding a displaced cation is slightly different from the type of octahedron normally occupied by a cation. The new site for the displaced cation is in fact less distorted than the

original anion octahedra from which it is moved. In the process described above a very narrow stacking fault in the anion arrangement has been formed in a plane parallel to XX of Fig. 41, and associated with this is a plane of cations having a density of occupation twice that of a normal plane. This fault is in some ways similar to that found at an antiphase domain boundary in an ordered structure⁽⁹⁴⁾. It differs from a simple antiphase domain boundary, however, because on each side of the fault cations occupy different types of octahedral interstices, and at the boundary both types of interstitial sites are occupied. This process can only occur in a structure such as rutile in which half the total number of interstitial cation sites are normally vacant. For example, let us consider a (101) plane of cations in normal rutile shown in Fig. 41, the sequence in cation position is:

circle - triangle - circle - triangle - .

In Fig. 43, where a (100) plane of vacancies has collapsed, the sequence in the same (101) plane is:

circle - triangle - circle - circle - triangle - circle - .

For this reason the fault of cation interstitials will be termed an antiphase boundary, furthermore a similar nomenclature has been used by other workers in this field.⁽⁸⁹⁾

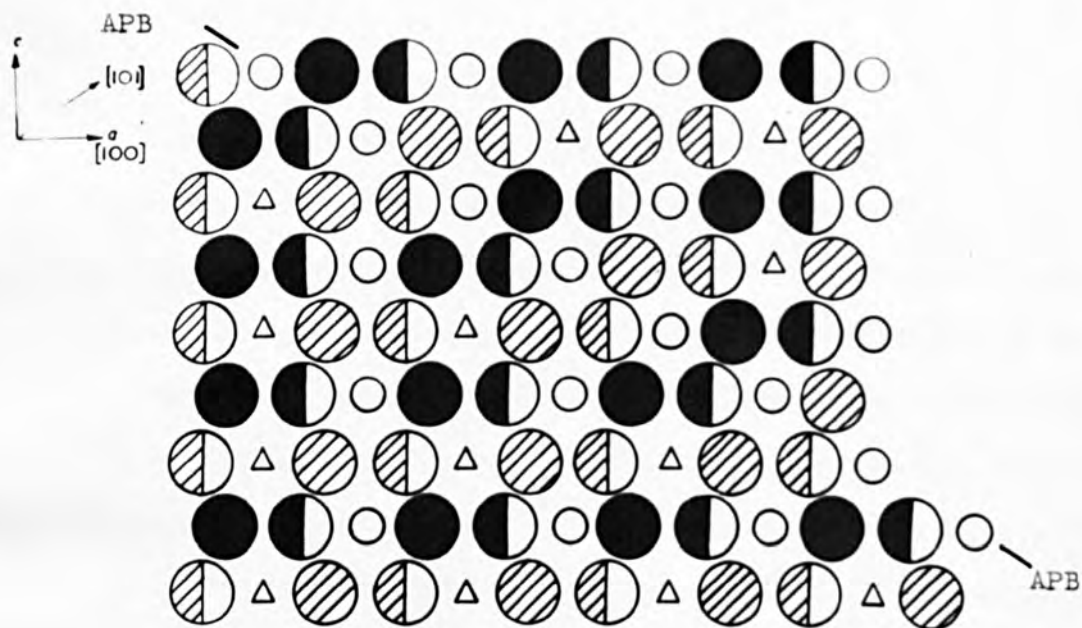


Fig. 44. Effect of removing the double plane of anions XX from Fig. 41(b) and moving the left-hand-side of YY by $\frac{1}{2}[101]$, relative to the right-hand-side. An APB consisting of a doubly occupied plane of cation interstitials is formed in a (101) plane.

So far we have considered the collapse of a cluster of anion vacancies on the $\{100\}$ planes in two directions. If the other two types of double planes suitable for clustering, i.e. $\{101\}$ and $\{110\}$, are considered in a similar way, it can be shown that only by a movement of $\frac{1}{2}\langle 101 \rangle$ can the octahedral arrangement of anions about cations be maintained at the fault. In Fig. 44 the effect of removing a (101) plane of anions, shown at YY in Fig. 41(b), and collapsing the structure by a displacement of $\frac{1}{2}[101]$ has been illustrated. A doubly occupied antiphase boundary of cation interstitials has been formed on a (101) plane. No attempt has been made to present a diagram showing the consequences of removing a (110) plane (ZZ, in Fig. 41(a)), since, because of the complicated arrangement of ions when projected on a (110) plane, such a figure is extremely confused. It can be shown, however, that an antiphase boundary of cations is formed in a (110) plane after displacing the structure by $\frac{1}{2}[101]$.

Thus it seems possible that anion vacancies cluster on double planes of anions of the type $\{100\}$, $\{101\}$ and $\{110\}$, and that the lattice can only be displaced by $\frac{1}{2}\langle 101 \rangle$ when the cluster collapses. It is important to note that in all of the cases considered there is an overall contraction of the lattice in the a direction coupled with a slight expansion in the c direction.

1.4. Variation of the Density of Rutile with Departure from Stoichiometric Composition

1.4.1. Theoretical

If x anion vacancies are created in unit mass of sample, without change in volume, then the density of the now non-stoichiometric sample of rutile ρ_n will be given simply by:

$$\rho_n = \rho_s (1 - kx) \quad (6.3)$$

where ρ_s is the density of stoichiometric rutile (4.2502 gm/cc) and k is equal to the reciprocal of the constant used to convert fractional changes in weight of a sample of rutile into concentrations of anion vacancies (see Sec. 9, Part III). The density of rutile will, therefore, decrease as departures from the stoichiometric composition occur.

The next step is to consider the case of condensation of vacancies, that is to say, the effect of creating x anion vacancies per unit mass of a sample of stoichiometric rutile, and then reducing its volume by an amount equal to the volume of anions removed. The decrease in volume of unit mass can be estimated from a knowledge of the ionic radius (r) of an oxygen ion, which is reported to be $1.45 \text{ \AA}^{(4)}$, and will be equal to $\frac{4}{3} \pi r^3 x N M^{-1} 10^{-24}$ cc. where N is Avogadro's Number and M the molecular weight of rutile. The density of a sample of

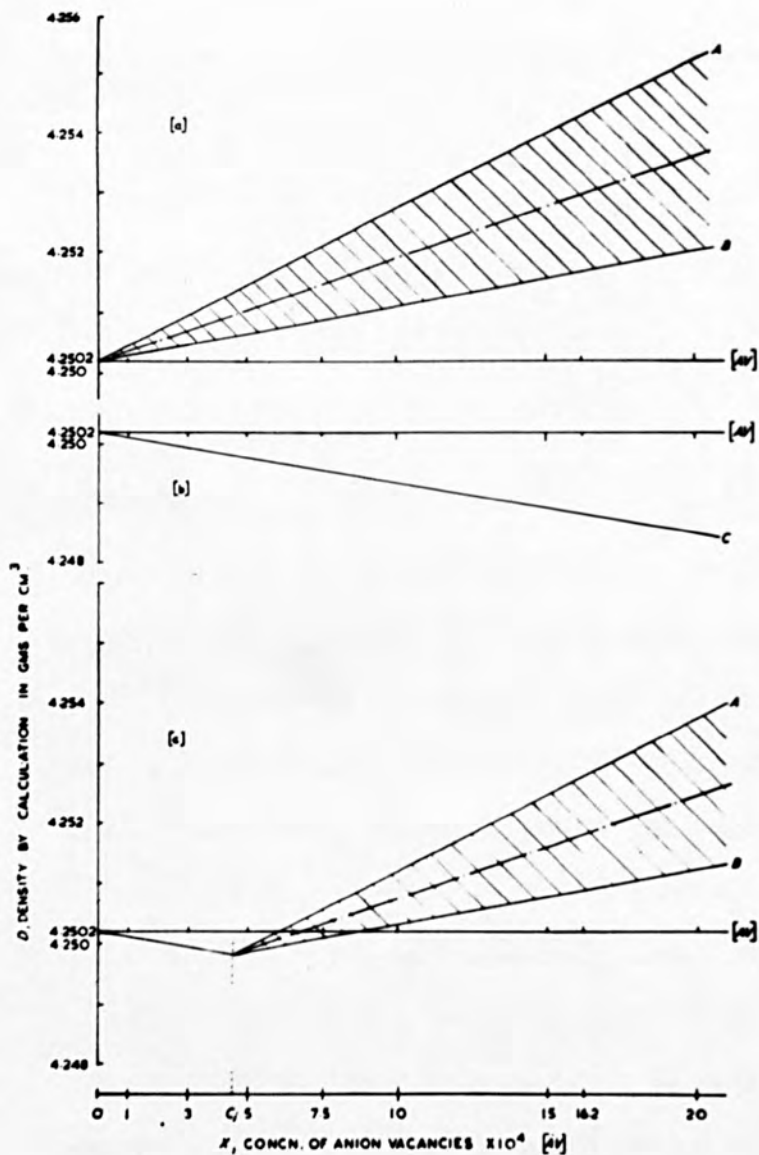


Fig. 45. Theoretical variation of the density of rutile on departure from the stoichiometric composition: (a) lattice collapse about a cubical volume, A, and a spherical volume, B; (b) on the creation of anion vacancies only; and (c) on creating anion vacancies up to a composition c_1 and then forming cation interstitials.

non-stoichiometric rutile in which the vacancies have collapsed will thus be given by:

$$\rho_n = \frac{\rho_s(1 - kx)}{1 - \frac{4\pi r^3 x n \rho_s}{3 \cdot 10^{24} M}} \quad (6.4)$$

Should be N

This formula has been derived on the assumption that the lattice collapses about anion vacancies which have a spherical volume. This case represents the minimum possible reduction in volume due to the collapse of vacancies. The case of reducing the volume by the largest amount must also be considered. Here it is assumed that the anion vacancies cluster to form a series of cubes of side equal to the diameter of an oxygen ion. Equation (6.4) now becomes:

$$\rho_n = \frac{\rho_s(1 - kx)}{1 - \frac{8r^3 x n \rho_s}{10^{24} M}} \quad (6.5)$$

Values of ρ_n have been calculated for a range of values of x for all three cases (see Appendix VI), and the data is presented in a graphical form in Fig. 45. Lines A and B in Fig. 45(a) correspond to ρ_n calculated according to equations (6.5) and (6.4) respectively. In practice it is to be expected that ρ_n will be within the shaded region lying between the lines A and B.

Earlier it was proposed that only anion vacancies are present in slightly non-stoichiometric rutile, while in highly non-stoichiometric rutile the anion vacancies collapse and give rise to excess cations at a fault. Thus the density of rutile would be expected to decrease in the initial stages of departure from stoichiometric composition, and then increase as the vacancies collapse. Thermodynamically, condensation of vacancies will occur when the free energy of a condensed vacancy is equal to the free energy of a free vacancy. Because of the entropy effect, the free energy of free vacancies will depend on their number, it being assumed that they are randomly distributed throughout the material. Thus at large departures from stoichiometric composition the density of free vacancies will remain constant at some value c_i as indicated in Fig. 45(c). The lines A and B shown in Fig. 45(a) must now be transposed so that their origin lies at the density ρ_n for which the concentration of free vacancies is c_i .

1.4.2. Experimental

The density of a sample containing a small concentration of anion vacancies has been found to be less than the density of stoichiometric rutile. A sample containing a high concentration of anion vacancies had, however, a density greater than that of

stoichiometric rutile, which can be taken as an indication that cation interstitials were present in this sample. Although only a few measurements of the density of samples of non-stoichiometric rutile of known composition were made, the observed trend agrees with the type of density variation calculated in the previous section.

It is interesting to compare the variation of the density of non-stoichiometric rutile found in the present investigation, with that which has been reported in the literature. Straumanis et al.⁽¹³⁾ state that the density of rutile decreases continuously with increasing departure from stoichiometric composition whilst Prener⁽⁶⁰⁾ finds the opposite. None reported, however, an initial decrease followed by an increase, as found in the present studies. Since all available data on the density changes is contradictory, there is obviously a need for a systematic re-investigation of the effects of departures from stoichiometric composition on the density of rutile.

1.5. Applicability of Proposed Defect-Model to Results of Other Workers

Having proposed a model for the defect structure of non-stoichiometric rutile, it is necessary to consider to what extent published data of other workers either supports or contradicts the model. The work of Buessem and Butler⁽¹⁹⁾, discussed in

Sec. 1.1, indicates that the departure from stoichiometric composition of rutile varies inversely as the one-sixth power of the oxygen pressure, from which it would be concluded that cation interstitials are not formed. However, these workers used high partial pressures of oxygen, and, therefore, were only concerned with small departures from the stoichiometric composition where anion vacancies would be expected to be present.

Recently, Kofstad⁽⁹⁵⁾ has reported that the composition of rutile varies inversely as the one-sixth-power of the oxygen pressure at extremely low partial pressures of oxygen (10^{-16} atm), from which it must again be concluded that cation interstitials are not formed. Kofstad, however, used a gaseous mixture of carbon monoxide and carbon dioxide, to obtain low partial pressures of oxygen. It is not known to what extent carbon enters the rutile and interferes with the defect structure of the material. If carbon goes into solution as C^{4-} ions, it may very well give rise to associated vacant anion sites in order to preserve electrical neutrality. In this way, a progressive increase in free vacancies, leading to a one-sixth power law, could well persist up to high departures from stoichiometric composition.

Straumanis et al.⁽¹³⁾ have reported that on departure from the stoichiometric composition, the a parameter of rutile decreases in magnitude, whilst the c parameter increases. The

composition of the samples studied by these workers was between 10^{-3} and 10^{-2} anion vacancies per molecule of rutile, which are relatively large departures from the stoichiometric composition compared with those studied in the present investigation. The decrease in the a parameter agrees with the contraction observed in the a direction in the dilatometric specimen at temperatures above 850°C . Unfortunately, Straumanis et al. did not study the effect of small departures from the stoichiometric composition on the lattice parameters of rutile, where from our results an increase in a would be expected. The increase in c parameter agrees with the dilatometric results.

As a result of an investigation into the effects of departures from stoichiometric composition on the dielectric constants of rutile, in the a and c directions, Hollander and Castro⁽⁹⁶⁾ have proposed that needle-like conducting regions oriented parallel to the c axis are present. The needles were thought to consist of trivalent cations in interstitial positions, and hence are very similar to the antiphase boundaries of cation interstitials discussed in previous sections. In our earlier discussion no one particular type of plane was selected as the most favourable for clustering of anion vacancies, but Hollander and Castro's results would best be explained in terms of planes of the type $\{100\}$ or $\{110\}$ which would in both cases lead to antiphase boundaries parallel to the c direction.

The optical absorption of rutile has been recently re-investigated by von Hippel et al.⁽⁹⁰⁾. In slightly non-stoichiometric rutile, produced by heating samples at temperatures of up to 900°C in oxygen at atmospheric pressure, the infra-red spectrum was found to differ little from that of stoichiometric rutile. This finding was interpreted as indicating that anion vacancies with one associated electron were present in the samples. In highly non-stoichiometric rutile, produced by heating samples in a vacuum at temperatures up to 950°C, a strong discolouration band was found, similar in type to that observed by other workers^(27,59). The band was thought to arise as the result of what is described by von Hippel et al. as 'lattice breakdown and chemical dislocations'. It is possible, therefore, to interpret this statement as meaning that the lattice collapses about clusters of anion vacancies so that stacking faults, or antiphase boundaries as we have called them, are formed.

Using electron spin-resonance techniques, Chester^(58,81) has shown that trivalent titanium ions can be detected in interstitial sites in samples of rutile which have been reduced in hydrogen, but cannot be detected in samples reduced in a vacuum. The former type of reducing condition leads to very large departures from the stoichiometric composition, but even on reduction in vacuo at the temperatures used by Chester⁽⁵⁸⁾,

cation interstitials would have been expected to be formed on the basis of the results obtained in the present studies. However, Chester did not carry out a very extensive study using vacuum-reduced rutile, and as a result was of the opinion^(58,81) that it was impossible to be dogmatic about whether or not interstitial cations are formed in rutile on reduction in vacuo.

Published data available at the present time would, therefore, in general, appear to support the model we have proposed for the defect structure of non-stoichiometric rutile. However, up to this stage in the discussion, only effects of departures from stoichiometric composition in a perfect crystal of rutile have been considered, and the model should now be extended to include real crystals containing dislocations. The origins of the driving force which causes a tendency for anion vacancies to cluster, and the factors affecting the choice of sites on which clustering will subsequently take place, must also be considered. In addition the electronic effects of non-stoichiometry in rutile have been neglected in the discussion so far. All of these factors will now be considered in greater detail.

1.6. Electronic Effects of Non-Stoichiometry in Rutile

When rutile departs from stoichiometric composition, two electrons are liberated for every oxygen atom removed.

These electrons must be accommodated in the material, and there exists a number of ways in which this can be done. These are as follows:-

- (i) Both electrons can be localised in the vacant anion site giving rise to an F' -centre⁽⁴⁹⁾.
- (ii) Since the excitation energy of a single electron out of an F' -centre is usually small, it is possible that only a single electron can be accommodated in a vacant anion site leading to the formation of an F -centre. The other electron can then either be free as a conduction electron, or associate itself with a cation adjacent to the anion vacancy forming, in the case of rutile, a trivalent titanium ion.
- (iii) Both electrons can be attached to adjacent cations forming a pair of trivalent ions and an uncharged vacancy.
- (iv) One electron can be attached to an adjacent cation forming a trivalent ion, the other electron, being free as a conduction electron.
- (v) The two electrons could both be in the conduction band.

Since the electrons will have different energies in these various states, the extent to which they will populate the states will be governed by temperature.

It has been suggested earlier that at high temperatures the electrons attach themselves to cations, which results in the formation of trivalent titanium ions at either normal cation sites at small departures, or interstitial positions at large departures from the stoichiometric composition. The suggestions are based solely on the results of the isothermal and dilatometric studies described earlier, since in the present investigation, no work on physical properties has been carried out to obtain data which could be used to test these views. Hence it is necessary to rely on existing published data for a discussion of their possible validity. Unfortunately most of the electronic effects of departures from stoichiometric composition in rutile have been studied only at room temperature and electronic equilibrium at high temperatures, which is particularly relevant to this discussion, cannot be retained in a sample on quenching⁽²¹⁾, and, therefore, remains for the present unknown.

Studies of the optical absorption of rutile at room temperature⁽⁵⁹⁾ have shown that at very small departures from the stoichiometric composition, anion vacancies with two associated electrons (F'-centres) are present. However, it is unlikely that F'-centres will exist at high temperatures. At larger departures from the stoichiometric composition only F-centres are considered to be present⁽⁵⁹⁾. Since two electrons are associated with the creation of an anion vacancy, and as an

F-centre consists of an anion vacancy with a single associated electron, the state of the other electrons must be either a free electron or a trivalent titanium ion.

On departure from the stoichiometric composition, rutile has been found to become highly paramagnetic, due to the formation of trivalent titanium ions⁽¹⁰⁾. At room temperature the magnitude of the magnetic susceptibility can be explained if it is assumed that only a fraction of the total number of available electrons are located at cation sites, and the remaining electrons are in states in which they make only a small contribution to the susceptibility⁽¹⁰⁾. An electron in an F-centre has this type of property^(25,49), so that the susceptibility data would seem to indicate that at room temperature both trivalent titanium ions and F-centres are present in non-stoichiometric rutile. From susceptibility measurements made at low temperatures⁽¹⁰⁾ it has been suggested that the number of trivalent ions decreases with decreasing temperature, whilst the number of F-centres increases by the transfer of electrons from trivalent ions to uncharged anion vacancies. Although no data has been reported at high temperatures, the opposite trend would be expected to occur when the temperature was increased. Support for this view can be gained from a consideration of the alkali halides, in which the concentration

of F-centres has been shown to decrease with increasing temperature^(25,49).

From studies of the electrical conductivity and Hall coefficient of non-stoichiometric rutile at high temperature, it has been concluded that conduction electrons are present. Breckenridge and Hosler⁽²⁷⁾ have suggested that the low mobility and high effective mass of these conduction electrons indicate that the conduction band is a narrow 3d-band. Morin⁽⁶²⁾ has postulated that a narrow conduction band will be present in the oxides of the early transition metals by overlap of the 3d-electronic levels of the cations. The band is expected to be empty in stoichiometric rutile when all cations are in the tetravalent state. Electrons may, however, be expected to be present in this band at high temperatures in non-stoichiometric rutile by excitation of the single electron associated with a trivalent titanium ion. The dielectric work of Hollander⁽⁹⁶⁾ and optical absorption results of von Hippel⁽⁹⁰⁾ also lend support to the view that trivalent cations are formed in non-stoichiometric rutile.

The picture of the electronic states which can be envisaged solely by consideration of the rather inadequate experimental data is rather confused. This is especially so because the electronic occupation of the various possible states

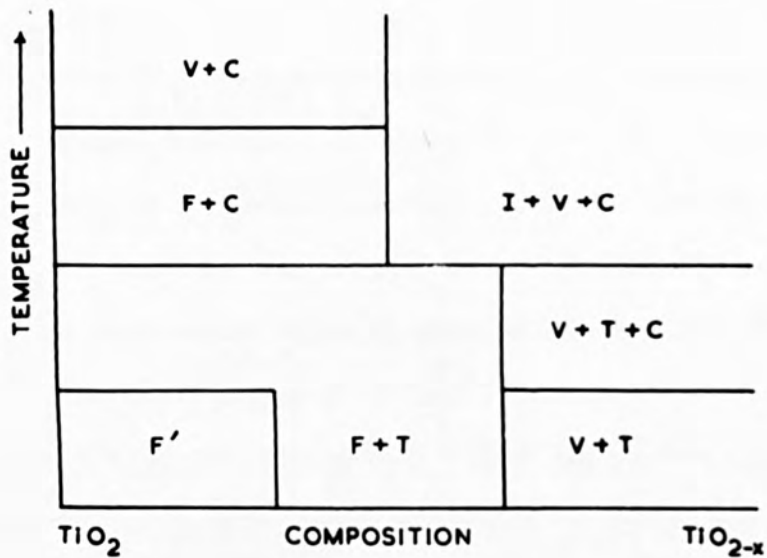


Fig. 46. A schematic diagram of the possible defect structure of non-stoichiometric rutile as a function of temperature and composition. (after McQuillan⁽⁹⁷⁾).

- F' - F' centre
- F - F-centre
- V - uncharged anion vacancy
- C - conduction electrons
- T - trivalent titanium ions at normal cation sites.
- I - trivalent titanium ions in interstitial positions

will be a function of both composition and temperature. As an illustration, in a purely diagrammatic form, of the type of behaviour which could ultimately be revealed, the nature of the defects in non-stoichiometric rutile as a function of temperature and composition has been sketched in Fig. 46.

Before discussing the origins of the driving force for the clustering of anion vacancies, we must consider which electronic state would most likely lead to clustering. It has been suggested that, at high temperatures, trivalent cations plus uncharged anion vacancies are likely to be present as defects in slightly non-stoichiometric rutile. The electrically neutral vacancies are in a very favourable condition for clustering, since they are uncharged and hence will not electrostatically repel each other. If, however, F-centres are present, it is difficult to envisage how clustering could take place, since, being negatively charged, they would repel each other.

The process by which the collapse of clustered anion vacancies gives rise to trivalent interstitial ions can be envisaged as follows. After collapse there is a plane of titanium ions having a population twice that of a normal cation plane in rutile, and hence there will be a large accumulation of positive charge at this position which must be shielded by conduction electrons. Thus collapse of vacancies can only be

expected when the material is no longer an insulator. Once collapse has taken place the interstitial cations can only remain if they reduce their ionic charge by capturing a conduction electron and becoming trivalent. The fault now consists essentially of a plane of Ti_2O_3 .

1.7. Origins of the Driving Force, and Possible Nuclei for Clustering

It has been suggested that uncharged anion vacancies are most likely to cluster, and so we must now consider the origins of the driving force which leads to clustering. The possibility of vacancies forming clusters in ionic solids has not received much attention in the past, and so once again it will be necessary to fall back on the use of effects which have been found to occur in metals.

A vacant lattice site has a strain energy associated with it⁽⁹²⁾, and in metals it has been shown from elasticity considerations that when two vacancies combine to form a divacancy, there is an overall reduction in strain energy⁽⁸⁶⁾. In addition, it has also been shown that when metals contain a high concentration of vacancies, the vacancies tend to condense, i.e. cluster, forming voids in the lattice^(94,98). Furthermore, divacancies can act as sites for nucleating voids⁽⁹²⁾. If these findings are extended to include rutile,

it would seem likely, since a lattice strain is associated with an anion vacancy, that at large departures from the stoichiometric composition anion vacancies, if uncharged, would tend to cluster. In so doing an overall reduction of the strain energy of the system occurs. As these processes are considered to be taking place at high temperatures, the effect of forming anion vacancy clusters on the entropy of the system will have to be taken into account. From a consideration of entropy alone, a system always tends to the state of maximum disorder⁽⁸⁶⁾ and so a random distribution rather than clusters of anion vacancies would be favoured in non-stoichiometric rutile. However, in order that clustering should take place, the resultant reduction in free energy of the system must more than compensate its decrease in entropy. A possible explanation for this is that the reduction in free energy is large owing to the high strain energy associated with an anion vacancy in an ionic solid⁽⁹²⁾.

It thus seems most probable that, in a perfect crystal, anion vacancies cluster on nuclei of di-anion vacancies. The model should now be extended to include imperfect, real crystals.

Many types of imperfection exist in a real crystal at high temperatures^(86,94), the majority of which are thermal points defects. In addition line defects or dislocations are

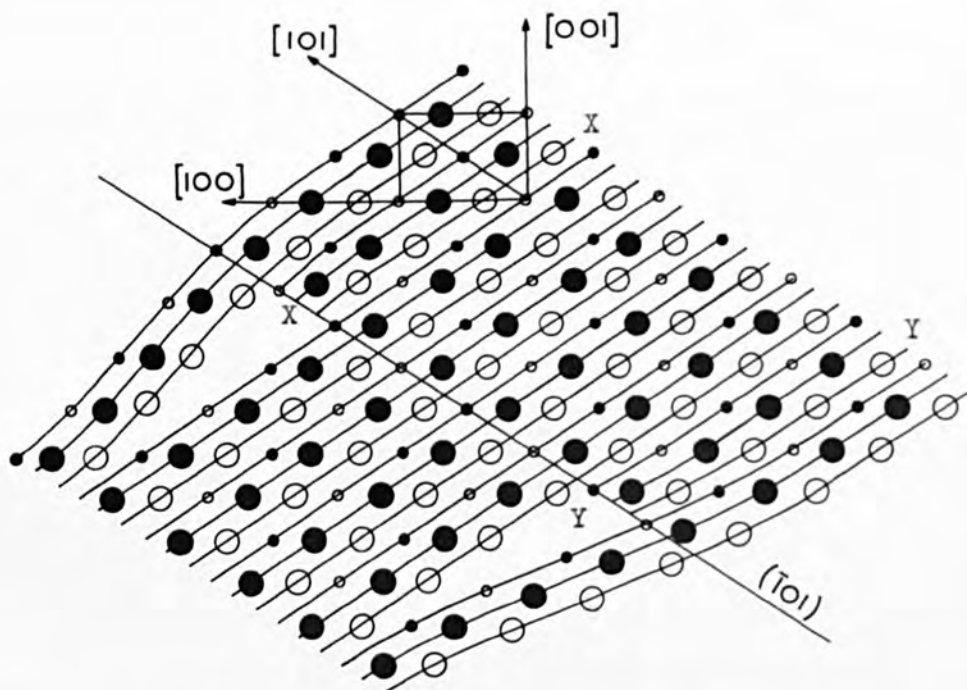


Fig. 47. Schematic diagram of partial dislocations on the $(\bar{1}01)$ system when viewed in the $[010]$ direction. Small and large circles represent cations and anions respectively. Full and open circles indicate ions in different planes. Anions and cations with the same symbol are not coplanar. Diagram after Ashbee⁽⁸⁹⁾.

present, which have been shown to interact with point defects^(92,94) and to act as sources and sinks for other defects^(94,98). In metals, dislocations can climb by accepting vacancies⁽⁹⁴⁾, which leads to a reduction in both the line energy of the dislocation and the strain energy associated with the vacancy⁽⁸⁶⁾. Similar types of interaction also occur in ionic solids for the same reasons⁽⁸⁶⁾.

Let us now consider a crystal of rutile containing dislocations. From a study of the mechanical properties of stoichiometric rutile, Ashbee⁽⁸⁹⁾ has shown that in rutile slip occurs mainly in $\langle 101 \rangle$ directions, even though a Burgers vector of $\langle a \ 0 \ c \rangle$ is not the shortest lattice vector. It was thus proposed⁽⁸⁹⁾ that the Burgers vector of dislocations gliding on a $\{101\} \langle 101 \rangle$ type of system were of the $\frac{1}{2}\langle a \ 0 \ c \rangle$, i.e. $\frac{1}{2}\langle 101 \rangle$ type. In consequence, superdislocations consisting of two partial dislocations separated by an antiphase boundary are formed on $\{101\}$ planes. The arrangement of the ions in a crystal of rutile containing a superdislocation of this type on a $(\bar{1}01)$ plane is shown in the diagram in Fig. 47. In the diagram the ionic arrangement of rutile has been simplified since only two, instead of four, different types of anion have been symbolised: anions on planes A and B, and planes C and D of Fig. 41(a) have been considered to be coplanar in Fig. 47.

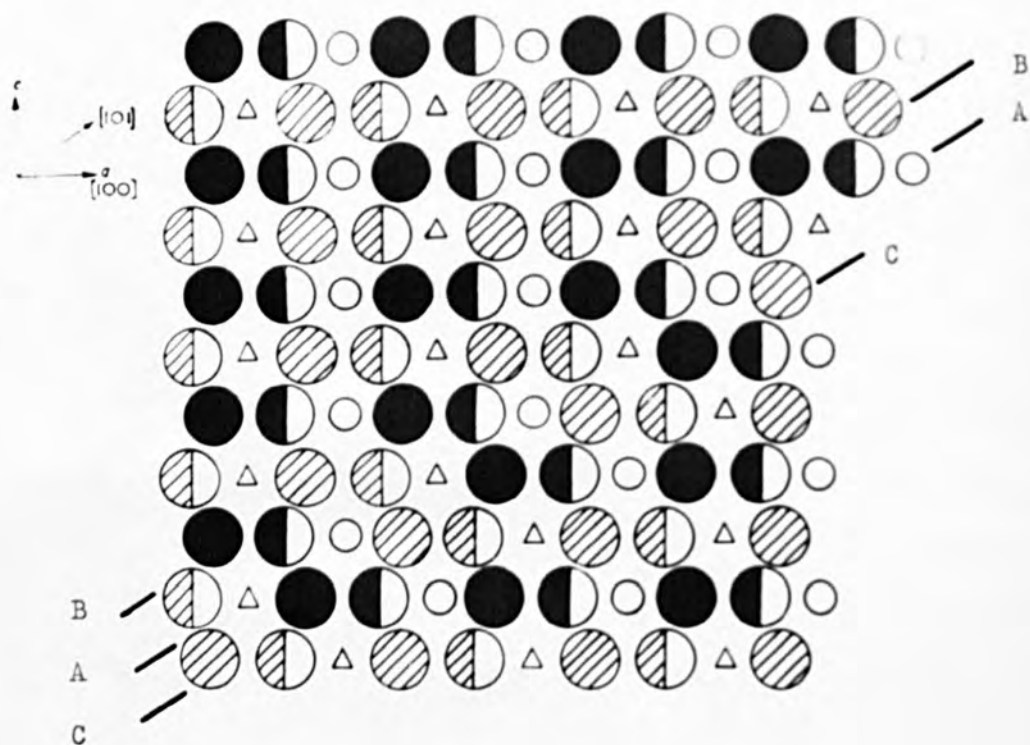


Fig. 48. Schematic diagram of the APB lying on the $(\bar{1}01)$ plane between X and Y in Fig. 47, redrawn using the same symbols as Fig. 41. The APB is indicated at AA.

A consequence of having an extended or superdislocation of the above type in rutile is that the Peierls-Nabarro⁽⁹⁴⁾ force opposing motion of the partial dislocations is smaller than in the non-extended case⁽⁹⁴⁾. If anion vacancies migrate to the ends of the antiphase boundary, the partial dislocations would be expected to climb, in an effort to reduce the strain energy of the system.

The process of clustering of anion vacancies on partial dislocations can be illustrated with reference to the diagram in Fig. 47. If clustering takes place on the double (101) planes of anions XX and YY, and a shear occurs in the appropriate direction by $\frac{1}{2}\langle 101 \rangle$, then the partial dislocations would move along XX and YY, in a $[\bar{1}01]$ direction.

It is also possible for anion vacancies to cluster on the double planes of anions adjacent to the antiphase boundary, i.e. in $(\bar{1}01)$ planes of Fig. 47. In order to consider this possibility, that part of the diagram, shown in Fig. 47, which includes the antiphase boundary, has been redrawn in Fig. 48 where the ions are represented by the symbols used in Fig. 41. In Fig. 48 the antiphase boundary has been indicated at AA, and can be seen to differ from that formed by a collapse of the lattice about a cluster of anions on an (101) plane (see Fig. 44). The former type of antiphase boundary consists

of alternate cation (open circles) and interstitial sites (open triangles), whereas the latter consists of cation sites only.

Let us now consider the consequences of clustering anion vacancies on the double plane (BB) immediately above the antiphase boundary shown at AA in Fig. 48. After removal of BB, followed by a shear in the appropriate direction of the type $\frac{1}{2}\langle 101 \rangle$, the antiphase boundary would become identical to the fault illustrated in Fig. 44. If, however, the double plane CC of Fig. 48 were removed, then it is impossible for a shear of the $\frac{1}{2}\langle 101 \rangle$ type to take place, since there are no interstitial sites in this direction. Instead, a shear of $[001]$ would have to take place in order that cations should move into interstitial positions. The possibility of this unusual type of shear has not been proposed in the foregoing, since it would normally only operate if clustering takes place in $\{001\}$ planes. It is doubtful if clustering could occur on these planes because, in addition to anions, they also contain cations. Thus it is proposed that a shear of $\langle 001 \rangle$ can only occur when anion vacancies cluster on antiphase boundaries forming part of a superdislocation in rutile. It is interesting to note that Hirthe⁽⁸⁸⁾ has reported that slip occurs in stoichiometric rutile by slip in an $\langle 001 \rangle$ direction on $\{110\}$ planes.

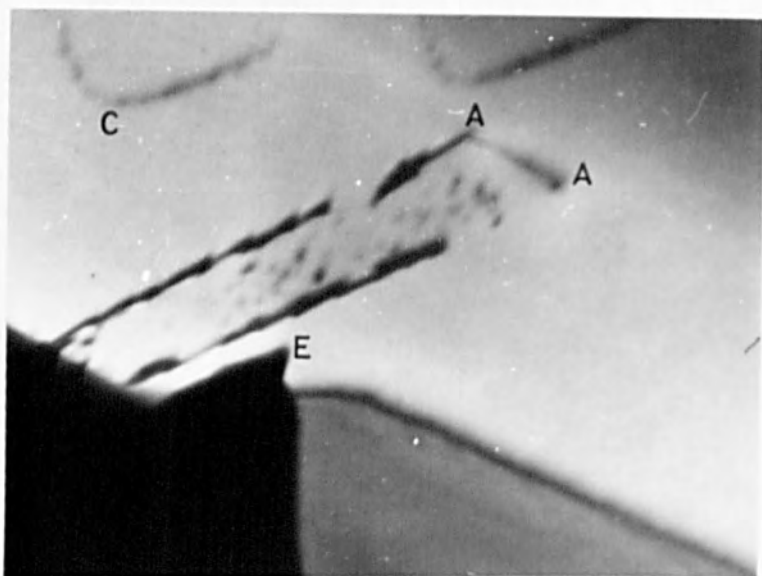


Fig. 49(e). Area of loop nearly equal to that of fault.

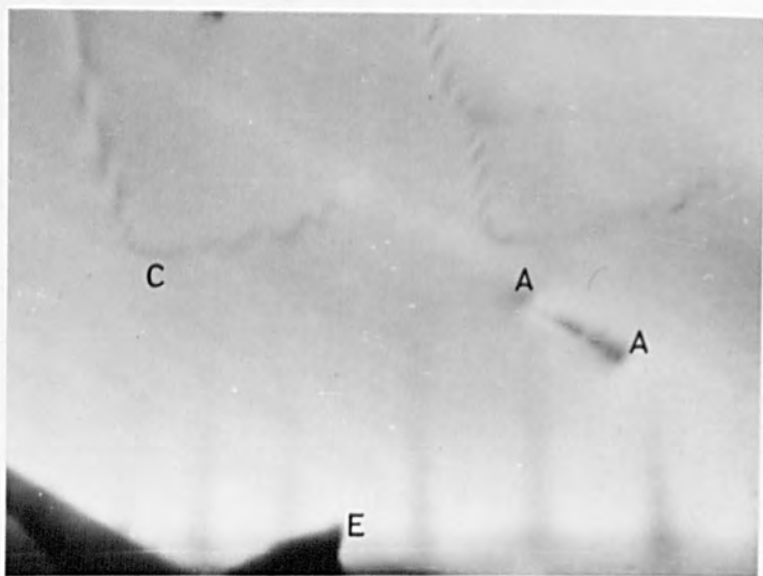


Fig. 49(f). Stacking fault removed. (Note that field of view slightly different to that in (a) to (e).)

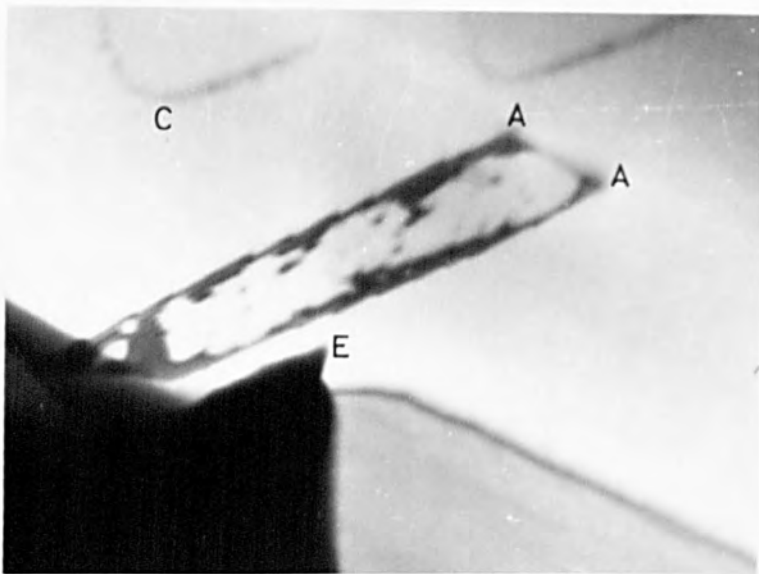


Fig. 49(c). Loops expanding and beginning to coalesce.

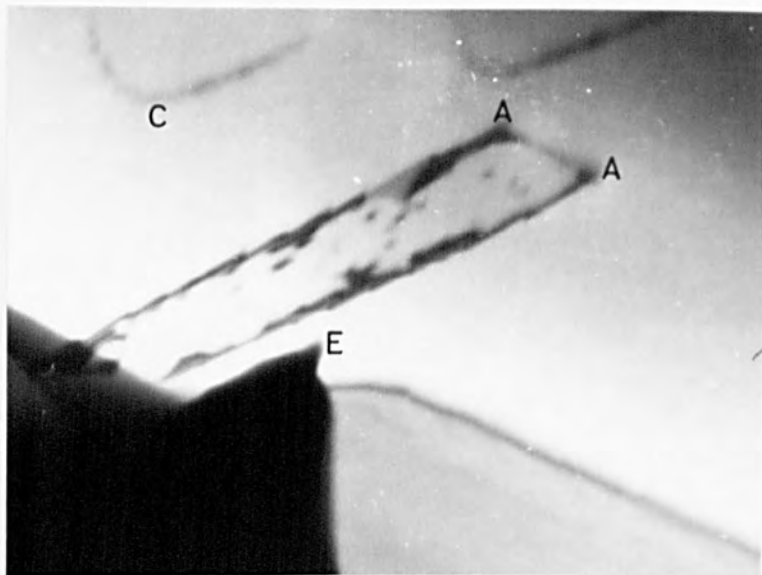


Fig. 49(d). Coalesced loops expanding.

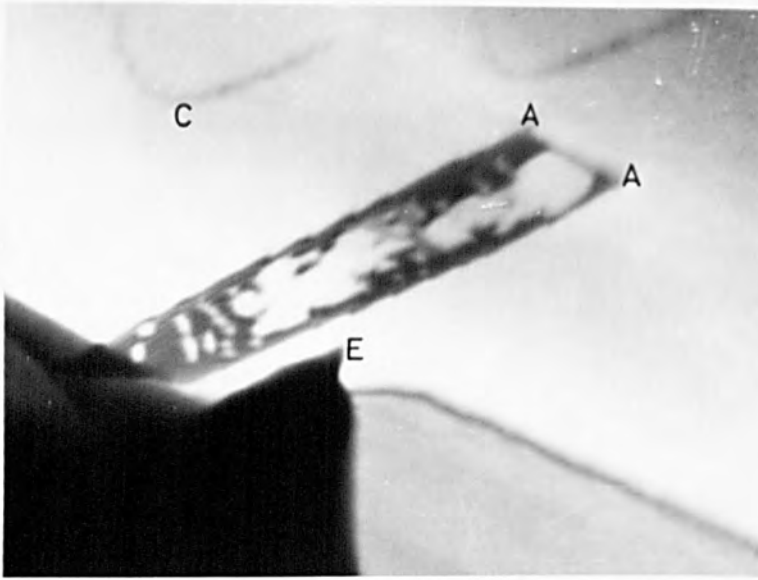


Fig. 49(a). Loops of vacancies nucleated on fault.

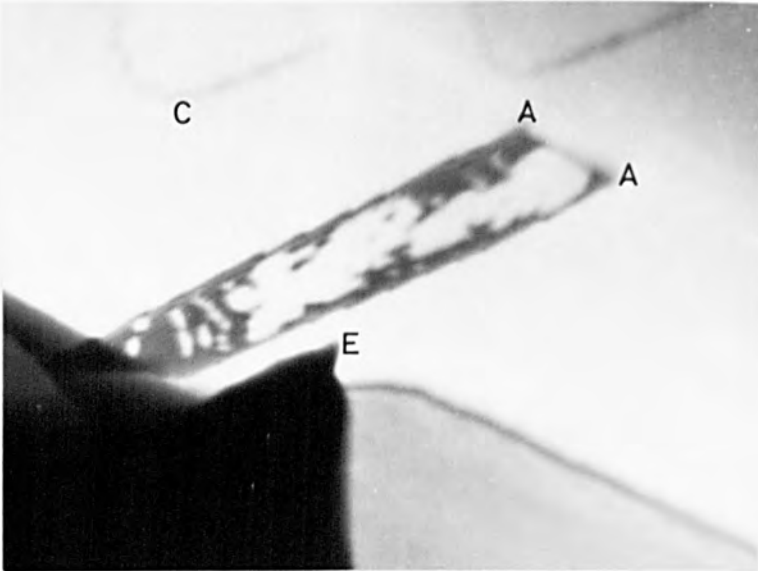


Fig. 49(b). Loops expanding.

Fig. 49. Sequence of electron micrographs (magnification X68,000) showing the growth of loops of anion vacancies on a stacking fault lying on a $\{101\}$ plane of rutile. Micrographs reproduced by kind permission of Smallman(99).

Ashbee⁽⁸⁹⁾ has reported that the strength of single crystals of rutile increases as departure from the stoichiometric composition occurs. A possible cause for the increase in strength could be that the boundary surrounding the collapsed disc of vacancies on $\{110\}$ and $\{100\}$ planes acts as sessile superdislocations. It would then be expected to interfere with slip on the usual $\{101\}$ planes. In a metal, sessile dislocations interfere with the normal process of slip, and lead to an increase in strength of the metal⁽⁹⁴⁾.

Very recently Smallman et al.⁽⁹⁹⁾ have obtained some evidence which shows that anion vacancies cluster in non-stoichiometric rutile. The evidence was obtained as a result of the direct observation, in an electron microscope, of the effects of non-stoichiometry on a thin flake of rutile. The flake was oriented with the (110) plane of the rutile structure in the plane of the flake. A stacking fault was observed continuously as the flake was heated and hence departed from the stoichiometric composition. The sequence of events which was observed is reproduced in the electron micrographs shown in Fig. 49, where a stacking fault lying on a $\{101\}$ plane of the flake is shown. When departure from the stoichiometric composition began to occur, loops of anion vacancies were nucleated in the fault (Fig. 49(a)). As the extent of departure increased the loops expanded and began to coalesce, as shown in

Figs. 49(b) and (c). The coalesced loops continued to expand (Figs. 49(d) and (e)) by the addition of vacancies, until eventually all that remained was the partial dislocation terminating the stacking fault, shown at AA in Fig. 49(f).

Up to the present time, however, no studies have been made using an electron microscope to see if clustering of anion vacancies takes place on stacking faults in $\{100\}$ and $\{110\}$ planes.

2. Maximum Extent of Non-Stoichiometry in Rutile

The main features resulting from the studies on the extent of departures from the stoichiometric composition produced by heating samples of rutile in a high vacuum are:

- (i) departures from the stoichiometric composition begin to occur at temperatures as low as 600°C ,
- (ii) at a fixed temperature the extent of the departure from the stoichiometric composition is larger the greater the degree of impurity of the material. The behaviour of the single-crystal sample of rutile is excluded from this generalisation.

Both of these features will now be discussed.

2.1. Non-Stoichiometry of Rutile at Low Temperatures

Up to the present time no data have been reported in the literature concerning departures from the stoichiometric composition in rutile at temperatures below 850°C. Czanderna and Honig⁽⁷³⁾ are of the opinion that any weight loss of a sample of rutile below 875°C can be attributed to dehydration of the sample, and that loss of oxygen only occurs above 875°C. In the present investigation it was found that misleading results on the non-stoichiometry of a sample of rutile could be obtained when it was used in the as-received condition. For this reason all samples of rutile were dehydrated under vacuum and re-oxidised under carefully controlled conditions before use. Furthermore, in order to remove any water which might have been adsorbed on the surface of the dehydrated specimens, they were always heated at a temperature of 400°C for 24 hours, in position in the microbalance, before commencing an experimental study. The final balance reading at this temperature was taken as the zero when computing subsequent losses in weight of the sample. By taking these precautions it is reasonable to assume that the weight losses observed at all temperatures above 400°C can be attributed directly to loss of oxygen from the samples of rutile.

The temperature at which departure from the stoichiometric composition first occurred in a sample of rutile, on

heating it in a high vacuum, was not determined in the present studies, but was shown to be in the temperature range 400°C to 600°C . Departures from the stoichiometric composition were not thought to have occurred below 400°C since the colour of a specimen remained white even after heating the specimen for 24 hours at this temperature in a vacuum of 10^{-5} mm of mercury. The colour of rutile changes from white to yellow when only a small concentration of vacant anion sites are created in the lattice^(23,27).

2.2. Maximum Extent of Non-Stoichiometry at Various Temperatures

Excluding for the present the behaviour of the single-crystal sample of rutile, the extent of departure from the stoichiometric composition, at a given temperature, was greater in a sample which was more impure. The data obtained using the single-crystal sample of rutile do not agree with this generalisation, and although this material was relatively impure in comparison to the high-purity rutile, it exhibited the smallest values of $[\text{AV}]$ found for any of the materials investigated at all temperatures below 1000°C . The single-crystal sample was the only massive sample examined; all other samples were in the form of a fine powder. It is possible, therefore, that insufficient time was allowed for equilibrium

to be reached at low temperatures in the single-crystal specimen because of the large diffusion path. The possibility that slow diffusion rates affect the behaviour is emphasised by the larger values of $[AV]$ obtained on reducing, in a vacuum, a single-crystal which had been crushed to a fine powder (see Fig. 38).

It is not possible at this stage to discuss in detail the way in which impurities lead to an increase in the extent of departure from the stoichiometric composition in rutile, since only incomplete chemical analyses of the impure samples are available. Furthermore, a systematic study of the effects of impurities could not be carried out, because of a lack of suitable facilities for preparing samples. Only general conclusions are, therefore, possible using the present data together with a knowledge of the major impurities present in the various samples.

From the analytical details of the samples (see Appendix III) the approximate number of Ti^{4+} ions which are replaced by impurity ions in the purified and technical rutile are:

TABLE VII

Sample	number of ions/ 10^4 ions of Ti^{4+}			
	Al^{3+}	Si^{4+}	Sb^{5+}	P^{5+}
Purified	<3	30	<6	<20
Technical	<3	60	>6	20

TABLE VIII

IMPURITY	CHANGE IN CONDUCTIVITY
WO_3	x 4000
MoO_3	x 0.5
<hr/>	
P_2O_5	x 1020
Sb_2O_5	x 833
V_2O_5	x 27
Ta_2O_5	x 4166
Nb_2O_5	x 5500
<hr/>	
SiO_2	x 3.3
ZrO_2	x 0.9
<hr/>	
B_2O_3	x 6
Al_2O_3	x 0.4
Fe_2O_3	x 0.5
Cr_2O_3	x 3.5
Ga_2O_3	x 0.4
Y_2O_3	x 0.1

Effect of various impurities (concentration of about 1 mole %) on the electrical conductivity of rutile ceramic at 250°C. Samples air-quenched from 1200° to 250°C (after Johnson⁽¹⁰⁰⁾).

The technical rutile contains more impurities in the tetravalent and pentavalent states compared with the purified rutile, and the sample of purified rutile containing 1 wt % niobium pentoxide contains an even larger concentration of ions in the pentavalent state than either of these materials. The values of $[AV]$ at a given temperature were greater in the niobium-doped material than in the technical rutile, and were greater in the latter than in the purified rutile. It would appear, therefore, that as the concentration of ions in the pentavalent state, and silicon ions in the tetravalent state increases, larger values of $[AV]$ are obtained at a given temperature. There is an interesting correlation between this observation and the effects of various oxides on the electrical conductivity of rutile, which have been reported by Johnson⁽¹⁰⁰⁾. The data obtained by Johnson is summarised in Table VIII, but the figures must be accepted with caution because little attention was paid to the state of reduction of the samples. It was found that the addition of pentavalent ions and also Si^{4+} ions to rutile led to an increase in electrical conductivity, whereas trivalent ions, with the exception of boron and chromium, led to a decrease. Furthermore, if ions in both the trivalent and pentavalent states were present in a sample, the electrical conductivity was found to be dependent on the relative numbers of each ion and the

relative magnitudes of their individual influences on the conductivity. In the present studies it is possible that a similar effect alters the extent of non-stoichiometry, since the purified, technical and niobium-doped rutile all contained approximately the same concentration of aluminium ions, but the relative concentration of impurities in the tetravalent and pentavalent states increased progressively from purified to niobium-doped rutile.

It would seem likely, therefore, that at a given temperature, larger departures from the stoichiometric composition can be induced in a sample by adding ions which cause an increase in the electrical conductivity of rutile; in general these are ions in the pentavalent state. By adding pentavalent ions, tetravalent titanium ions must be converted into trivalent ions, in order to preserve electroneutrality of the crystal, and the conductivity will depend, amongst other factors, on the concentration of Ti^{3+} ions. A stoichiometric sample of impure rutile is thus no longer an insulator, since electrons are present in a conduction band, and this appears to alter the non-stoichiometric defect structure of rutile. At this stage, however, it is only possible to suggest that the defect structure of non-stoichiometric rutile can be altered by the electronic effects associated with the

presence of impurity ions. A detailed explanation of the role played by impurity ions will only be obtained after further work of an extensive and systematic nature has been carried out.

3. Future Work

Further investigations which would aid in obtaining a better understanding of the defect structure of non-stoichiometric rutile, and the effects of impurities, are outlined below:

(a) A more detailed study of departures from the stoichiometric composition as a function of both high and low partial pressures of oxygen, and over a wider temperature range. Information of this nature would lead to a more accurate determination of the precise dependence of $[AV]$ on oxygen pressure. This work could be carried out using the micro-balance described earlier, but would be more satisfactory if a heavier specimen were to be used, to give correspondingly greater increases in weight. It would also be advantageous to dispense with the platinum specimen container, the oxidation of which caused the present studies to be restricted to fairly low temperatures. Such a procedure would be possible if measurements were made using either a single-crystal or sintered-powder specimen, and suspending them from a single-crystal

fibre of sapphire: this technique has recently been used by Walker⁽¹⁰²⁾.

(b) A study of the effects of non-stoichiometry on the physical properties, e.g. density, electrical conductivity, Hall coefficient, magnetic susceptibility, of rutile under carefully controlled conditions of temperature and oxygen pressure.

(c) A systematic investigation of the effects of impurities on the non-stoichiometric defect structure of rutile, using samples containing known amounts of chosen elements. A good starting material for these studies would be the high-purity rutile used in some of the studies described earlier.

(d) Electron microscopy examinations of thin flakes of rutile to determine if clustering of anion vacancies occurs on $\{100\}$ and $\{110\}$ planes.

VII REFERENCES

1. Schwarzkopf, P. and Kieffer, R. "Refractory Hard Metals"; MacMillan (1953)
2. Campbell, I.E. "High Temperature Technology"; J. Wiley (1956)
3. Baur, W.H. Acta Cryst. 2 (1956) 515
4. Grant, F.A. Rev. Mod. Phys. 31 (1959) 646
5. Bevan, H., Dawes, S.V. and Ford, R.A. Spectrochimica Acta 13 (1958) 43
6. Born, M. and Bollnow, O.F. Naturwiss 13 (1925) 559
7. Lennard-Jones, J.E. and Dent, B.M. Phil. Mag. 3 (1927) 1204
8. Syrkin, Y.K. and Dyatkina, M.E. "The Structure of Molecules and the Chemical Bond"; Butterworths (1950)
9. Hannay, N.B. and Smyth C.P. J. Am. Chem. Soc. 68 (1946) 171
10. Ehrlich, P. Z. Electrochem. 45 (1939) 362
11. Assayag, P., Dode, M. and Faivre, R. Compt. Rend. 240 (1955) 1212
12. Andersson, S. et al. Acta Chem. Scand. 11 (1957) 1641
13. Straumanis, M.E. Ejima, T. and James, W.T. Acta Cryst. 14 (1961) 493
14. DeVries, R. and Roy, R. J. Am. Ceram. Soc. 33 (1954) 370
15. White, J. Trans. Brit. Ceram. Soc. 56 (1957) 553
16. Cubicotti, D. J. Am. Chem. Soc. 73 (1951) 2032
17. Domagala, R.F. and McPherson, D.J. Trans. A.I.M.E. 200 (1954) 238
18. Williams, J. et al. Trans. Brit. Ceram. Soc. 56 (1957)

19. Buessem, W.R. and Butler, S.R. Article 2, "Kinetics of High Temperature Processes"; Ed., Kingery, W.D.: M.I.T. - J. Wiley (1959)
20. Nasu, N. Sci. Rpts. Tohoku Imp. Univ. 25 (1936) 510.
21. Kroger, F.A. and Vink, H.J. Solid State Phys. 3 (1956) 307
22. Hurlen, T. Acta Chem. Scand. 13 (1959) 365
23. Crowmeyer, D.C. Phys. Rev. 87 (1952) 876
24. Earle, M.D. ibid 61 (1942) 56
25. Dekker, A.J. "Solid State Physics"; MacMillan (1958)
26. Cusack, N. "The Electrical and Magnetic Properties of Solids": Longmans (1958)
27. Breckenridge, R.G. and Hosler, W.R. Phys. Rev. 91 (1953) 793
28. Hollander, L.E. and Castro, P.L. ibid 119 (1960) 1882
29. Hollander, L.E., Diesel, T.J. and Vick, G.L. ibid 117 (1960) 1467
30. Hauffe, K., et al. Z. Electrochem. 56 (1952) 937
31. Hutson, A.R. Chapter 13, "Semiconductors", Ed: Hannay, N.B.: Reinhold (1959)
32. Meyer, S. Ann. Physik 69, (1899) 236
33. Wedekind, E. and H ausknecht, P. Ber. Dent. Chem. Ges. 46, (1913) 3763
34. Berkman, S. and Zocher, H. Z. Physik Chem. 124 (1926) 322
35. Huttig, G.F. Z. anorg. und allgem. Chem. 224 (1935) 225

36. Raychaudhuri, D.P. and Sengupta, P.N. Indian J. Phys. 10 (1936) 253
37. Zimens, K. and Hedval, J. Svensk. Kem. Tidsk. 52 (1941) 12
38. Hill, F.N. and Selwood P.W. J. Am. Chem. Soc. 71 (1949) 2522
39. Reyerson, L.H. and Honig, J.M. ibid 75 (1953) 3920
40. Gray, T.J., McCain, C.C., and Masse, N.G. J. Phys. Chem. 63 (1959) 472
41. Senftle, F.E., Pankey, T. and Grant, F.A. Phys. Rev. 120 (1960) 820
42. Bates, L.F. "Modern Magnetism": Cambridge University Press (1951)
43. Gray, T.J. et al. "Defect Solid State", Interscience Publishers (1957)
44. Zerfoss, S., Stokes, H. and Moore, C.H. J. Chem. Phys. 16 (1948) 1166
45. Schmidt, W. Ann. Phys. 9 (1902) 919
46. Berberich, L.J. and Bell, M.E. J. App. Phys. 11 (1940) 681
47. von Hippel, A. et al. Ind. Eng. Chem. 38 (1946) 1097
48. Bunting, R., Shelton and Creamer, J. Res. Nat. Bur. Stds. 38 (1947) 337
49. Mott N.F. and Gurney, R.W. "Electronic Processes in Ionic Crystals": Oxford University Press (1957)
50. Parker, R.A. and Wasilik, J.H. Phys. Rev. 120 (1960) 1631
51. Srivastava, K.G. Tech. Rpt. 127 (1958), Lab. Insuln. Res. M.I.T.
52. Srivastava, K.G. Phys. Rev. 119 (1960) 516

53. Cronemeyer, D.C. and Gilleo, M.A. Phys. Rev. 82 (1951) 975
54. Soffer, B.H. J. Chem. Phys. 35 (1961) 940
55. Moore, C.H. Trans. A.I.M.E. 184 (1949) 194
56. Verneuil, A. Compt. rend. 135 (1902) 791
57. Frederikse, H.P.R. J. App. Phys. 32 (1962) 2211 (Suppl.)
58. Chester, P.F. Westinghouse Res. Rpt. 908C901-P.3(1961)
59. Cronemeyer, D.C. Phys. Rev. 113 (1959) 1222
60. Prener, J.S. (G.E. Laboratories, Schenectady) Private Communication
61. Mauer, F.A. and Bolz, L.H. Nat. Bur. Stds., Wright Air Devel. Cen. Tech. Rpt. 55-473 (1955)
62. Morin, F.J. Bell Sys. Tech. J. 37 (1958) 1045
63. Goodenough, J.B. Phys. Rev. 117 (1960) 1442
64. Dunitz, J.D. and Orgel, L.E. J. Phys. Chem. Solids 3 (1957) 20
65. Hume-Rothery, W. "Atomic Theory for Students of Metallurgy": Institute of Metals (1955)
66. Morin, F.J. Phys. Rev. Letters 3 (1959) 34
67. Hasiguti, R.R. et al. J. Phys. Soc. Japan 16 (1961) 2223
68. Rees, A.L.G. "Chemistry of the Defect Solid State": Methuen (1954)
69. Sachse, H.B. and Nichols, G.L. Anal. Chem. 33 (1961) 1349
70. Aronson, S. J. Electrochem. Soc. 108 (1961) 312
71. Smakula, A. Methods of Expt. Phys - Solid State Phys. - 6 (1959) 283
72. Kingery, W.D. "Property Measurements at High Temperatures": M.I.T. - J. Wiley (1959)

73. Czanderna, A.W. and Honig, J.M. J. Phys. Chem. 63 (1959) 620
74. Gulbransen, E.A. Adv. in Catalysis V (1953) 119
75. Gulbransen, E.A. and Andrew, K.F. Trans. A.I.M.E. 185 (1949) 515
76. Rhodin, R.N. Adv. in Catalysis V (1953) 39
77. Topping, J. "Errors of Observation and Their Treatment": Institute of Physics (1957)
78. Jones, D.W. (University of Birmingham)
Private Communication
79. Cox, B. (U.K.A.E.A., Harwell)
Private Communication
80. Gast, T. Z. Angew. Physik 8 (1956) 167
81. Chester, P.F. (C.E.G.B., Leatherhead)
Private Communication
82. Ells, C. Ph.D. Thesis, University of Birmingham (1957)
83. Sartorius-Weke (Göttingen)
Private Communication
84. Kennard, E.H. "Kinetic Theory of Gases": McGraw-Hill (1938)
85. Crookes, W. Quart. J. Sci. 12 (1875) 337
86. Swalin, R.A. "Thermodynamics of Solids": J. Wiley (1962)
87. Basterfield, J. Ph.D. Thesis, University of Birmingham (1962)
88. Hirthe, W.M. Ph.D. Thesis, Northwestern University (1961)

89. Ashbee, K.H.G. Ph.D. Thesis, University of Birmingham (1962)
90. von Hippel, A.,
Kalnajz, J. and
Westphal, W.B. J. Phys. Chem. Solids 23 (1962) 779
91. Seitz, F. Rev. Mod. Phys. 34 (1962) 656
92. van Bueren, H.G. "Imperfections in Crystals":
N-Holland (1960)
93. Pauling, L. "Nature of the Chemical Bond":
Cornell U.P. (1940)
94. Smallman, R.E. "Modern Physical Metallurgy":
Butterworths (1962)
95. Kofstad, P. J. Phys. Chem. Solids 23 (1962) 1579
96. Hollander, L.E. and
Castro, P.L. J. App. Phys. 33 (1962) 3421
97. McQuillan, A.D. (University of Birmingham)
Private Communication
98. Seitz, F. Acta Met. 1 (1953) 355
99. Smallman, R.E.,
Ashbee K.H.G. and
Williamson, K. Proc. Roy. Soc.
(To be published)
100. Johnson, G.H. J. Am. Ceram. Soc. 36 (1953) 97
101. Thorpes, "Dictionary of Applied Science" 10
102. Walker, R.F. Vac. Microbalance Techniques
1 (1961) 87

VIII ACKNOWLEDGEMENTS

The work described in this thesis was carried out in the Department of Physical Metallurgy under the general direction of Professor G.V. Raynor, F.R.S. Financial support for the work came from the U.K.A.E.A. (Dounreay) and for the studentship from D.S.I.R.

The author would like to express particular thanks to Professor A.D. McQuillan who supervised the project, and whose advice and help at all stages of the work have been greatly appreciated. Thanks are also extended to Dr. R.E. Smallman for stimulating discussions and for making available unpublished electron micrographs.

I am indebted to Miss H. Wright for typing the manuscript, to Miss V. Russell for help in preparing the diagrams and to Miss J. Wain for help with the photographs.

Finally I should like to express my sincere gratitude to my wife for her unceasing encouragement and her self-sacrifice during the past three years.

Table IA.

Atomic notation	Ionic notation	Schottky's notation	Rees's notation	Effective charge (in electron charges)
MgO	$Mg^{2+}O^{2-}$	MgO	$Mg^{2+}O^{2-}$	
V_{Mg}	$V^{2+}_{Mg^{2+}}$ or $V_{C^{2+}}$	$Mg\Box^{\times}$	$(p_2 \Box^+)$	0
V_{Mg}'	$(V^{+}_{Mg^{2+}})'$ or $(V_{C^+})'$	$Mg\Box'$	$(p \Box^+)$	-1
V_{Mg}''	$(V_{Mg^{2+}})''$ or $(V_C)''$	$Mg\Box''$	\Box^+	-2
V_O	$V^{2-}_{O^{2-}}$ or $V_{A^{2-}}$	$O\Box^{\times}$	$(e_2 \Box^-)$	0
V_O^{\bullet}	$(V^{-}_{O^{2-}})^{\bullet}$ or $(V_{A^-})^{\bullet}$	$O\Box^{\bullet}$	$(e \Box^-)$	+1
$V_O^{\bullet\bullet}$	$(V_{O^{2-}})^{\bullet\bullet}$ or $(V_A)^{\bullet\bullet}$	$O\Box^{\bullet\bullet}$	\Box^-	+2
Mg_i	Mg_i	MgO^{\times}	$(e_2 Mg^{2+} \Delta)$	0
Mg_i^{\bullet}	$(Mg_i^+)^{\bullet}$	MgO^{\bullet}	$(e Mg^{2+} \Delta)$	+1
Li_{Mg}	$(Li^{+}_{Mg^{2+}}\oplus)$	$Li\bullet^{\times}(Mg)$	$(p Li^{+} \Box^+)$	0
Li_{Mg}'	$(Li^{+}_{Mg^{2+}})'$	$Li\bullet'(Mg)$	$(Li^{+} \Box^+)$	-1
Ga_{Mg}	$(Ga^{3+}_{Mg^{2+}}\ominus)$	$Ga\bullet^{\times}(Mg)$	$(e Ga^{3+} \Box^+)$	0
Ga_{Mg}^{\bullet}	$(Ga^{3+}_{Mg^{2+}})^{\bullet}$	$Ga\bullet^{\bullet}(Mg)$	$(Ga^{3+} \Box^+)$	+1
Cl_O	$(Cl^{-}_{O^{2-}}\ominus)$	$Cl\bullet^{\times}(O)$	$(e Cl^{-} \Box^-)$	0
Cl_O^{\bullet}	$(Cl^{-}_{O^{2-}})^{\bullet}$	$Cl\bullet^{\bullet}(O)$	$(Cl^{-} \Box^-)$	+1
Mn_{Mg}	$Mn^{2+}_{Mg^{2+}}$	$Mn\bullet^{\times}(Mg)$	$(Mn^{2+} \Box^+)$	0
Mn_{Mg}^{\bullet}	$(Mn^{3+}_{Mg^{2+}})^{\bullet}$	$Mn\bullet^{\bullet}(Mg)$	$(Mn^{3+} \Box^+)$	+1
$Mn_{Mg}^{\bullet\bullet}$	$(Mn^{4+}_{Mg^{2+}})^{\bullet\bullet}$	$Mn\bullet^{\bullet\bullet}(Mg)$	$(Mn^{4+} \Box^+)$	+2

Comparison of various notations of centres for the case MgO (after Kröger and Vink⁽²¹⁾).

Symbols:

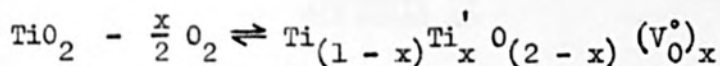
Atomic and Ionic:

- \ominus, \oplus ... free electrons, holes
 - $\cdot, ' , \grave{}$... positive, negative charge
 - $\grave{}$... interstitial site; ∇ ... vacant lattice site
- Schottky⁽⁸⁸⁾:
- \bullet ... lattice site; \circ ... interstitial site
 - \square ... vacancy; \times ... uncharged
 - $\cdot, ' , \grave{}$... positive, negative charge
- Rees⁽⁶⁸⁾:
- \square^+, \square^- ... vacant cation, anion lattice site
 - Δ ... interstitial; e, p ... quasi-free electron, hole

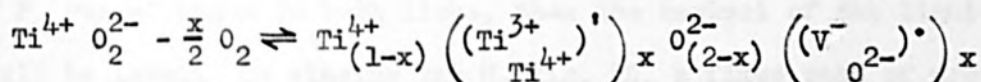
APPENDIX I

In Section 2 the various defects that could be produced in non-stoichiometric rutile were described in terms of the ionic notation used by Kroger and Vink⁽²¹⁾. This notation was used since the crystal bonding in rutile is to a large extent ionic in nature. However, the defects could equally well have been described in terms of the atomic notation used by the same authors, in which no assumptions are made regarding the crystal bonding. These two notations are compared in the first two columns of Table IA, for the case of MgO. When considering rutile it is evident that a vacant oxygen site with one associated electron will be $(V_{O}^{-}2^{-})^{\circ}$ in the ionic notation, whereas V_{O}° in the atomic notation.

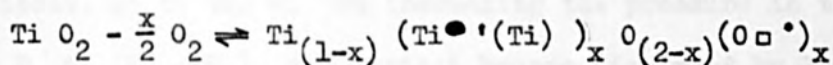
In Table IA two other notations, due to Schottky⁽⁸⁸⁾ and Rees⁽⁶⁸⁾, are indicated so that it is possible to compare the manner in which some of the defects in MgO are expressed in terms of four different notations in general use. With the aid of Table IA a defect reaction expressed in terms of one notation can be translated into any of the other notations. As an example let us consider the formation of oxygen (anion) vacancies, with one associated electron, and Ti^{3+} ions, at normal (cation) lattice sites, when x atoms of oxygen are lost from a molecule of stoichiometric rutile. Expressing the loss in terms of the atomic notation⁽²¹⁾,



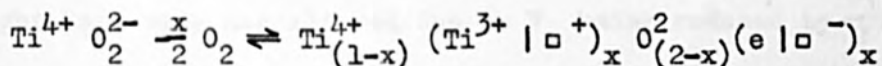
In terms of the ionic notation⁽²¹⁾:



In the notation due to Schottky⁽⁸⁸⁾:



In the notation due to Rees⁽⁶⁸⁾:



In a similar way the other defect reactions given in Section 2 can be expressed in terms of each of the notations given in Table IA.

APPENDIX II

If the dibutyl manometer contained argon at a pressure of P_A cms of argon in both limbs, then the menisci of the liquid would be level. On closing tap H, Fig. 20, a fixed mass of argon at a pressure P_A is trapped in the volume V_0 above the right hand meniscus, up to tap H. On increasing the pressure in the system by P_0 to $(P_0 + P_A)$, the menisci become displaced by l_1 cms, but P_0 is not proportional to l_1 since the pressure of the argon on the right hand side has altered due to V_0 being reduced by $\frac{l_1}{2}k$, where k is the cross-sectional area of the manometer tube. Thus:

$$\text{Pressure at X} = P_0 + P_A$$

$$\text{Pressure at Y} = P'_A$$

$$\therefore P_0 + P_A - P'_A = Fl_1 \quad (\text{AII.1})$$

where F is the factor for converting l_1 to cms of mercury.

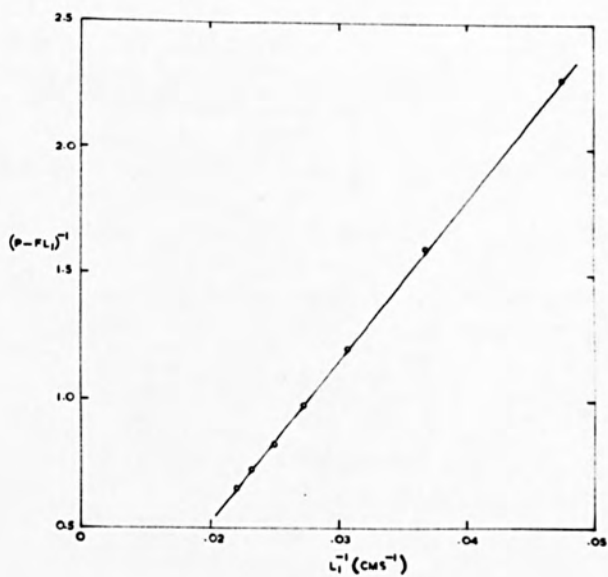
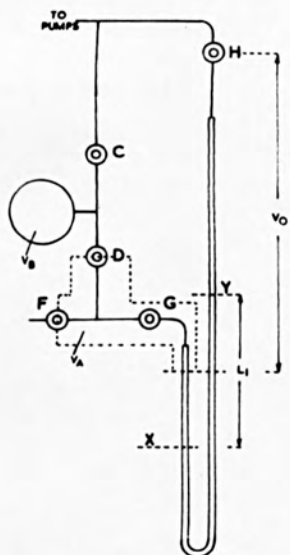
Now a fixed mass of gas on the right hand side, originally at pressure P_A and in volume V_0 , has been compressed to a pressure P'_A in a volume $(V_0 - \frac{l_1}{2}k)$ i.e. from the Gas Laws ($P_1V_1 = P_2V_2$):-

$$P_A V_0 = P'_A (V_0 - \frac{l_1}{2}k) \quad (\text{AII.2})$$

Substitution of (AII.1) in (AII.2) gives:

$$P_A V_0 = (P_A + P_0 - Fl_1)(V_0 - \frac{l_1}{2}k)$$

which on rearrangement gives:-



(a)

(b)

Fig. IA. (a) The volume V_A of the apparatus, and
 (b) the graph used to calculate the volume V_0 .

$$P_A \frac{l_1 k}{2} = (P_o - Fl_1)(V_o - \frac{l_1 k}{2})$$

$$\therefore P_o = \frac{P_A l_1 k}{(2V_o - l_1 k)} + Fl_1 \quad (\text{AII.3})$$

Thus the amount by which the pressure in the system has increased (P_o) above the known basic pressure of argon (P_A) can be calculated from l_1 , provided V_o and k are known.

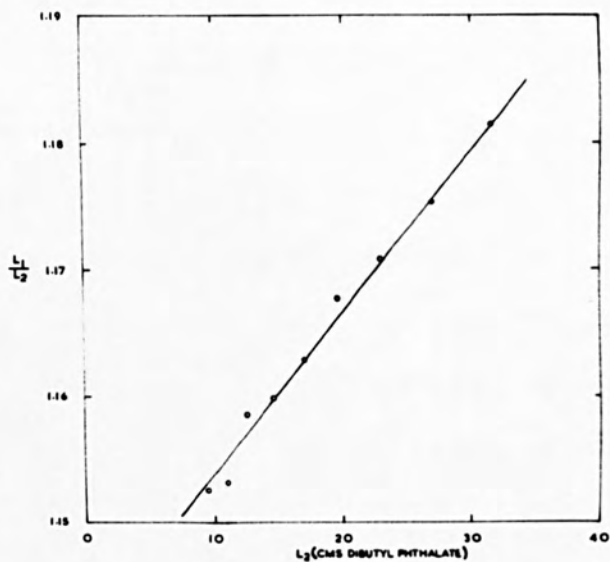
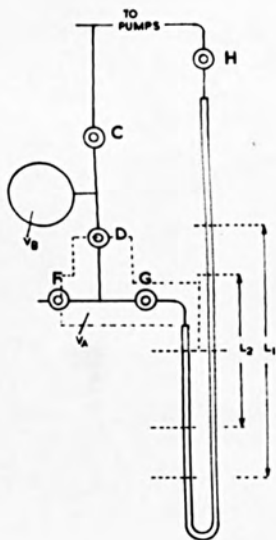
In order to calculate V_o , known pressures of argon (P), measured using the mercury manometer, were admitted to the dibutyl manometer, with an initial pressure of P_A cms of argon in the right hand limb. The corresponding displacements, l_1 , of the menisci were measured. In order to obtain V_o graphically, equation (AII.3) was rearranged to give:

$$(P_o - Fl_1)^{-1} = \frac{2V_o}{kP_A} \cdot l_1^{-1} - \frac{1}{P_A} \quad (\text{AII.4})$$

In this case P_o is given by $(P - P_A)$.

On plotting $(P_o - Fl_1)^{-1}$ vs l_1^{-1} a straight line was obtained (see Fig. 1A(b)) whose slope was $\frac{2V_o}{kP_A}$. A more accurate value of the slope was obtained by treating the data by a least squares analysis.

Before, however, V_o could be calculated, the cross-sectional area of the manometer tube had to be derived. Unfortunately the diameter of the tube was unknown, although the tube was known to be of precision bore. The method of finding k is given below: With the right hand limb of the manometer evacuated, argon was admitted to the system (with taps F and C, Fig. 2A(a), closed) to



(a)

(b)

Fig. 2A. (a) The known volume V_B of the apparatus, and
 (b) the graph used to the cross-sectional area of the manometer tube.

give a displacement of l_1 cms i.e. the argon was at a pressure of $F.l_1$ cms of mercury. Tap D was closed, thus isolating argon at a pressure $F.l_1$ in the volume V_B which was accurately known. The gas in the system was then pumped away. Tap D was opened and the gas in V_B , at pressure $F.l_1$, was expanded into the system causing a displacement of l_2 cms of the dibutyl menisci. The volume into which the gas had expanded was V_A , the volume of the part of the system up to the position where the menisci were normally level (see Fig. 2A(a)), plus $\frac{l_2}{2}k$. From the Gas Laws i.e. $P_1V_1 = P_2V_2$:-

$$F.l_1.V_B = F.l_2 \left(V_B + V_A + \frac{l_2}{2}k \right)$$

$$\text{i.e. } \frac{l_1}{l_2} = \frac{V_B + V_A}{V_B} + \frac{k}{2V_B} \cdot l_2 \quad (\text{AII.5})$$

On plotting $\frac{l_1}{l_2}$ vs l_2 a straight line was obtained (Fig. 2A(b)) whose slope was $\frac{k}{2V_B}$. In order to obtain a more accurate value of the slope, the data was treated by a least squares analysis. Since V_B was known accurately, k could be calculated.

By finding V_0 and k in the above manner, the dibutyl manometer was used to measure small pressures of oxygen in the system, although the latter was under a basic pressure of 70 mm of argon.

APPENDIX III

The impurities present in the high-purity rutile
were as follows* :

TiO ₂	99.99%
SiO ₂	0.0028%
Al ₂ O ₃	0.0008%
Sn	< 20 ppm
Nb ₂ O ₅	< 20 ppm
ZrO ₂	< 20 ppm
P ₂ O ₅	< 20 ppm
Cr ₂ O ₃	< 2 ppm
Pb	< 10 ppm
Sb ₂ O ₅	< 20 ppm
V ₂ O ₅	< 10 ppm
Cu	< 10 ppm
As ₂ O ₃	< 10 ppm

Analytical details of the other materials were supplied by Hopkin and Williams Ltd., unless otherwise indicated.

* The author is indebted to Mr. J. Whitehead, British Titan Products Ltd., for kindly supplying these figures.

Technical rutile:

Al_2O_3	< 0.02%*
SiO_2	0.54%*
P_2O_5	0.52%
Pb	< 0.02%
Cr_2O_3	< 10 ppm
V_2O_5	< 10 ppm
Fe_2O_3	60 ppm
Cu	12 ppm

Purified rutile: this material is prepared from technical rutile in order to reduce, in particular, the arsenic and antimony content.

Al_2O_3	< 0.02%*
SiO_2	0.26%
As	< 1 ppm
Sb	< 200 ppm

Single crystal rutile:

Al_2O_3	0.06%*
SiO_2	1.10%*

*The author is indebted to Mr. J. Whitehead, British Titan Products Ltd., for kindly supplying these figures.

APPENDIX IV

Specimen: high purity rutile

Average Temp. °C	Fractional Weight Loss $\times 10^{-4}$	[AV] $\times 10^{-3}$
(a) No dehydration - as received powder		
514.5	0	0
705.0	3.88	1.935
860.0	5.00	2.498
907.5	5.11	2.554
997.0	5.19	2.591
1332.0	7.08	3.533
(b) Dehydration: subsidiary furnace, temperature 1025°C.		
	$\times 10^{-6}$	$\times 10^{-5}$
358.0	0	0
586.5	7	3.5
658.0	21	10.6
754.5	25	12.5
819.5	26	12.9
876.0	27	13.7
916.0	37	18.4
961.0	38	19.2
1009.0	43	21.5

Specimen: purified rutile.

Pressure of Oxygen mm	Fractional Weight Uptake $\times 10^5$	Decrease in [AV] $\times 10^4$	[AV] in Sample $\times 10^4$
Temperature = 843.7°C [AV] _{VAC} = 8.40×10^4			
1.525	4.65	2.32	6.08
2.506	5.44	2.72	5.68
3.966	6.66	3.33	5.07
5.657	8.15	4.07	4.33
7.643	8.77	4.38	4.02
10.753	8.91	4.45	3.95
17.115	9.44	4.71	3.69
Temperature = 900.5°C [AV] _{VAC} = 11.14×10^{-4}			
1.729	8.07	4.03	7.11
2.839	9.41	4.70	6.44
4.601	9.94	4.96	6.18
7.655	10.33	5.16	5.98 ?
11.718	11.59	5.79	5.35
18.631	11.86	5.92	5.22
Temperature = 945.6°C [AV] _{VAC} = 12.67×10^{-4}			
2.038	9.32	4.65	8.02
3.364	{ 11.66	5.82	6.85
5.530	{ 11.41	5.70	6.97
8.839	{ 13.27	6.62	6.05
14.709	14.14	7.06	5.61
20.105	15.22	7.60	5.07
	15.29	7.63	5.04

Pressure of Oxygen mm	Fractional Weight Uptake $\times 10^5$	Decrease in [AV] $\times 10^4$	[AV] in Sample $\times 10^4$
Temperature = 999.5°C $[AV]_{VAC} = 11.50 \times 10^{-4}$			
1.585 3.293 6.050 9.329 13.933 32.361	5.80 7.59 8.46 9.58 10.40 12.40	2.90 3.79 4.22 4.79 5.19 6.19	8.60 7.71 7.28 6.71 6.31 5.31
Temperature = 968°C (sample 2) $[AV]_{VAC} = 9.81 \times 10^{-4}$			
3.096 6.716 10.669 12.674 15.598 23.238	8.41 9.50 10.19 10.56 10.65 11.55	4.20 4.74 5.09 5.27 5.32 5.77	5.61 5.07 4.72 4.54 4.49 4.04

Specimen: purified rutile

Average Temp. °C	Fractional Weight Loss $\times 10^{-5}$	[AV] $\times 10^{-4}$
(a) Dehydration: subsidiary furnace, temperature 1025°C.		
387.5	0	0
562.0	3.5	1.81
645.0	4.9	2.50
746.0	7.4	3.70
812.5	9.9	4.99
869.0	11.0	5.51
919.0	{ 14.6	7.27
	{ 14.0	6.92
968.0	{ 19.0	9.47
	{ 19.7	9.86
1018.0	23.4	11.71
1071.0	37.2	18.59
(b) Doped with 1 wt. percent Nb_2O_5 Dehydration: integrated with oxidation.		
	$\times 10^{-4}$	$\times 10^{-4}$
399.0	0	0
595.5	0.63	3.14
665.0	1.20	5.98
760.0	1.62	8.10
836.0	2.05	10.22
901.5	3.81	19.05
962.5	5.79	28.90
1020.5	10.26	51.23

Specimen: technical rutile

Average Temp. °C	Fractional Weight Loss $\times 10^{-5}$	[AV] $\times 10^{-4}$
Dehydration: subsidiary furnace, temperature 1025°C.		
372.0	0	0
575.5	7.2	3.58
665.5	10.0	5.01
776.5	11.2	5.57
876.0	13.2	6.61
944.0	16.9	8.44
1011.0	32.7	16.31
1071.5	73.8	35.33

Specimen: single crystal rutile

Average Temp. °C	Fractional Weight Loss $\times 10^{-6}$	[AV] $\times 10^{-5}$
(a) Massive.		
331.0	0	0
484.0	0	0
698.0	13	6.5
808.0	16	8.0
886.5	18	9.0
960.0	22	11.0
1063.0	{ 34	17.0
	{ 43	21.5
1277.5	319	159.9
(b) Crushed.		
	$\times 10^{-4}$	$\times 10^{-3}$
496.0	1.92	.957
586.0	2.92	1.458
688.5	4.35	2.171
796.5	5.84	2.917
869.0	6.88	3.432
949.0	{ 6.91	3.448
	{ 7.67	3.832
1098.0	{ 13.94	6.959
	{ 16.34	8.158

APPENDIX V

Dilatometry data:

Temp. °C	$\frac{\Delta l}{l}$ OBS $\times 10^3$	$\frac{\Delta l}{l}$ CALC $\times 10^3$	δ $\times 10^3$	Temp. °C	$\frac{\Delta l}{l}$ OBS $\times 10^3$	$\frac{\Delta l}{l}$ CALC $\times 10^3$	δ $\times 10^3$
Parallel <u>a</u> Direction				Parallel <u>c</u> Direction			
156.5	2.303	2.271	+0.032	165.4	1.532	1.483	+0.049
214.5	3.141	3.113	+0.028	213.0	1.882	1.910	-0.028
256.0	3.700	3.715	-0.015	242.2	2.162	2.172	-0.010
308.0	4.469	4.470	-0.001	286.0	2.549	2.565	-0.016
354.0	5.095	5.137	-0.042	329.0	2.962	2.950	+0.012
405.5	5.829	5.885	-0.056	374.6	3.347	3.359	-0.012
455.5	6.598	6.610	-0.012	437.0	3.896	3.919	-0.023
503.0	7.286	7.299	-0.013	488.2	4.370	4.378	-0.008
555.0	8.135	8.054	+0.081	536.3	4.846	4.809	+0.037
-	-	-	-	-	-	-	-
601.0	8.846	8.722	+0.124	573.2	5.176	5.140	+0.036
655.5	9.740	9.512	+0.228	609.9	5.547	5.469	+0.078
709.5	10.669	10.296	+0.373	650.1	5.931	5.830	+0.101
762.5	11.553	11.065	+0.488	684.8	6.263	6.141	+0.122
806.0	12.275	11.696	+0.579	730.8	6.684	6.552	+0.132
860.0	13.078	12.480	+0.598	758.7	6.995	6.803	+0.192
911.5	13.870	13.227	+0.643	808.7	7.445	7.252	+0.193
957.5	14.443	13.895	+0.548	836.6	7.734	7.502	+0.232
1002.0	14.982	14.541	+0.441	891.7	8.256	7.996	+0.260
				938.0	8.698	8.411	+0.287
				982.6	9.175	8.811	+0.364

APPENDIX VI

The density of a sample of rutile:

(a) containing x anion vacancies per molecule is given by:

$$\rho_n = \rho_s (1 - kx) = 4.2502 (1 - 0.2003x)$$

(b) containing x anion vacancies, and if the volume of the sample is decreased by collapse about a spherical volume of anion vacancies, is given by:

$$\rho_n = \rho_s \frac{(1 - kx)}{1 - Vx}$$

where $V = \frac{4}{3} \pi r^3 N M^{-1} 10^{-24} 4.2502 = 0.4171$.

(c) containing x anion vacancies and if a collapse about a cube occurs, is given by:

$$\rho_n = \rho_s \frac{(1 - kx)}{1 - Cx}$$

where $C = 8 r^3 N M^{-1} 10^{-24} 4.2502 = 0.7973$.

x $\times 10^4$	ρ_n (a)	ρ_n (b)	ρ_n (c)
1	4.25011	4.25029	4.25045
5	4.24977	4.25066	4.25147
10	4.24935	4.25112	4.25274
15	4.24892	4.25158	4.25401
20	4.24850	4.25205	4.25529